ISSN 1410-1675

BULLETIN OF THE MARINE GEOLOGY

VOLUME 39 • NUMBER 1 • JUNE 2024

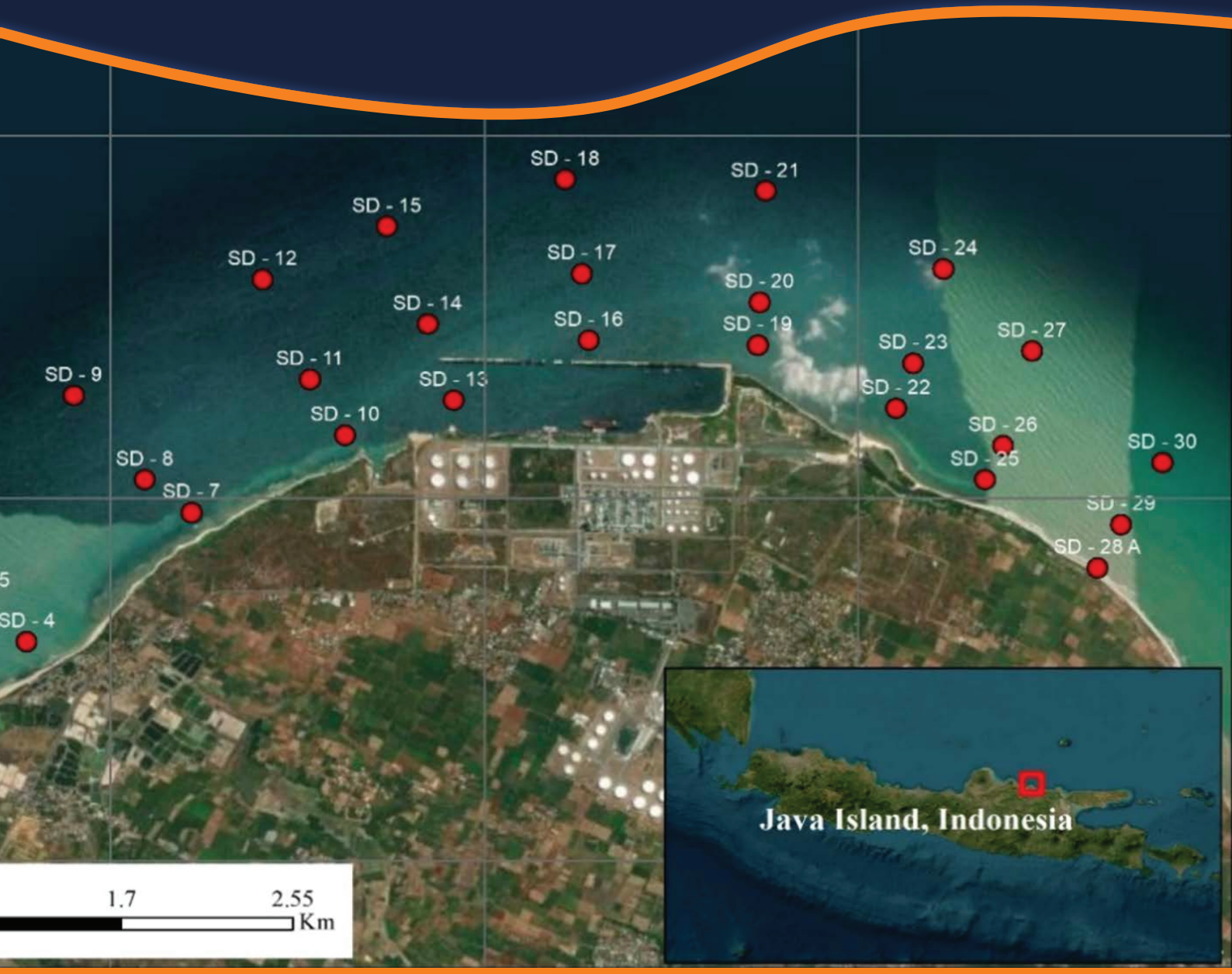

BoMG	VOL. 39	NO. 1	PAGE 1-68	BANDUNG, JUNE 2024	ISSN 1410-6175

Accredited : RISTEK-BRIN 200/M/KPT/2020

MARINE GEOLOGICAL INSTITUTE
GEOLOGICAL AGENCY
MINISTRY OF ENERGY AND MINERAL RESOURCES

BALAI BESAR SURVEI DAN PEMETAAN GEOLOGI KELAUTAN
BADAN GEOLOGI
KEMENTERIAN ENERGI DAN SUMBER DAYA MINERAL

BULLETIN OF THE MARINE GEOLOGY

Vol. 39, No. 1, June 2024

For communication of this publications, please contact :
MARINE GEOLOGICAL INSTITUTE
Dr. Junjunan 236, Bandung-40174, Indonesia
Telephone : +62-22-6032020, 6032201, Fax : +62-22- 6017887
E-mail : ejournal.p3gl@gmail.com

Cover Figure : Bed load sampling location of TPPI Tuban Port, East Java, Indonesia (Source: Rachman, et al, 2024)

Preface

This year marks the deadline for re-accrediting the Bulletin of the Marine Geology. The publication of its first edition in 2024 is a key component of the re-accreditation process with the Ministry of Education, Culture, Research, and Technology. The Marine Geological Institute credits its editorial board, general division, and legal cooperation and information sub-division for their collaboration in completing the inaugural edition.

Featuring five articles from different scientific disciplines, all written by field experts, the Editorial Board extends its gratitude to all who contributed to the submission and review of papers. The papers tells us an impact of environmental factors on coastal ecosystems, with each topics addresses different aspects of how pollutants, ocean energy, sediment dynamics, heavy metals, and tidal patterns can affect the health and resilience of coastal environments.

The first paper highlights the potential risks of PAH pollutants released into the Indramayu Coast from anthropogenic activities, emphasizing the need for further awareness and periodic monitoring to detect carcinogenic PAHs. The second paper explores the seasonal and intra-seasonal variability of ocean thermal energy as a clean energy alternative, with fluctuations ranging between 280.09 GW and 295.65 GW, demonstrating its potential as a renewable energy resource. The third paper emphasizes the importance of understanding sediment dynamics to support the revitalization of ports and ensure the sustainability of port operations through effective solutions. The fourth paper reveals the increased pollution in coral reef environments due to heavy metal lead (Pb) content from rapid industrial development and ship traffic, with surface water Pb concentrations exceeding threshold levels and posing potential harm to the coral reef ecosystem. The last article discusses Tidal Harmonic Analysis and Prediction to support Early Warning for Coastal Flooding, highlighting the importance of accurate tide predictions in providing early warning, mitigation, and adaptation to frequent coastal flooding in at-risk coastal areas.

By submitting research findings to be published in this periodical, you, as top-tier scientists, will help us in our endeavours to make the Bulletin of Marine Geology reputable, prestigious, and respectable. Enjoy reading this edition.

Bandung, June 2024
Warm regards,

Editorial Board

ISSN 1410-6175

BULLETIN OF THE MARINE GEOLOGY

Vol. 39, No. 1, June 2024

Contents

POLYCYCLIC AROMATIC HYDROCARBONS (PAHs) IN INDRAMAYU COASTAL, WEST JAVA: DISTRIBUTION, SOURCE, AND ECOLOGICAL RISK ASSESSMENT
Deny Yogaswara, Dede Falahudin, Ita Wulandari, Edward Edward, Ricky Rositasari, Ukis Shofarudin ---------- **1-14**
DOI : http://dx.doi.org/10.32693/bomg.39.1.2024.850

SEASONAL AND INTRA-SEASONAL VARIABILITY OF OCEAN THERMAL POTENTIAL ENERGY IN THE INDONESIAN EXCLUSIVE ECONOMIC ZONE
Totok Suprijo, Gandhi Napitupulu, Nining Sari Ningsih, Denny Basardo Jonatan Sinaga, Audi Rachman ---------- **15-27**
DOI : http://dx.doi.org/10.32693/bomg.39.1.2024.866

SEDIMENT CHARACTERISTICS TO SUPPORT THE REVITALIZATION OF TPPI TUBAN PORT, EAST JAVA, INDONESIA
Reno Arief Rachman, Mardi Wibowo, Aloysius Bagyo Widagdo, Nurkhalis Rahili, Rizaldi Caesar Yuniardi, Hamzah Haru Radityo Suharyanto, Affandy Hamid, Aris Subarkah, Suranto Suranto, Hanah Khoirunnisa ---------- **28-41**
DOI : http://dx.doi.org/10.32693/bomg.39.1.2024.874

STUDY OF HEAVY METAL LEAD (PB) CONTENT IN THE CORAL REEF ENVIRONMENT OF PANJANG ISLAND, BANTEN
Ahmad Al Fauzan, Dwi Amanda Utami, Rima Rachmayani, Ayu Utami Nurhidayati ---------- **42-58**
DOI : http://dx.doi.org/10.32693/bomg.39.1.2024.862

TIDAL HARMONIC ANALYSIS AND PREDICTION TO SUPPORT EARLY WARNING FOR COASTAL FLOODING
Randi Firdaus, Nurul Tazaroh, Oky Surendra, Eko Prasetyo, Riris Adriyanto ---------- **59-68**
DOI : http://dx.doi.org/10.32693/bomg.39.1.2024.863

POLYCYCLIC AROMATIC HYDROCARBONS (PAHs) IN INDRAMAYU COASTAL, WEST JAVA: DISTRIBUTION, SOURCE, AND ECOLOGICAL RISK ASSESSMENT

POLISIKLIK AROMATIK HIDROKARBON (PAH) DI PESISIR INDRAMAYU, JAWA BARAT: DISTRIBUSI, SUMBER, DAN KAJIAN RISIKO EKOLOGI

Deny Yogaswara*, Dede Falahudin, Ita Wulandari, Edward, Ricky Rositasari, Ukis Shofarudin

Research Center for Oceanography - National Research and Innovation Agency (BRIN), Jalan Pasir Putih Raya, Ancol Timur, Jakarta Utara 14430 - Indonesia

*Corresponding author: deny.yogaswara@brin.go.id

(Received 16 Agustus 2023; in revised from 04 September 2023 accepted 22 May 2024)

DOI : 10.32693/bomg.39.1.2024.850

ABSTRACT: PAH pollutants from anthropogenic activities were released into Indramayu Coast and could potentially have negative effects on the environment. This study aimed to determine the distribution, source, and ecological risks of PAHs in the area. Seawater and sediment samples were collected and stored in glass bottles at 4 °C and then further processed in the laboratory. The samples were extracted with dichloromethane and n-hexane and then fractionated using a silica gel column, and finally injected into a Gas Chromatography-Mass Spectrometer (GCMS). The distribution of PAH compounds was detected in all sampling stations in varying amounts. PAH with low molecular weight (two to three rings) was predominant in seawater samples, while high molecular weight (four rings) was predominant in sediments. In addition, by using the molecular diagnostic ratio, the PAH source in Indramayu Coast was detected to be pyrogenic and petrogenic processes that come from anthropogenic activities. Exposure to PAH concentrations in this study posed a lower risk to sediment-dwelling organisms. However, further awareness and periodic monitoring are required to detect carcinogenic PAHs.

Keywords: polycyclic aromatic hydrocarbons (PAHs), pollutants, Indramayu Coast, ecological risk

ABSTRAK: *Polutan PAH yang berasal dari kegiatan antropogenik dilepaskan ke Pesisir Indramayu dan berpotensi menimbulkan dampak negatif terhadap lingkungan. Penelitian ini bertujuan untuk mengetahui distribusi, sumber, dan risiko ekologi PAH di pesisir Indramayu. Sampel air laut dan sedimen diambil dan disimpan dalam botol kaca pada suhu 4°C untuk kemudian dianalisis lebih lanjut di laboratorium. Sampel diekstraksi dengan diklorometana dan n-heksana kemudian difraksinasi menggunakan kolom silika gel, lalu diinjeksikan ke alat Gas Chromatography-Mass Spectrometer (GCMS). Konsentrasi PAH terdeteksi dalam air laut dan sedimen masing-masing sebesar 190-400 ng/L dan 8,3-45 ng/g. PAH dengan berat molekul rendah (dua sampai tiga cincin) dominan dalam sampel air laut, sedangkan PAH dengan berat molekul sedang (empat cincin) dominan dalam sedimen. Selain itu, dengan menggunakan rasio diagnostik molekuler, sumber PAH di Pesisir Indramayu terdeteksi dari proses pirogenik dan petrogenik serta berasal dari aktivitas antropogenik. Paparan konsentrasi PAH dalam penelitian ini mempunyai risiko lebih rendah terhadap organisme penghuni sedimen. Namun, kesadaran lebih lanjut dan pemantauan berkala diperlukan untuk mendeteksi PAH yang bersifat karsinogenik.*

Kata Kunci: *Polisiklik Aromatik Hidrokarbon (PAH), Polutan, Pesisir Indramayu, Risiko Ekologi*

INTRODUCTION

Polycyclic aromatic hydrocarbons (PAHs) are the most abundant and widespread persistent organic pollutants in aquatic environments (Neşer et al., 2012; Mehdinia et al., 2015). Attention to these pollutants is increasing due to their toxic, mutagenic, and carcinogenic effects on organisms and human health (Ravindra et al., 2008). Unlike other organic hydrophobic contaminants (Charles et al., 2012), PAHs are continuously produced and released into the environment by the pyrolysis of fossil fuels (UNEP 2001; Mastral et al., 2003). Coastal and marine ecosystems are particularly vulnerable to PAHs (Glad et al., 2017), which mostly come from terrestrial area and the ocean itself. Furthermore, seasonal variations might affect hydrodynamic processes in Indramayu Coast and hence the transportation of PAHs in ecosystems and accumulate PAHs in seawaters, sediments (Liu et al., 2016), and marine biota (Farrington 2020; Yogaswara et al., 2021).

In aquatic ecosystems, low molecular weight PAHs are found in the dissolved phase; however, those of heavier molecules (having four or more aromatic rings) are mostly adsorbed onto sediment particles (Veerasingam et al., 2016). PAHs evaporate into the atmosphere and incorporate into aerosol particles and then can be deposited on the sea surface, where they aggregate with marine particulate organic matter (POM) (Akyüz and Çabuk 2010). Once in the water column, biogeochemical processes play a role in the transfer of contaminants bound in suspended particles to the sediment surface (Portet-Koltalo et al., 2013). Therefore, sediment is the main receptor and reservoir of PAH (Chen et al., 2020).

Indramayu coastal is a neritic sea in the northern Java (Widhiarno and Muliati 2016) and is influenced by several factors, including population growth, industrialization, and rapid economic development (Sodikin 2011; Wulandari et al., 2019). These anthropogenic activities have a detrimental effects and have become a potential source of PAHs (Tong et al., 2019; Zhao et al., 2021) for which the Cimanuk River might carry PAHs to the estuary through surface runoff (Paryono et al., 2017; Sholeh et al., 2018). Therefore, Indramayu CoastIndramayu Coast requires intensive environmental quality monitoring.

This study was conducted to analyze the levels, sources, and potential ecological risks of PAHs in the environment of Indramayu Coast. Furthermore, it provides information to understand PAHs levels as an environmental database, the management of organic pollution in the Indramayu coastal area, the sources of risk, and the mapping of exposure to PAHs to the coastal environment.

METHODS AND MATERIALS

Sampling site

Seawater and sediments were collected using an acrylic glass Van Dorn water sampler and a stainless steel Van Veen grab, respectively, from 18 stations in the Estuary of Cimanuk River and Indramayu Coast, West Java Province, in April 2017 (Figure 1). All samples were kept in an ice box at a temperature of 4 °C, for further analysis in the laboratory.

Sediment characteristics

The granulometric method was used to analyze the particle size of the sediments. Briefly, 50 g of wet sediment was weighed, dried in an oven at 80 °C for 12 h, homogenized with distilled water, and filtered through stratified sieves with mesh sizes of 4, 2, 1, 0.5, 0.25, 0.125, and 0.063 mm (Wentworth, 1922; Blair and McPherson, 1999).

Sample analysis

One liter of seawater was collected and filtered using Whatman Grade GF/C Glass Microfiber Filter Papers (pore size: 0.45 µm; diameter: 47 mm). The filtrate was extracted three times using a liquid-liquid extraction method and shaken using a vertical shaker at 150 rpm for 5 min with dichloromethane (30 mL), n-hexane (30 mL), and a dichloromethane-n-hexane mixture (1:1 v/v, 30 mL). The mixture was then fractionated using sodium sulfate and silica gel-60, with 15 mL of n-pentane-dichloromethane (40:60) and then it was evaporated and injected into the Gas Chromatography-Mass Spectrometer (GCMS) ISQ-LT 1310 Thermo Scientific (Khozanah et al., 2019).

Furthermore, 10 g of sediment was extracted using a solvent similar to the seawater samples, in an ultrasonic water bath for 30 min at 30 °C (Yamaguchi and Lee 2010). Subsequently, activated copper was added to remove the sulfur containing material. Moreover, the sample was fractionated by silica gel-60 with 15 mL of n-pentane:dichloromethane mixture (2:3, v/v). Finally, it was evaporated and injected into a GCMS ISQ-LT 1310 Thermo Scientific (Khozanah et al., 2019).

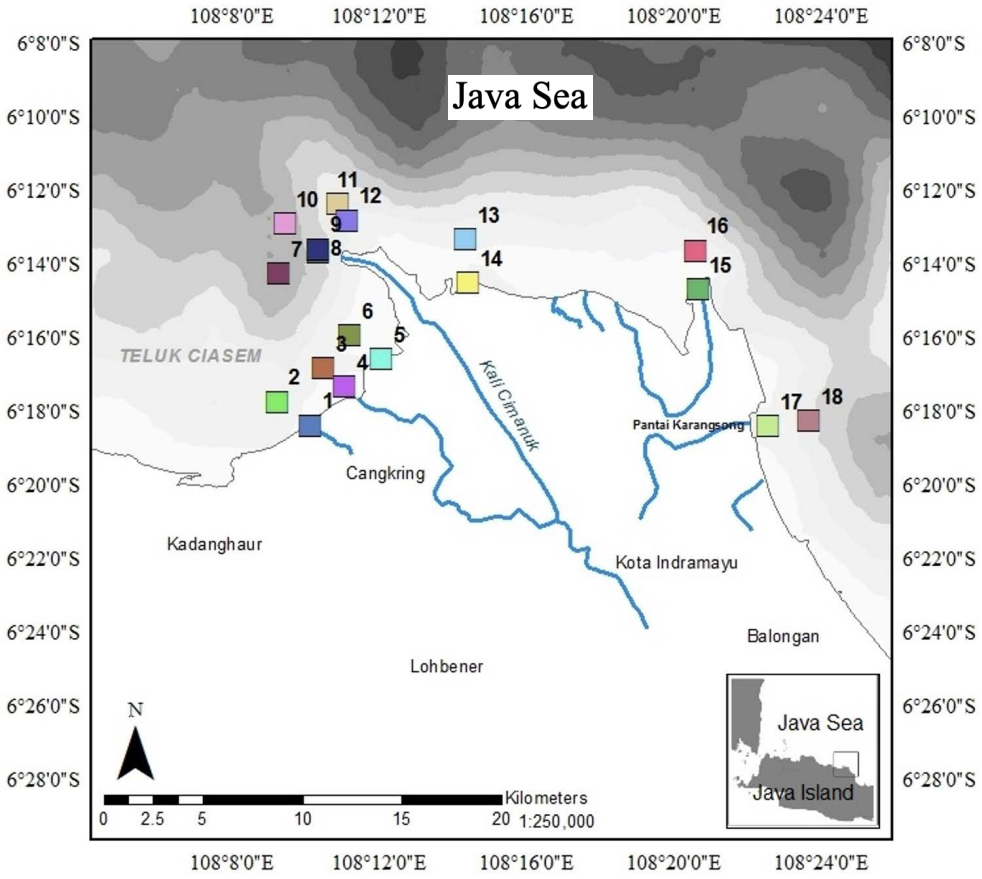

Figure 1. Field sampling of seawater and sediment samples at 18 stations in Indramayu Coast, West Java.

GCMS condition

PAHs were determined using a GCMS ISQ-LT 1310 Thermo with a column TG5-SilMs (30 m length, 0.25 mm ID). The GC oven was set at 50 °C (hold for 0.5 minutes), and then it was set with an initial temperature of 160 °C for 15 minutes, which increased the temperature to 290 ^{o}C with a gas rate of 10 ^{o}C/min (hold for 13 minutes). Finally, the temperature was raised to 300 ^{o}C and held for 4 minutes. The gas system used helium gas at a rate of 1.2 mL/min (with constant flow), with a splitless time mode of 0.5 minutes. The MS detector was set at an ionization potential/electron energy of +70 eV with ion sources and interface temperature of 230 ^{o}C and 250 ^{o}C respectively. Ion mass data (m/z) was recorded between 50-750 scans per second. PAH compounds were identified based on the mass spectra and retention times using the full scan method.

The average recovery of the blank spiked standard was 60% and it was performed separately. The GCMS performance was carried out separately against external standards QTM PAH mix CRM47930 immediately before injecting the sample. A blank sample procedure was performed to identify contaminants during PAH analysis in the laboratory.

Identification of pollution source

Diagnostic ratios were used to identify the potential sources of PAHs in seawater and sediments (Table 1) (Yunker et al., 2002; Ke et al., 2017). In general, PAHs can be classified into three groups based on differences in the number of rings: low molecular weight PAHs (2-3 rings), medium molecular weight PAHs (4 rings), and high molecular weight PAHs (5-6 rings). Different distributions of the number of rings may indicate different PAH sources (Baumard et al., 1998). In this method, the diagnostic ratios fluoranthene (Flt)/(fluoranthene (Flt) + pyrene (Pyr)), Anthracene (Ant)/(Anthracene (Ant) + Phenenathrene (Phe)), Benzo [a] Anthracene (BaA)/(Bezo [a] Anthracene (BaA) + Chrysene (Chry)), Indeno (123-cd) pyreine (Ind)/(Indeno (1,2,3-cd) pyrene (Ind) + Benzo (g,h,i) perylene (B(ghi)P)), and Benzo (a) pyrene (BaP)/Benzo (ghi) Perylene (B(ghi)P) were used as indicators in the study of PAH compounds (Yang et al., 2020).

Table 1. Molecular diagnostic ratio of PAHs to determine pollution source

PAH Ratio	Range	Source	Reference
∑LMW/∑HMW	< 1	Pyrogenic	(Tobiszewski and Namieśnik 2012)
	> 1	Petrogenic	
Ant/(Ant+Phe)	< 0.1	Petrogenic	(Ravindra et al., 2008)
	> 0.1	Pyrogenic	
Flt/(Flt+Pyr)	< 0.4	Petrogenic	(De La Torre-Roche et al., 2009)
	0.4-0.5	Fossil fuel combustion	
	> 0.5	Grass, wood, coal combustion	
BaA/(BaA+Chry)	0.2-0.35	Coal combustion	(Yunker et al., 2011)
	> 0.35	Vehicle emission	
	< 0.2	Petrogenic	
Ind/(Ind+B(g,h,i)P)	< 0.2	Petrogenic	
	0.2-0.5	Petroleum combustion	
	> 0.5	Grass, wood, coal combustion	
BaP/B(ghi)P	< 0.6	Non-traffic emission	(Katsoyiannis et al., 2007)
	> 0.6	Traffic emission	

Distribution of PAH

PAH distribution is determined based on the distribution of the types of PAH compounds detected at each sampling station. Typically, PAH levels will decrease or degrade as they move farther from the mainland or coastline and towards the open sea.

Environmental ecological risk evaluation

The ecological risk assessment of PAHs in sediments was evaluated using sediment quality guidelines, such as the effect range level (ERL), effect range medium (ERM), threshold effects level (TEL), and probable effects level (PEL) (MacDonald et al., 1996; CCME 1999). The adverse biological effects of PAHs in sediment were predicted to occur infrequently (<ERL/TEL), occasionally (ERL/TEL > concentrations < ERM/PEL), and frequently (>ERM/PEL) (Yang et al., 2020). In addition, it is significant to examine the sediment particles as organic contaminants. Therefore, sediment quality guidelines (ISQG value) were necessary to evaluate the effect of contaminated sediment in the marine environment (ANZECC 2000). For four carcinogenic PAHs, e.g., chrysene, benzo (a) pyrene, benzo (a) anthracene, and benzo (k) fluoranthene (PAH_4), were calculated based on the total number of carcinogenic PAH detected in seawater and sediment samples.

Statistical Analysis

For statistical analysis of the significance level (p) of PAH distribution among sampling stations, a one-way ANOVA was applied. To gain a better understanding of the relationship between PAH concentration and the characteristics of sediment from each station investigated, the obtained results were subjected to principal component analysis (PCA) by using the Paleontological Statistics software package for education and data analysis (Past) 4.13.

RESULTS

PAHs level in seawater and sediment

The PAHs levels in seawater ranged from 190 ng/L to 400 ng/L, with a mean value of 279.4 ng/L. The highest PAH concentration was found at Station 1, whereas the lowest total PAH level was detected at Station 12. PAH concentrations in sediments ranged from 8.3-45 ng/g wet weight (ww) with a mean value of 18.5 ng/g, and the highest PAHs level was detected at station 1 and the lowest at station 2 (Figure 2).

Characteristics and distribution of PAHs

PAHs with three rings were more prevalent than those with two or more rings in seawater, meanwhile, PAHs with four rings were more prevalent in sediment. Anthracene was detected massively in seawater, followed by fluorene, fluoranthene, and pyrene. In sediment, anthracene was also predominant, followed by fluoranthene, pyrene, and benzo (a) anthracene (Figure 3).

The composition of PAHs in seawater and sediment samples varied at each sampling station. A large number of PAH compounds were detected in seawater and sediment samples at station 1 (Figure 4).

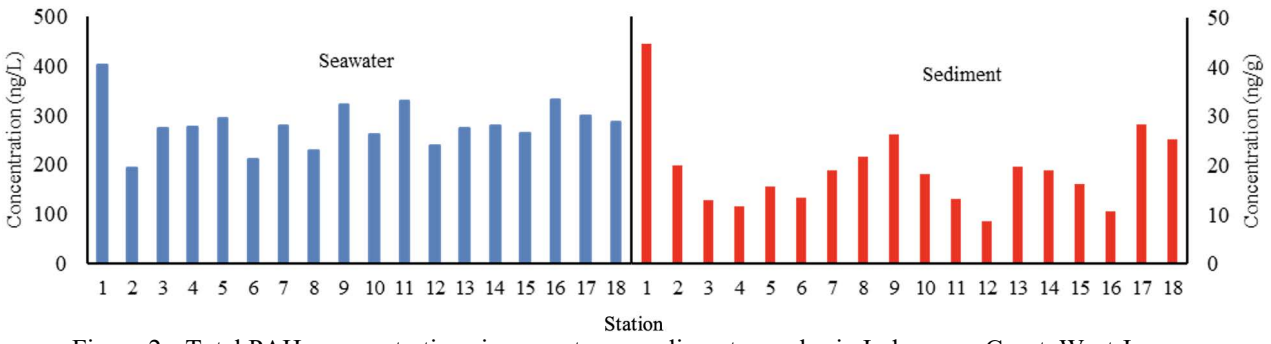

Figure 2. Total PAHs concentrations in seawater an sediment samples in Indramayu Coast, West Java.

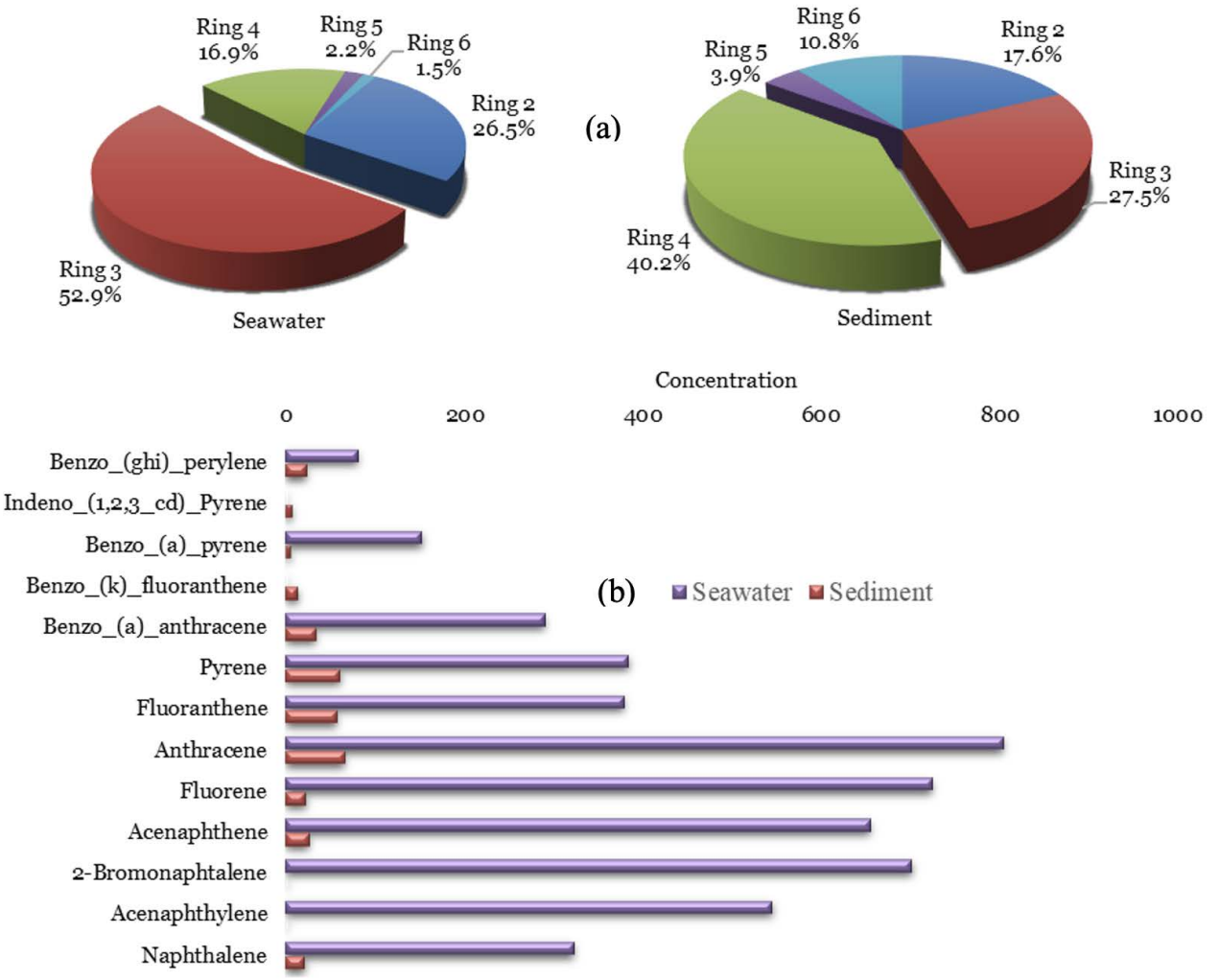

Figure 3. Ring composition (a) and distribution of PAH congeners (b) in seawater (ng/L) and sediment (ng/g) samples in Indramayu Coast, West Java.

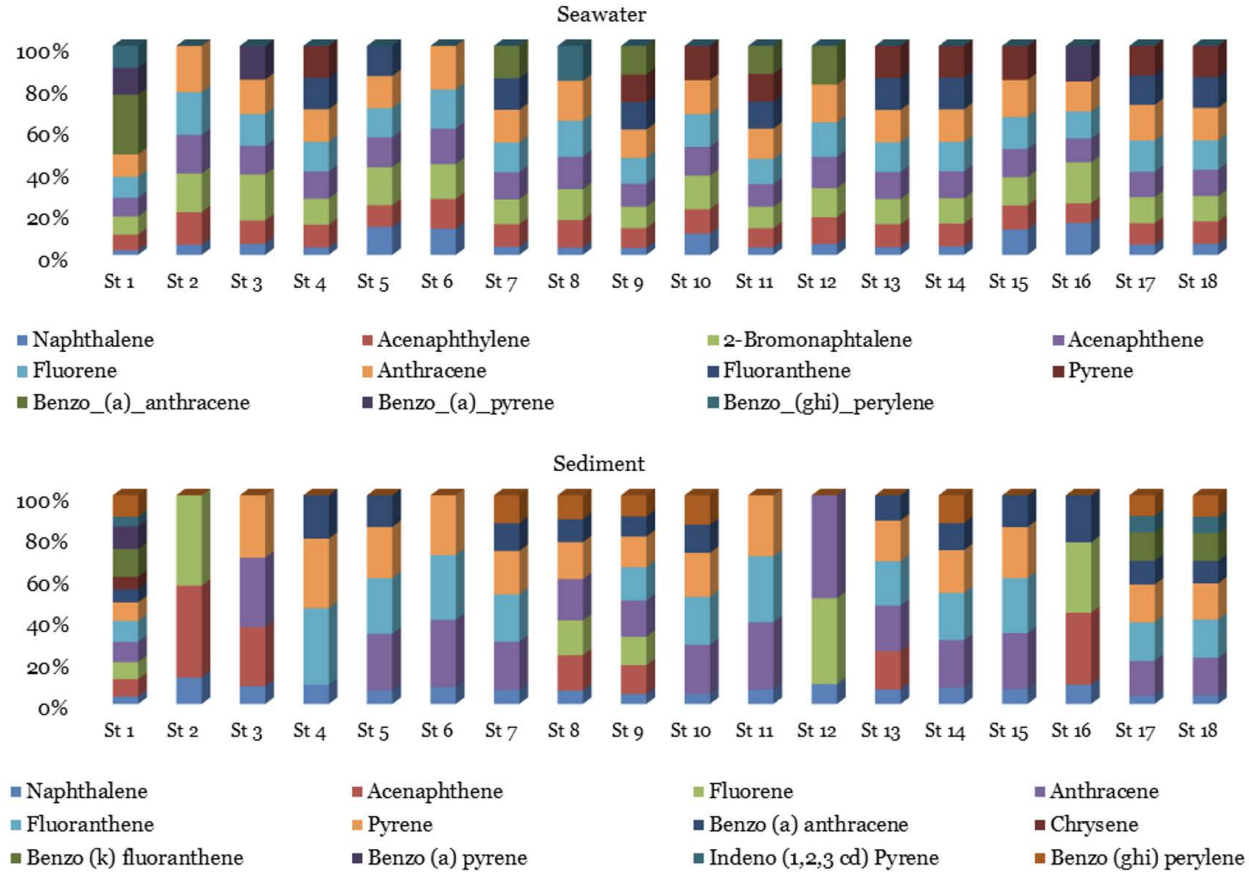

Figure 4. PAH congeners composition in seawater and sediment samples from each station in Indramayu Coast, West Java.

DISCUSSIONS

PAHs in seawater and sediment

In general, the Indramayu waters can be described as unpolluted by PAH substances, given that their concentration levels are below the threshold limit set by the sediment quality guidelines of CCME (1999) and ANZECC (2000). The highest PAH concentrations in seawater were observed at station 1, located near the harbor and crossed by the ship line. Ship dock activities and fishing boat traffic are sources of PAH in water (Chen et al., 2020; Yogaswara et al., 2020). In addition, the deposition of particulate matter from the atmosphere can be a potential source of PAHs (Tong et al., 2019). The Indramayu Coast is located in the Java Sea and is influenced by two monsoon regimes, the northwest and southeast monsoons, which affect the variability of rainfall, riverine input, winds, waves, and sea currents (Koropitan et al., 2009). According to several previous studies, these physical oceanographic parameters can affect the distribution of organic pollutants in water (Zhao et al., 2021).

The PAHs levels in seawater are higher than in other sites on Java, such as Cilincing Waters, Jakarta Bay (Yogaswara et al., 2020). Moreover, these levels are still higher in comparison to those observed in several other countries, such as the Xiamen Coast - China, the Mediterranean Sea - France (Guigue et al., 2014), the Tyyhenian Sea - Italy (Cincinelli et al., 2001), and the Pier Estuary, New Jersey - USA (Gigliotti et al., 2002). The high PAHs was detected in this study could be due to the nearby crude oil refinery of PT Pertamina and the potential for crude oil leakage from the loading and unloading of tankers via single-point mooring (SPM) (Sinurat et al., 2016).

The highest level of polycyclic aromatic hydrocarbons (PAHs) was found in the sediment samples at Station 1 due to its location near a shipping port in an estuary area. The lower level at Station 2 could be attributed to the hydrophobic nature of organic pollutants and the hydrodynamic conditions in the coastal area. Several factors contribute to the accumulation of these pollutants in the sediment samples, such as the dramatic increase in shipping activity over the last two decades. In addition, offshore or onshore gas and oil exploration and production activities are potentially due to oil spills, which contribute to increasing chemical

pollution in coastal and ocean areas (Tornero and Hanke 2016). Their low solubility and hydrophobic nature cause them to be adsorbed onto suspended particulates and carried by rivers, which eventually spread and sunk into the sediment in estuaries and coastal waters (Duan et al., 2015). This leads to their persistent accumulation in high concentrations (Li and Li 2017). In addition, the deposition of organic pollutants can be affected by the hydrodynamic conditions in the area (Kang et al., 2017) and potentially occur in the various PAHs distributions in each sampling in Indramayu Coast.

The average PAHs levels in the sediment samples were lower than those along the Java Sea, such as Banten Bay (Khozanah and Yogaswara 2017), Jakarta Bay (Yogaswara et al., 2020), and Cirebon Waters (Khozanah et al., 2019). This is likely due to the lower industrial activity in Indramayu than the other four sites. Additionally, PAH levels decreased with an increasing distance from the estuary, suggesting that human activities have less of an impact on the open sea (Yang et al., 2020). In estuaries, PAH compounds generally originate from river discharges. However, hydrodynamic conditions such as currents, tides, winds, and waves influences high PAH levels in rivers (Mehdinia et al., 2015). Furthermore, the ANOVA test showed statistical significance ($p < 0.05$) of PAH distribution in seawater and sediment samples among sampling stations, particularly sampling stations close to the mainland, as the main sources of anthropogenic activities and riverine input.

PAHs with four or more rings tend to be detected in sediment samples because they are persistent and accumulate in sediment particulates. In contrast, PAHs with lower rings (two to three rings) are more commonly detected in seawater samples because of their hydrophobicity, meaning they stay in seawater (Tong et al., 2019). Furthermore, based on the classification of contaminated water proposed by Maliszewska-Kordybach (1996), the PAH concentrations in sediments can be divided into four categories: (a) uncontaminated (<200 ng/g), (b) weakly contaminated (200-600 ng/g), (c) contaminated (600-1000 ng/g), and (d) heavily contaminated (>1000 ng/g). Consequently, according to this category, sediments from the Estuary of Cimanuk River and Indramayu Coast are uncontaminated by PAHs. Anthracene was the predominant compound detected in seawater and sediment samples, while benzo (ghi) perylene and chrysene were the less detected compounds in seawater and sediment samples (Figure 3). Generally, anthracene originates from the petrochemical and manufacturing industries, while benzo (ghi) perylene originates from motor vehicle emissions (Abdel-Shafy and Mansour, 2016). Several PAHs congeners that were not detected in seawater or sediment samples had concentrations below the detection limit of 1 ng/L.

PAHs Distribution

The distribution of PAHs was significant at station 1, indicating that during seawater sampling, PAHs were distributed around this site. As hydrophobic compounds, PAHs tend to float and spread on the surface of the air, and due to hydrodynamical processes, PAH compounds sank into the water column and being accumulated in sediment over a long period of time (Tong et al., 2019). Therefore, the concentration of PAH compounds at the seawater surface is higher in general than at the sediment surface. Furthermore, the accumulation of PAHs generally occurred in the estuary, while at the station 1, it was detected to be a significant location for the distribution of these pollutants because it is located in the estuary area. Hence, an estuary is often used as a long-term monitoring site due to its ability to accumulate and deposit organic pollutants over a long period of time (Wang et al., 2017). Furthermore, degradation of PAHs in sediments is low for high molecular weight (HMW) group PAH compounds and under anaerobic conditions. PAH levels near the coastal sampling stations (e.g., station 1, 5, 8, 9, 15, and 17) are consistently higher in comparison to sampling stations in the open sea, indicating a decline in PAH concentrations as they move away from the coast. The distribution of PAHs in coastal waters is strongly influenced by hydrodynamic conditions and the aggregation of organic pollutants with particulate matter (Mehdinia et al., 2015).

The distribution of pollutants in coastal and marine environments is impacted by the size of particles and the amount of clay in sediment (Yang et al., 2020). This research uncovered that at each sampling station, there were varying dominant sediment characteristics. Generally, silt particles were predominant sediment characteristic for the whole sampling station, and followed by clayish silt, silty sand, and sand (Table 2). In addition, PCA analysis was figure out for 85.5% of the total variances in profile of PAH rings in particle size of sediment samples (Figure 5). About 56.4% of total variances on the first principal components is characterized by clayish silt, sand, silty

sand, and silt. Furthermore, about 29.1% of total variances on the second principal (PC2) is dominated by silt, clayish silt, sand, and silty sand. The PCA analysis in correlation between particle size of sediment and PAH ring depicted a minor significant correlation in each sampling station. Each particle size of sediment has a various accumulation of type of PAH ring and is not related to each other. This indicates that the dominant sediment characteristics were not necessarily associated with high levels and ring molecules of PAHs. This is a normal occurrence in the changing aquatic ecosystems of estuarine and coastal areas (Timoney and Lee 2011). According to a study by Duan et al. (2015), Gu et al. (2017), and Lohmann et al. (2005), have demonstrated that sediment characteristics have less effect on the accumulation of organic contaminants in sediments.

Identification and source of PAHs

The molecular weight ratio (low and high) and molecular diagnostic ratio (MDR) indicated that the source of PAH pollutants came from pyrogenic and petrogenic processes (Table 2). Pyrogenic sources were predominantly derived from seawater samples, whereas petrogenic sources were predominantly derived from sediment samples. In addition, particulate organic pollutants can also come from atmospheric deposition, thereby contributing to the

Table 2. Sediment characteristics at each sampling station in Indramayu Coast, West Java

Station	Sediment Characteristic	Station	Sediment Characteristic	Station	Sediment Characteristic
St 1	Clayish silt	St 7	Silt	St 13	Clayish silt
St 2	Silt	St 8	Silt	St 14	Sand
St 3	Silt	St 9	Silt	St 15	Silt
St 4	Silty sand	St 10	Silt	St 16	Silt
St 5	Silty sand	St 11	Clayish silt	St 17	Silt
St 6	Clayish silt	St 12	Silt	St 18	Silt

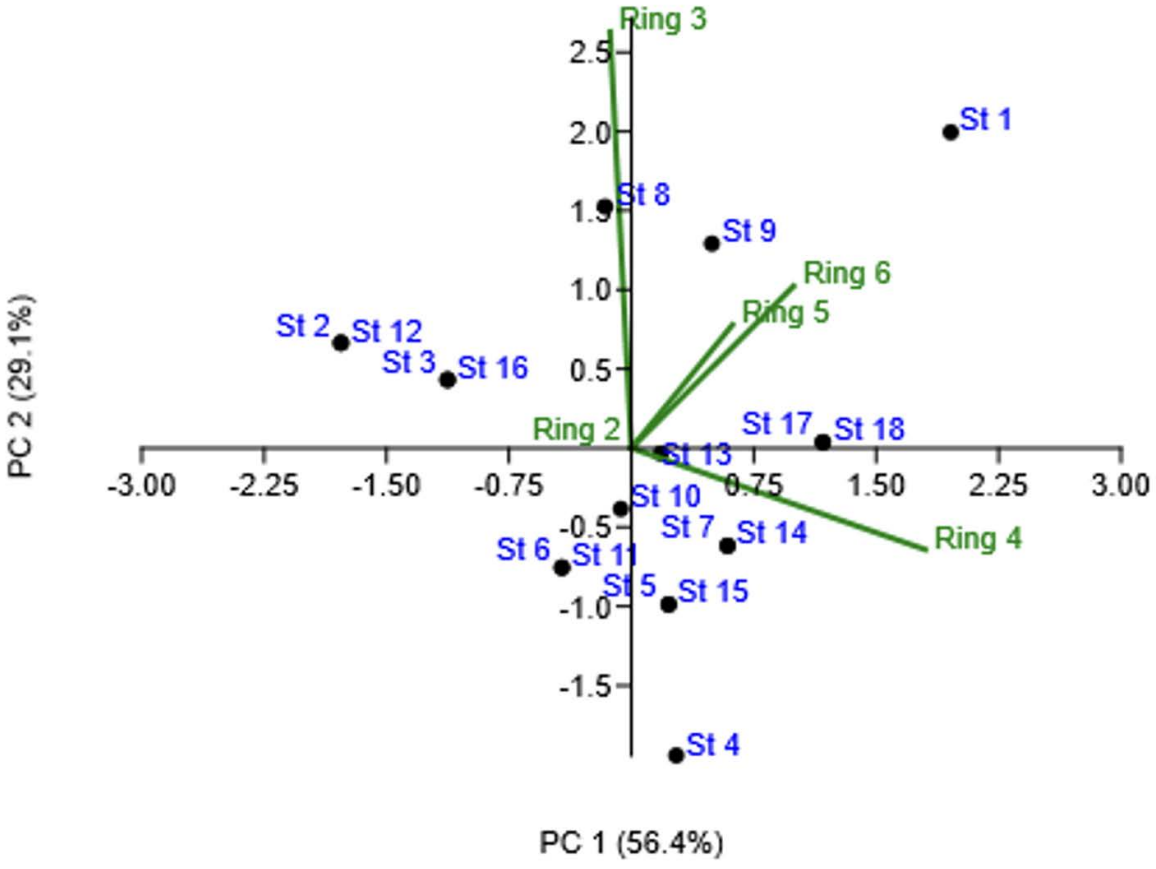

Figure 5. PCA analysis to identify the correlation between ring of PAHs and sampling stations in Indramayu Coast, West Java.

accumulation of pollutants in the marine environment as well (Galarneau, 2008). In this study, it suggests that the PAH pollutants come from both sources, petrogenic sources potentially come from oil spills and oil seeps from Kilang Balongan Pertamina Indramayu, shipping and boat discharge, as well as input from riverine and municipal waste water. Meanwhile, pyrogenic source potentially come from the atmospheric deposition of particulate matter and the combustion emission of vehicles from mainland and boat activities in Eretan and Karangsong fishing ports, Indramayu.

PAHs potentially originate from both pyrogenic and petrogenic sources. Pyrogenic sources generally originate from industrial emissions or fuel combustion from ships or automobile discharge, transport through the atmosphere, and dispersion through water periods of time (Li et al., 2015).

Environmental ecological risk

Based on sediment quality guidelines, the relationship between PAHs levels and ERL and ERM criteria can reveal whether PAHs adversely affect benthic communities and organisms (Han et al., 2019). The results showed that the selected individual PAH level below the sediment quality threshold did not negatively affect the biota in the sediment (CCME, 1999; ANZECC, 2000). However, it is still necessary to be more aware of the potential ecological risks posed by sedimentary PAHs over the long term, particularly in estuaries.

For carcinogenic risk evaluation, the risks for seven carcinogenic PAHs, benzo (k) fluoranthene (BkF), benzo (a) anthracene (BaA), benzo (a) pyrene

Table 3. Identification of PAHs source in Indramayu Coast, West Java

Station	∑LMW/∑HMW		Ant/(Ant+Phe)		Flt/(Flt+Pyr)		BaA/(BaA+Chry)	
	Sdm	Swt	Sdm	Swt	Sdm	Swt	Sdm	Swt
St 1	0.42	0.93	1.00	1.00	0.53	nc	0.51	1.00
St 2	nc	nc	nc	1.00	nc	nc	nc	nc
St 3	2.35	5.20	1.00	1.00	nc	nc	nc	nc
St 4	0.10	2.29	nc	1.00	0.52	0.50	1.00	nc
St 5	0.51	5.95	1.00	1.00	0.52	1.00	1.00	nc
St 6	0.68	nc	1.00	1.00	0.52	nc	nc	nc
St 7	0.43	2.27	1.00	1.00	0.52	1.00	1.00	1.00
St 8	1.49	4.98	1.00	1.00	nc	nc	1.00	nc
St 9	0.98	1.50	1.00	1.00	0.52	0.50	1.00	1.00
St 10	0.40	5.09	1.00	1.00	0.52	nc	1.00	nc
St 11	0.64	1.53	1.00	1.00	0.52	0.49	nc	1.00
St 12	nc	4.39	1.00	1.00	nc	nc	nc	1.00
St 13	0.89	2.27	1.00	1.00	0.52	0.50	1.00	nc
St 14	0.44	2.30	1.00	1.00	0.52	0.50	1.00	nc
St 15	0.51	5.14	1.00	1.00	0.52	nc	1.00	nc
St 16	3.43	4.84	nc	1.00	nc	nc	1.00	nc
St 17	0.26	2.54	1.00	1.00	0.50	0.50	1.00	nc
St 18	0.28	2.38	1.00	1.00	0.51	0.50	1.00	nc

Note: nc = not calculated, Sdm = Sediment, Swt = Seawater

hydrodynamic processes (Castro-Jiménez et al., 2012). In addition, pyrogenic sources can originate from river flow inputs carried from estuaries to the high seas (Chen et al., 2020). Petrogenic sources usually originate from the contamination of crude oil or petroleum fuel products that are spilled to the ocean, directly spread in the water, and aggregated by organic particulates (Tobiszewski and Namieśnik 2012). Furthermore, they sink and gradually accumulate in sediments over long

(BaP), benzo (b) fluoranthene (BbF), indeno (cd - 1,2,3) perylene (IND), chrysene (Chr), and dibenzo (a,h) anthracene (DBahA), in the aquatic environment have the potential to occur, especially the type of BaP, which is carcinogenic (Mu et al., 2014; Li and Li 2017). The four carcinogenic PAHs (PAH_4) based on regulation of EU-Commission (2011) were detected from a total of seven types of PAH congeners that were categorized as

Table 4. Sediment analysis of ecological risk (ng/g) in Indramayu Coast, West Java

PAHs	ERL	ERM	TEL	PEL	ISQG-Low	ISQG-High	This study (average)
Naphthalene	160	2100	34.6	391	-	-	1.1
Acenaphthene	16	500	6.7	88.9	16	500	3.7
Fluorene	19	540	21.2	144	19	540	3.6
Anthracene	85.3	1100	46.9	245	85	1100	4.4
LMW	**280.3**	**4240**	**109.4**	**868.9**	**120**	**2140**	**12.8**
Fluoranthene	600	5100	113	1494	600	5100	4.3
Pyrene	665	2600	153	1398	665	2600	4
Benzo (a) anthracene	261	1600	74.8	693	261	1600	2.4
Chrysene	384	2800	108	846	384	2800	2.7
Benzo (a) pyrene	430	1600	88.8	763	430	1600	4.9
HMW	**2340**	**13700**	**537.6**	**5194**	**2340**	**13700**	**18.3**
Total	**2620.3**	**17940**	**647**	**6062.9**	**2460**	**15840**	**31.2**

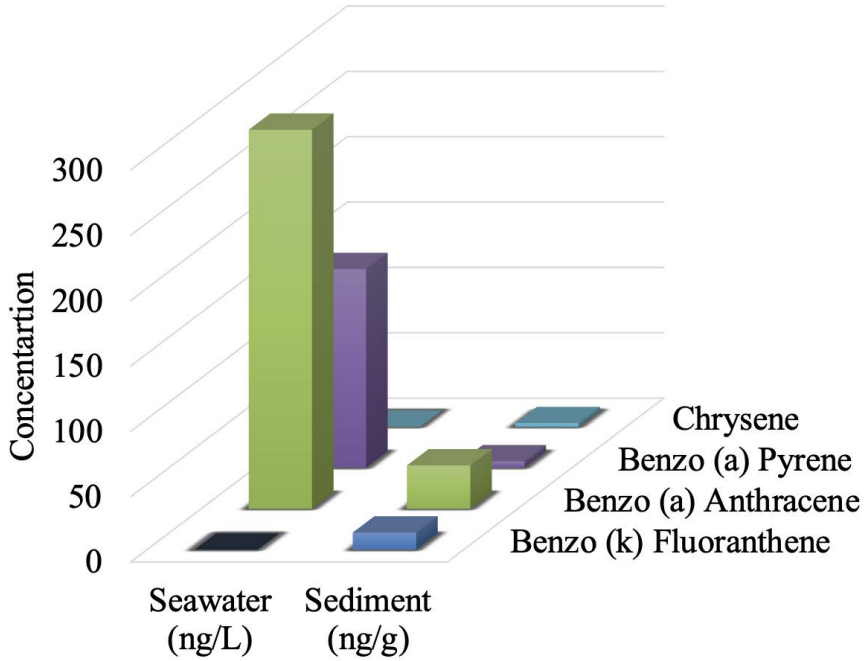

Figure 6. Identification of carcinogenic PAHs in Indramayu Coast, West Java

carcinogenic, such as chrysene, benzo (a) pyrene, benzo (a) anthracene, and benzo (k) fluoranthene (Figure 6). Two carcinogenic PAHs were detected in the seawater samples, whereas four were detected in the sediment samples. The carcinogenic PAHs benzo (a) anthracene had the highest levels in both the seawater and sediment samples. With the presence of four carcinogenic PAHs in this area, it is important to be concerned about the health risks both marine organisms and humans. In particular, the carcinogen BaP can disrupt the reproductive system and trigger the occurrence of cancer cells (Zhao et al., 2021).

CONCLUSSIONS

This study figured out that the low molecular weight PAHs (two to three rings) are the main PAHs profile in seawater, while medium molecular weight (four rings) PAHs are most detected in sediments. As they move towards the open sea, PAH concentrations will generally decrease or undergo degradation, away

from the land or coast. It is assumed that input from anthropogenic and industrial activities on land is a possible source of PAH pollutants in this coastal environment, both from pyrogenic and petrogenic. The ecological risk posed by the levels of PAHs in the sediments was observed to be relatively low. Nevertheless, further investigation is required, as carcinogenic PAHs have been noticed at some field stations along Indramayu coastal. The existence of four carcinogenic PAHs in this vicinity warrants attention towards potential health risks for both marine organisms and humans.

ACKNOWLEDGEMENTS

This research was funded through the IPK LIPI (BRIN) priority program in fiscal year 2017. The authors would like to thank all personnel involved in the field sampling and analysis in the laboratory.

REFERENCES

Abdel-Shafy, H.I., Mansour, M.S.M., 2016. A review on polycyclic aromatic hydrocarbons: Source, environmental impact, effect on human health and remediation. *Egyptian Journal of Petroleum*. 25: 107-123. doi:10.1016/j.ejpe.2015.03.011.

Akyüz, M., Çabuk, H., 2010. Gas-particle partitioning and seasonal variation of polycyclic aromatic hydrocarbons in the atmosphere of Zonguldak, Turkey. *Science of the Total Environ*ment, 408(22): 5550-5558. doi:10.1016/j.scitotenv.2010.07.063.

ANZECC, 2000. *Australian and New Zealand Guidelines for Fresh and Marine Water Quality*. 1(4): 314. ISBN 09578245 0 5.

Baumard, P., Budzinski, H., Michon, Q., Garrigues, P., Burgeot, T., Bellocq, J., 1998. Origin and bioavailability of PAHs in the Mediterranean Sea from mussel and sediment records. *Estuarine, Coastal, and Shelf Science*. 47(1): 77-90. doi:10.1006/ecss.1998.0337.

Blair, T.C., McPherson, J.G., 1999. Grain-size and textural classification of coarse sedimentary particles. *Journal of Sedimentary Research*. 69(1): 6-19. doi:10.2110/jsr.69.6.

Castro-Jiménez, J., Berrojalbiz, N., Wollgast, J., Dachs, J., 2012. Polycyclic aromatic hydrocarbons (PAHs) in the Mediterranean Sea: Atmospheric occurrence, deposition and decoupling with settling fluxes in the water column. *Environmental Pollution Journal*. 166: 40-47. doi:10.1016/j.envpol.2012.03.003.

CCME, 1999. *Canadian Sediment Quality Guidelines for The Protection of Aquatic Life*. Polycylic Aromatic Hydrocabrons (PAHs).

Charles, F., Nozais, C., Pruski, A.M., Bourgeois, S., Méjanelle, L., Vétion, G., Rivière, B., Coston-Guarini, J., 2012. Ecodynamics of PAHs at a peri-urban site of the French Mediterranean Sea. *Environmental Pollution Journal*. 171: 256-264. doi:10.1016/j.envpol.2012.07.034.

Chen, C.F., Ju, Y.R., Su, Y.C., Lim, Y.C., Kao, C.M., Chen, C.W., Dong, C.D., 2020. Distribution, sources, and behavior of PAHs in estuarine water systems exemplified by Salt River, Taiwan. *Marine Pollution Bulletin.* 154. doi:10.1016/j.marpolbul.2020.111029.

Cincinelli, A., Stortini, A.M., Perugini, M., Checchini, L., Lepri, L., 2001. Organic pollutants in sea-surface microlayer and aerosol in the coastal environment of Leghorn - (Tyrrhenian Sea). *Marine Chemistry Journal.* 76(1-2): 77-98. doi:10.1016/S0304-4203(01)00049-4.

De La Torre-Roche, R.J., Lee, W.Y., Campos-Díaz, S.I., 2009. Soil-borne polycyclic aromatic hydrocarbons in El Paso, Texas: Analysis of a potential problem in the United States/ Mexico border region. *Journal of Hazardous Materials.* 163(2-3): 946-958. doi:10.1016/J.JHAZMAT.2008.07.089.

Duan, X., Liu, J., Zhang, D., Yin, P., Li, Y., Li, X., 2015. An assessment of human influences on sources of polycyclic aromatic hydrocarbons in the estuarine and coastal sediments of China. *Marine Pollution Bulletin.* 97(1-2): 309-318. doi:10.1016/j.marpolbul.2015.05.071.

EU-Commission, 2011. Commission Regulation (EU) No. 835/2011 of 19 August 2011. Amending Regulation (EC) No. 1881/2006 as regards maximum levels for polycyclic aromatic hydrocarbons in foodstuffs. *Official Journal of the European Union*. L 215(835): 4-8.

Farrington, J.W., 2020. Need to update human health risk assessment protocols for polycyclic aromatic hydrocarbons in seafood after oil spills. *Marine Pollution Bulletin.*

150: 110744. doi:10.1016/j.marpolbul.2019.110744.

Galarneau, E., 2008. Source specificity and atmospheric processing of airborne PAHs: Implications for source apportionment. *Atmospheric Environment*. 42(35): 8139-8149. doi:10.1016/j.atmosenv.2008.07.025.

Gigliotti, C.L., Brunciak, P.A., Dachs, J., Glenn, T.R., Nelson, E.D., Totten, L.A., Eisenreich, S.J., 2002. Air-water exchange of polycyclic aromatic hydrocarbons in the New York-New Jersey, USA, Harbor Estuary. *Environmental Toxicology and Chemistry*. 21(2): 235-244. doi:10.1002/etc.5620210203.

Glad, M., Bihari, N., Jaksic, Z., Fafandel, M., 2017. Comparison between resident and caged mussels: Polycyclic aromatic hydrocarbon accumulation and biological response. *Marine Environmental Research*. 129: 195-206. doi:10.1016/j.marenvres.2017.06.004.

Gu, Y., Li, H., Lu, H., 2017. Polycyclic aromatic hydrocarbons (PAHs) in surface sediments from the largest deep plateau lake in China : Occurrence, sources and biological risk. Ecological Engineering. 101: 179-184. doi:10.1016/j.ecoleng.2017.02.007.

Guigue, C., Tedetti, M., Ferretto, N., Garcia, N., Méjanelle, L., Goutx, M., 2014. Spatial and seasonal variabilities of dissolved hydrocarbons in surface waters from the Northwestern Mediterranean Sea: Results from one year intensive sampling. *Science of the Total Environment*. 466-467: 650-662. doi:10.1016/j.scitotenv.2013.07.082.

Han, B., Zheng, L., Lin, F., 2019. Risk assessment and source apportionment of PAHs in surface sediments from Caofeidian Long Island, China. *Marine Pollution Bulletin*. 145(May): 42-46. doi:10.1016/j.marpolbul.2019.05.007.

Kang, M., Yang, F., Ren, H., Zhao, W., Zhao, Y., Li, L., Yan, Y., Zhang, Y.J., Lai, S., Zhang, Y.Y., 2017. Influence of continental organic aerosols to the marine atmosphere over the East China Sea: Insights from lipids, PAHs and phthalates. *Science of the Total Environment.* 607-608: 339-350. doi:10.1016/j.scitotenv.2017.06.214.

Katsoyiannis, A., Terzi, E., Cai, Q.Y., 2007. On the use of PAH molecular diagnostic ratios in sewage sludge for the understanding of the PAH sources. Is this use appropriate? *Chemosphere*. 69(8): 1337-1339. doi:10.1016/J.CHEMOSPHERE.2007.05.084.

Ke, C.L., Gu, Y.G., Liu, Q., Li, L.D., Huang, H.H., Cai, N., Sun, Z.W., 2017. Polycyclic aromatic hydrocarbons (PAHs) in wild marine organisms from South China Sea: Occurrence, sources, and human health implications. *Marine Pollution Bulletin.* 117(1-2): 507-511. doi:10.1016/j.marpolbul.2017.02.018.

Khozanah, and Yogaswara, D., 2017. Concentrations of PAHs (Polycyclicaromatic Hydrocarbons) Pollutant in Sediment of The Banten Bay. *Bulletin of the Marine Geology*. 32: 61-66. ejournal.mgi.esdm.go.id/bomg

Khozanah, Yogaswara, D., Wulandari, I., Edward, Hindarti, D., Falahudin, D., 2019. Concentration, spatial distribution, and source apportionment of polycyclic aromatic hydrocarbons (PAHs) in marine surface sediments from Cirebon coastal water, West Java, Indonesia. *AIP Conference Proceeding*. 2175(020066): 1-6. doi:10.1063/1.5134630.

Koropitan, A.F., Ikeda, M., Damar, A., Yamanaka, Y., 2009. Influences of physical processes on the ecosystem of Jakarta Bay : a coupled physical - ecosystem model experiment. *ICES Journal of Marine Science.* 66: 336-348.

Li, J., Dong, H., Zhang, D., Han, B., Zhu, C., Liu, S., Liu, X., Ma, Q., Li, X., 2015. Sources and ecological risk assessment of PAHs in surface sediments from Bohai Sea and northern part of the Yellow Sea, China. *Marine Pollution Bulletin.* 96(1-2): 485-490. doi:10.1016/j.marpolbul.2015.05.002.

Li, J., Li, F., 2017. Polycyclic aromatic hydrocarbons in the Yellow River estuary: Levels, sources and toxic potency assessment. *Marine Pollution Bulletin.* 116(1-2): 479-487. doi:10.1016/j.marpolbul.2016.11.043.

Liu, L., Liu, R., Yu, W., Xu, F., Men, C., Wang, Q., Shen, Z., 2016. Risk assessment and uncertainty analysis of PAHs in the sediments of the Yangtze River. *Marine Pollution Bulletin.* doi:10.1016/j.marpolbul.2016.08.009.

Lohmann, R., Macfarlane, J.K., Gschwend, P.M., 2005. Importance of Black Carbon to

Sorption of Native PAHs , PCBs , and PCDDs in Boston and New York Harbor Sediments. *Environmental Science Tehcnology* 39(1): 141-148.

Macdonald, D.D., Carr, R.S., Calder, F.D., Long, E.R., Ingersoll, C.G., 1996. Development and evaluation of sediment quality guidelines for Florida coastal waters. *Ecotoxicology*. 5: 253-278.

Maliszewska-Kordybach, B., 1996. Polycyclic aromatic hydrocarbons in agricultural soils in Poland: preliminary proposals for criteria to evaluate the level of soil contamination. Appl Geochemistry. 11:1-7.

Mastral, A.M., Callen, M.S., Lopez, J.M., Murillo, R., Garcia, T., Navarro, M.V., 2003. Critical review on atmospheric PAH. Assessment of reported data in the Mediterranean basin. *Fuel Processing Technology.* 80(2): 183-193. doi:10.1016/S0378-3820(02)00249-7.

Mehdinia, A., Aghadadashi, V., Fumani, N.S., 2015. Origin, distribution and toxicological potential of polycyclic aromatic hydrocarbons in surface sediments from the Bushehr coast, The Persian Gulf. *Marine Pollution Bulletin.* 90(1-2): 334-338. doi:10.1016/j.marpolbul.2014.09.021.

Mu, L., Peng, L., Liu, X., Song, C., Bai, H., Zhang, J., Hu, D., He, Q., Li, F., 2014. Characteristics of polycyclic aromatic hydrocarbons and their gas/particle partitioning from fugitive emissions in coke plants. *Atmospheric Environment.* 83: 202-210. doi:10.1016/j.atmosenv.2013.09.043.

Neşer, G., Kontas, A., Ünsalan, D., Altay, O., Darilmaz, E., Uluturhan, E., Küçüksezgin, F., Tekoğul, N., Yercan, F., 2012. Polycyclic aromatic and aliphatic hydrocarbons pollution at the coast of Aliaĝa (Turkey) ship recycling zone. *Marine Pollution Bulletin.* 64(5): 1055-1059. doi:10.1016/j.marpolbul.2012.02.019.

Paryono, Damar, A., Susilo, S.B., Dahuri, R., Suseno, H., 2017. Sedimentasi Delta Sungai Citarum, Kecamatan Muara Gembong, Kabupaten Bekasi. *Jurnal Penelitian Pengelolaan Daerah Aliran Sungai.* 1(1): 49-59.

Portet-Koltalo, F., Ammami, M.T., Benamar, A., Wang, H., Le Derf, F., Duclairoir-Poc, C., 2013. Investigation of the release of PAHs from artificially contaminated sediments using cyclolipopeptidic biosurfactants. *Journal of Hazardous Materials.* 261: 593-601. doi:10.1016/j.jhazmat.2013.07.062.

Ravindra, K., Sokhi, R., Van Grieken, R., 2008. Atmospheric polycyclic aromatic hydrocarbons: Source attribution, emission factors and regulation. *Atmospheric Environment.* 42(13): 2895-2921. doi:10.1016/J.ATMOSENV.2007.12.010.

Sholeh, M., Pranoto, P., Budiastuti, S., Sutarno, S., 2018. Analysis of Citarum River pollution indicator using chemical, physical, and bacteriological methods. *AIP Conference Proceeding.* 2049. doi:10.1063/1.5082473.

Sinurat, M.E.B., Ismanto, A., Hariyadi, H., 2016. Analisis Pola Sebaran Tumpahan Minyak Mentah (Crude Oil) dengan Pendekatan Model Hidrodinamika dan Spill Analysis di Perairan Balongan, Indramayu, Jawa Barat. *Jurnal Oseanografi.* 5(2): 218-226. http://ejournal-s1.undip.ac.id/index.php/jose%0AANALISIS.

Sodikin, S., 2011. Karakteristik Dan Pemanfaatan Sumberdaya Pesisir Dan Laut Di Kawasan Pantai Kabupaten Indramayu. *Jurnal Geografi Gea*. 11(2): 200-208. doi:10.17509/gea.v11i2.1630.

Timoney, K.P., Lee, P., 2011. Polycyclic aromatic hydrocarbons increase in athabasca river delta sediment: Temporal trends and environmental correlates. *Environmental Science and Technology.* 45(10): 4278-4284. doi:10.1021/es104375d.

Tobiszewski, M., Namieśnik, J., 2012. PAH diagnostic ratios for the identification of pollution emission sources. *Environmental Pollution.* 162: 110-119. doi:10.1016/j.envpol.2011.10.025.

Tong, Y., Chen, L., Liu, Y., Wang, Y., Tian, S., 2019. Distribution, sources and ecological risk assessment of PAHs in surface seawater from coastal Bohai Bay, China. *Marine Pollution Bulletin.* 142: 520-524. doi:10.1016/j.marpolbul.2019.04.004.

Tornero, V., Hanke, G., 2016. Chemical contaminants entering the marine environment from sea-based sources: A review with a focus on European seas. *Marine*

Pollution Bulletin. 112(1-2): 17-38. doi:10.1016/j.marpolbul.2016.06.091.

UNEP, 2001. Final Act of the Plenipotentiaries on the Stockholm Convention on Persistent Organic Pollutants. *United Nation environment Program Chemical, Geneva, Switzertland.* Geneva.

Veerasingam, S., Saha, M., Suneel, V., Vethamony, P., Rodrigues, A.C., Bhattacharyya, S., Naik, B.G., 2016. Characteristics, seasonal distribution and surface degradation features of microplastic pellets along the Goa coast, India. *Chemosphere*. 159: 496-505. doi:10.1016/j.chemosphere.2016.06.056.

Wang, C., Zou, X., Li, Y., Zhao, Y., Song, Q., Yu, W., 2017. Pollution levels and risks of polycyclic aromatic hydrocarbons in surface sediments from two typical estuaries in China. *Marine Pollution Bulletin.* 114(2): 917-925. doi:10.1016/j.marpolbul.2016.11.027.

Wentworth, C.K., 1922. A Scale of Grade and Class Terms for Clastic Sediments. *The Journal of Geology*. 30(5): 377-392.

Widhiarno, F., Muliati, Y., 2016. Peramalan Gelombang di Perairan Kabupaten Indramayu dengan Pemodelan Numerik SWAN 41.01A. *RekaRacana: Jurnal Online Teknik Sipil Institut Teknologi Nasional*. 2(4): 160-171.

Wulandari, I., Yogaswara, D., Khozanah, Edward, Rositasari, R., Falahudin, D., 2019. Pengukuran Total Petroleum Hidrokarbon (TPH) Melalui Pendekatan Kadar Minyak-Lemak dalam Sedimen di Perairan Delta Cimanuk, Jawa Barat. *Oseanologi dan Limnologi di Indonesia*. 4(2): 123. doi:10.14203/oldi.2019.v4i2.272.

Yamaguchi, C., Lee, W., 2010. A cost effective, sensitive, and environmentally friendly sample preparation method for determination of polycyclic aromatic hydrocarbons in solid samples. *Journal of Chromatography A*. 1217(44): 6816-6823. doi:10.1016/j.chroma.2010.08.055.

Yang, W., Zhang, H., Lang, Y., Li, Z., 2020. Pollution status of PAHs in surface sediments from different marginal seas along China Mainland: A quantitative evaluation on a national scale. *Environmental Pollution*. 263: 114431. doi:10.1016/j.envpol.2020.114431.

Yogaswara, D., Prartono T., Satya, A., 2020. Distribusi Spasial dan Analisis Risiko Ekologi Senyawa Polisiklik Aromatik Hidrokarbon (PAH) di Perairan Cilincing - Teluk Jakarta. *Oseanologi dan Limnologi di Indonesia.* 5(3): 209. doi:10.14203/oldi.2020.v5i3.325.

Yogaswara, D., Prartono, T., Satya, A., 2021. Occurrence and Source Apportionment of Polycyclic Aromatic Hydrocarbons (PAHs) in Green Mussel (Perna viridis) from Cilincing Waters of Jakarta Bay, Indonesia. *Squalen Bulletin of Marine and Fisheries Postharvest and Biotechnology*. 16(1): 29-40. doi:10.15578/squalen.484.

Yunker, M.B., Ikonomou, M.G., Sather, P.J., Friesen, E.N., Higgs, D.A., Dubetz, C., 2011. Development and validation of protcols to differentiate PCB patterns between farmed and wild salmon. *Environmental Science and Technology*. 45(6): 2107-2115. doi:10.1021/es1038529.

Yunker, M.B., MacDonald, R.W., Vingarzan, R., Mitchell, H., Goyette, D., Sylvestre, S., 2002. PAHs in the Fraser River basin: a critical appraisal of PAH ratios as indicators of PAH source and composition. *Organic Geochemistry.* 33: 489-515.

Zhao, Y., Li, J., Qi, Y., Guan, X., Zhao, C., Wang, H., Zhu, S., Fu, G., Zhu, J., He, J., 2021. Distribution, sources, and ecological risk assessment of polycyclic aromatic hydrocarbons (PAHs) in the tidal creek water of coastal tidal flats in the Yellow River Delta, China. *Marine Pollution Bulletin.* 173(PB): 113110. doi:10.1016/j.marpolbul.2021.113110.

SEASONAL AND INTRA-SEASONAL VARIABILITY OF OCEAN THERMAL POTENTIAL ENERGY IN THE INDONESIAN EXCLUSIVE ECONOMIC ZONE

VARIABILITAS MUSIMAN DAN INTRA-MUSIMAN DARI ENERGI POTENSIAL PANAS LAUT DI ZONA EKONOMI EKSLUSIF INDONESIA

Totok Suprijo[1,2*], Gandhi Napitupulu[2], Nining Sari Ningsih[2], Denny Basardo Jonatan Sinaga[1], Audi Rachman[1]

[1] Coastal Oceanography Laboratory, Faculty of Earth Sciences and Technology, Bandung Institute of Technology, Bandung, Indonesia
[2] Research Group of Oceanography, Faculty of Earth Sciences and Technology, Bandung Institute of Technology, Bandung, Indonesia

*Corresponding author: totok.suprijo@itb.ac.id

(Received 20 January 2024; in revised from 30 January 2024; accepted 22 May 2024)

DOI : 10.32693/bomg.39.1.2024.866

ABSTRACT: Ocean thermal energy is a promising marine renewable energy resource that can be developed as a clean energy alternative for Indonesia, which is in the equatorial or tropical region. This study assesses the potential of ocean thermal energy as a renewable energy source in the Indonesian Exclusive Economic Zone (EEZ) by estimating the monthly, seasonal, and intra-seasonal variability of ocean thermal energy conversion (OTEC) resources. The Indonesian EEZ spans from 6°N to 11°S and 95°E to 139°E, covering an area of 3,495,698.72 km². Using temperature data from simulations of the Hybrid Coordinate Ocean Model (HYCOM), the study evaluates the potential of OTEC resources over a 50-year period (from January 1964 to December 2013) with a spatial resolution of 0.125°. Estimation of OTEC potential power resources was based on temperature differences at depths of 20 m and 1000 m, following the hybrid cycle working principle.The results of the estimations indicate that the area has a monthly average potential power of 289.73 GW. The estimation also reveals seasonal and intra-seasonal variability in this potential energy, with fluctuations ranging from 280.09 GW in August to 295.65 GW in December, influenced by phenomena such as ENSO (El Niño Southern Oscillation) and IOD (Indian Ocean Dipole). In the Indonesian EEZ, the average potential thermal power decreases to 288.23 GW during an El Niño event and increases to 291.72 GW during a La Niña event. The IOD phenomenon has a similar effect, with potential decreasing to 281.82 GW during a positive IOD event and rising to 292.64 GW during a negative IOD event.

Keywords: Indonesian Exclusive Economic Zone (EEZ), intra-seasonal variability, seasonal variability, ocean thermal energy conversion (OTEC)

ABSTRAK: *Energi panas laut adalah sumber daya energi terbarukan yang menjanjikan dan dapat dikembangkan sebagai alternatif energi bersih bagi Indonesia, yang berada di daerah khatulistiwa atau tropis. Kajian ini mengevaluasi potensi energi panas laut sebagai sumber energi terbarukan di Zona Ekonomi Eksklusif (ZEE) Indonesia dengan memperhitungkan variabilitas bulanan, musiman, dan intra-musiman dari konversi sumber daya energi panas laut (OTEC). ZEE Indonesia meliputi wilayah dari 6°Lintang Utara hingga 11°Lintang Selatan dan dari 95°Bujur Timur hingga 139°Bujur Timur, dengan luas mencapai 3.495.698,72 km². Dengan menggunakan data suhu dari simulasi Model Oseanografi Koordinat Hibrida (HYCOM), kajian ini mengevaluasi potensi sumber daya OTEC selama periode 50 tahun (Januari 1964 hingga*

Desember 2013) dengan resolusi spasial 0,125°. Estimasi sumber daya potensial energi OTEC didasarkan pada perbedaan suhu di kedalaman 20 m dan 1000 m, mengikuti prinsip kerja siklus hibrida. Hasil estimasi menunjukkan bahwa wilayah ZEE-Indonesia memiliki potensi daya rata-rata bulanan sebesar 289,73 GW. Hasil estimasi juga mengungkapkan adanya variabilitas musiman dan intra-musiman dari sumberdaya energi panas laut yang berfluktuasi dengan berkisaran dari 280,09 GW pada bulan Agustus dan 295,65 GW pada bulan Desember, serta dipengaruhi oleh fenomena seperti ENSO (El Niño Southern Oscillation) dan IOD (Indian Ocean Dipole). Di ZEE Indonesia, potensi rata-rata sumber daya panas laut mengalami penurunan menjadi 288,23 GW saat terjadi El Niño dan meningkat menjadi 291,72 GW pada peristiwa La Niña. Fenomena IOD memiliki efek serupa, potensi sumberdaya menurun menjadi 281,82 GW saat peristiwa IOD positif dan meningkat menjadi 292,64 GW ketika IOD negatif.

Kata Kunci: *Zona Ekonomi Eksklusif (ZEE) Indonesia, variabilitas intra-musiman, variabilitas musiman, konversi energi termal lautan (OTEC)*

INTRODUCTION

Ocean energy offers long-term carbon emission reduction potential. However, it is unlikely to make a significant contribution in the short term before 2020, as it is still in a nascent stage of development. All ocean energy technologies, except for tidal dams, are still conceptual, undergoing research and development, or are in the prototype and pre-commercial demonstration stages (Von Jouanne & Brekken, 2017). The performance of ocean energy technologies is expected to gradually improve as experience is gained and new technologies can access low-quality resources (Chu et al., 2020). Whether these technical advances will result in sufficient cost reductions to enable widespread deployment of ocean energy is a critical uncertainty in assessing the future role of ocean energy in climate change mitigation (Topper et al., 2019). While technical potential is not expected to be a major global barrier to ocean energy deployment, resource characteristics will require that local communities in the future choose among several available ocean technologies to suit local resource conditions (Rudolph et al., 2020).

Indonesia also has abundant resources for solar, wind, and ocean energy development. The country is located along the equator and covers a total tropical ocean area of approximately 7.9 million square kilometers, including the exclusive economic zone (Lubchenco & Haugan, 2023). Tropical seas naturally collect solar energy and absorb billions of watts of energy from the sun in the form of solar radiation every day (Merchant et al., 2019). Intense solar illumination and longer days result in significant warming of the upper 10 to 150 m of the ocean, resulting in warm ocean surface waters (27-29 °C) (Serban et al., 2021). This temperature difference represents a significant amount of potential energy, which would be a completely renewable energy source (Clemente et al., 2021). In addition to power generation using a method known as ocean thermal energy conversion (OTEC), this potential energy could be extracted to support heating, cooling, and transportation applications (Aresti et al., 2023).

For an OTEC factory to be economical, a temperature difference of about 20 °C is required. A temperature difference of this magnitude is available between surface water and water at a depth of 1000 m at most locations within 20° of the equators (Herrera et al., 2021; Langer et al., 2020). The electrical resources that can be extracted using OTEC plants from the world's oceans were estimated by a simple time-domain model of the one-dimensional ocean thermal structure (Bernal et al., 2022; Nihous, 2007). The published steady-state results were further extended by dividing the potential OTEC production region into one-degree "squares" and by allowing operational adjustment of OTEC operations. In that study, the 'OTEC production region' was based on the annual average temperature difference between 20 and 1000 m of water depth (Nihous, 2007). The study increased the estimated steady-state maximum OTEC electrical power from about 3 TW to 5 TW (Nihous, 2018). Recent results from the study, which assessed the OTEC rate with a high-resolution (0.125°×0.1251°) ocean general circulation model, indicated a global OTEC net maximum of about 12-14 TW (Rajagopalan & Nihous, 2013). Based on the vertical temperature difference criterion, a synthesis of relevant information to assess the feasibility of OTEC development in Indonesian waters was initiated (Bhuiyan et al., 2022). Utilizing temperature vertical profiles, a similar study to identify potential sites for OTEC development in Indonesian waters was conducted (Nihous, 2018). Although both previous studies have described potential locations

for OTEC development, they did not estimate the number of electrical resources in the Indonesian waters.

This research aims to analyze the potential of ocean heat energy contained in the EEZ of Indonesian waters. Furthermore, knowing the seasonal and intra-seasonal variability of the potential for ocean thermal energy in the Indonesian EEZ based on simulation data from 1964 to 2013. The influence of intra-seasonal variability consists of the El Nino Southern Oscillation (ENSO) and the Indian Ocean Dipole (IOD).

METHODS AND MATERIALS

Data

The study area of this research is the Indonesian waters, with coordinates of 6°N - 11°S and 95°E - 139°E (Figure 1a). The data used in this study are temperature data from the 3-dimensional hydrodynamic model Hybrid Coordinate Ocean Model (HYCOM). This data comes from research conducted by Rachmayani et al. (2023). The temperature data used is the monthly temperature at two depths, namely 20 m and 1000 m, in the period of January 1964 to December 2013 (50 years). This data has a spatial resolution of 0.125°×0.125°, resulting in a grid size of 353 × 137.

Sea surface temperature data (20 m) from buoy measurements were used to validate the surface temperature data (20 m) from the model. Buoy data were obtained from the Triangle Trans-Ocean Buoy Network (TRITON) measurement station in the Pacific Ocean and the Research Moored Array for African-Asian-Australian Monsoon Analysis and Prediction (RAMA) in the Indian Ocean, obtained from the National Oceanic and Atmospheric Administration (NOAA). Details of the validation of field data and model data are shown in Table 1, with the location of the stations shown in Figure 1a. Validation of model data with observation data has a bias value of 0.09 to 0.62 °C, indicating that the model temperature data is quite close to the field measurement data.

The average ocean temperatures at 20 m (Figure 1b) and 1000 m (Figure 1c) depths during 1964-2013 were 29.30 °C and 4.3 °C, respectively. The amount of variation in the temperature of Indonesian waters at a depth of 20 m can be shown through the standard deviation value. The standard deviation of Indonesian water temperature at a depth of 20 m ranges from 0.30 °C to 1.88 °C. The standard deviation of Indonesian water temperature at 1000 m depth ranges from 0.02 °C to 0.51 °C. This shows the

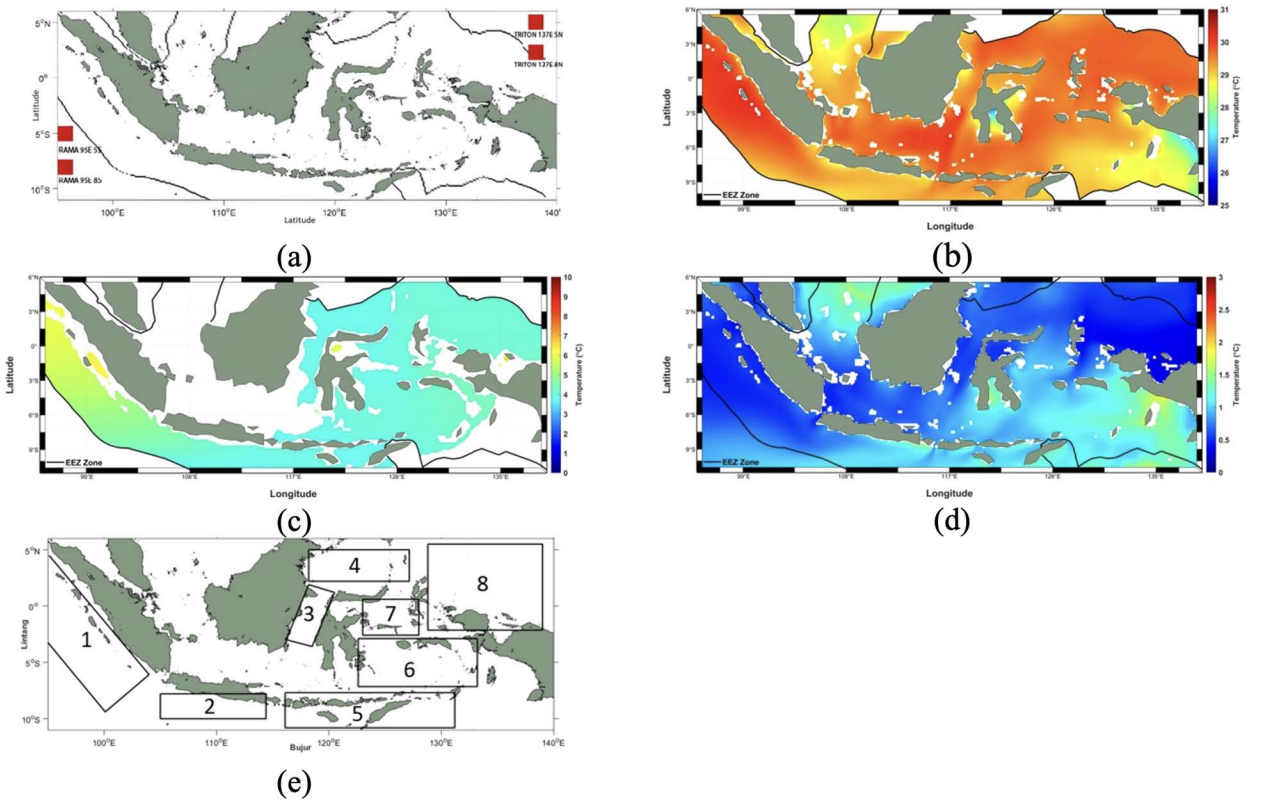

Figure 1. (a) Location points of measurement data of TRITON and RAMA stations. Average depth temperature of (b) 20 m and (c) 1000 m during 1964-2013. (d) The standard deviation of Indonesian water temperature at 20 m depth. (e) Division of the study area into eight observation areas.

stability of Indonesian water temperature at a depth of 1000 m. The small standard deviation indicates that the temperature in these waters tends to be stable.

In this study, the study area was divided into eight regions, as shown in Figure 1e, with details in Table 2. The division of the study area was conducted to determine how much influence the regional phenomenon has on each study area.

Data on the Oceanic Niño Index (ONI) and Dipole Mode Index (DMI) are utilized to examine variations in ocean temperature and power potential about the ENSO and IOD phenomena. ONI data was acquired from NOAA's Climate Prediction Center, while DMI data was obtained from NOAA's Physical Science Laboratory.

Table 1. Validation of model data with field measurement data.

Coordinate Point	Period	Bias (℃)	*RMSE* (℃)
2° N; 137° E	May 1992 – May 2013	0.44	0.42
5° N;137° E	May 1993 – August 2007	0.62	0.54
5° S; 95° E	November 2001 – October 2012	0.37	0.49
8° S; 95° E	November 2009 – December 2013	0.09	0.51

Table 2. Details of the division of the study area

Region	Longitude	Latitude
Region 1 (Indian Ocean)	95° E; 104° E	9.4° S; 4.5° N
Region 2 (South of Java)	105° E; 114.4° E	10° S; 7.8° S
Region 3 (Makassar Strait)	116.2° E; 120.5° E	3.6° S; 1.9° N
Region 4 (Sulawesi Sea)	118.2° E; 127.25° E	2.2° N; 5.5° N
Region 5 (Sawu Sea and Arafura Sea)	116.1° E; 131.2° E	10.8° S; 7.7° S
Region 6 (Banda Sea and Seram Sea)	122.6° E; 133.2° E	7.16° S; 2.9° S
Region 7 (Maluku Sea)	123° E; 128° E	2.6° S; 0.6° S
Region 8 (Pacific Ocean)	128.8° E; 139° E	2.5° S; 5.5° N

Method

OTEC is an old idea that solar energy is stored as heat in the mixed layer (surface) of tropical oceans (Nihous, 2005). The heat in the ocean can be utilized for electrical energy through OTEC. The working principle of OTEC is based on the thermodynamic cycle, the Rankine cycle, which can convert heat into work. Based on the way of working, OTEC can be divided into three types, namely Open Cycle, Closed Cycle, and Hybrid Cycle (Aresti et al., 2023).

The working principle of the Open Cycle is to use warm water at sea level to drive the turbine. A mass of warm water is pumped into a low-pressure container, causing the water to boil. The water vapor will drive the turbine to generate electricity. The vapor will be re-condensed using a mass of cold water from the depths (Herrera et al., 2021). The working principle of the Closed Cycle is to utilize the temperature difference between warm water and cold water used as working fluid (ammonia is generally used) to complete the Rankine cycle (Zhang et al., 2021). The warm water mass is used to vaporize the working fluid, and then the working fluid vapor will pass through the generator to generate electricity. The cold-water mass is used to make the working fluid liquid again so that it can be used to repeat the cycle. The working principle of the Hybrid Cycle is to use the advantages of the Open Cycle and Closed Cycle. A mass of warm seawater is put into a low-pressure container so that the water will boil. The water vapor is used to vaporize the low-pressure fluid that will drive the turbine to generate electricity (Wang et al., 2022). The water vapor will be re-condensed using a mass of cold water (Masutani & Takahashi, 2001).

OTEC power potential is obtained by calculating the temperature difference (ΔT) between 20 m and 1000 m depth using the working principle of the Hybrid Cycle (equation 1). Based on Nihous (2007), OTEC can be operated if ΔT has a value of more than 20 °C. The value of each parameter for the OTEC calculation is shown in Table 3.

$$P_{net} = \frac{Q_{cw}\rho c_p \epsilon_{tg}}{8T}\left\{\frac{3\gamma}{2(1+\gamma)}\Delta T^2 - 0.18\Delta T^2 - 0.12\left(\frac{\gamma}{2}\right)^{2.75}\Delta T^2\right\} \quad (1)$$

The total power potential is obtained by summing up all the power from each existing data grid with Equation 2.

$$\sum_{m=0}^{353}\sum_{n=0}^{137} P_{(m,n)} \quad (2)$$

where m is the grid longitude, n is the grid latitude, and P is the power potential value at the grid latitude and longitude.

Model data validation was performed to ensure that the data was fit for research. Validation is done

Table 3. Parameter values for OTEC calculation

Parameter	Value	Unit	Meaning of symbol
Q_{cw}	2.43	m^3/s	Cold water discharge
ρ	1025	kg/m^3	Density of seawater
c_p	4000	J/kg°C	Specific heat of seawater
ε_{tg}	0.85	-	Turbogenerator efficiency
γ	2	-	Comparison of Q_{cw} with Q_{ww}
ΔT	$\Delta T(x,y)$	°C	Difference between T_{20} and T_{1000}
T	$T(x,y)$	°C	20 m depth temperature

by comparing model data with observation data through bias and *RMSE* calculations with the formulation by Thomson and Emery (2014) as follows:

$$bias = \frac{1}{n}\sum_{i=1}^{n}(T_m - T_0) \quad (3)$$

$$RMSE = \sqrt{\frac{1}{n}\sum_{i=1}^{n}(T_m - T_0)^2} \quad (4)$$

where T_m is the modeled temperature (°C), T_0 is the observed temperature (°C), n is the amount of data.

RESULTS AND DISCUSSION

Seasonal Variations in Indonesian Waters Temperatures

The average temperature value for each month can be seen in Table 4. The highest average temperature was in April at 29.72 °C and the lowest was in August at 28.61 °C. This is influenced by the apparent movement of the sun. In April, the sun is just above the equator moving north, so the average sea surface temperature is high. Meanwhile, in August, just above the equator, the sun is moving south, towards the equator. This causes the average value of surface temperature in Indonesian waters to be low.

The average ocean temperature at 20 m depth in Indonesian waters varies seasonally, as shown in Figure 2. The average ocean temperature at 20 m depth in the west monsoon season is 29.40 °C, in the first transition season 29.62 °C, in the east monsoon season 28.92 °C, and in the second transition season 29.26 °C.

In the west monsoon season (Figure 2a), the temperature of the waters in the northern part of Indonesia at a depth of 20 m is lower than in the southern part of Indonesia. This is due to the position of the sun south of the equator, so the temperature of the waters in southern Indonesia is higher. In the transitional season (Figure 2b), the average value of surface temperature is also high because the position of the sun is just above the equator. Whereas in the east monsoon season (Figure 2c), the position of the sun is north of the equator, so the temperature of the waters of northern Indonesia is higher. In addition, during the east monsoon season, there is cooling in the upwelling zone south of Java and the Arafura Sea, where the water mass moves to the Java Sea and the Karimata Strait, so to compensate for this, there is an increase in cold water mass from depth (Qu et al., 2015).

The average ocean temperature at 1000 m depth in the west monsoon season is 4.30 °C (Figure 2e), in the first transition season 4.34 °C (Figure 2f), in the east monsoon season 4.27 °C (Figure 2g), and in the second transition season 4.31 °C (Figure 2h). The temperature at a depth of 1000 m does not have a significant difference every season because the influence of the sun is not significant to the change in temperature at a depth of 1000 m. The variation of temperature at a depth of 1000 concerning season and year is <0.5 °C, so the depth of 1000 is used as a reference depth for calculating OTEC values.

Table 4. Average Temperature Values at 20 m Depth in the Indonesian Sea

Month	Temperature (°C)		Month	Temperature (°C)	
	20 m	1000 m		20 m	1000 m
January	29.31	4.29	July	28.83	4.29
February	29.25	4.32	August	28.61	4.32
March	29.47	4.35	September	28.82	4.35
April	29.72	4.35	October	29.31	4.35
May	29.68	4.33	November	29.65	4.33
June	29.30	4.29	December	29.65	4.29

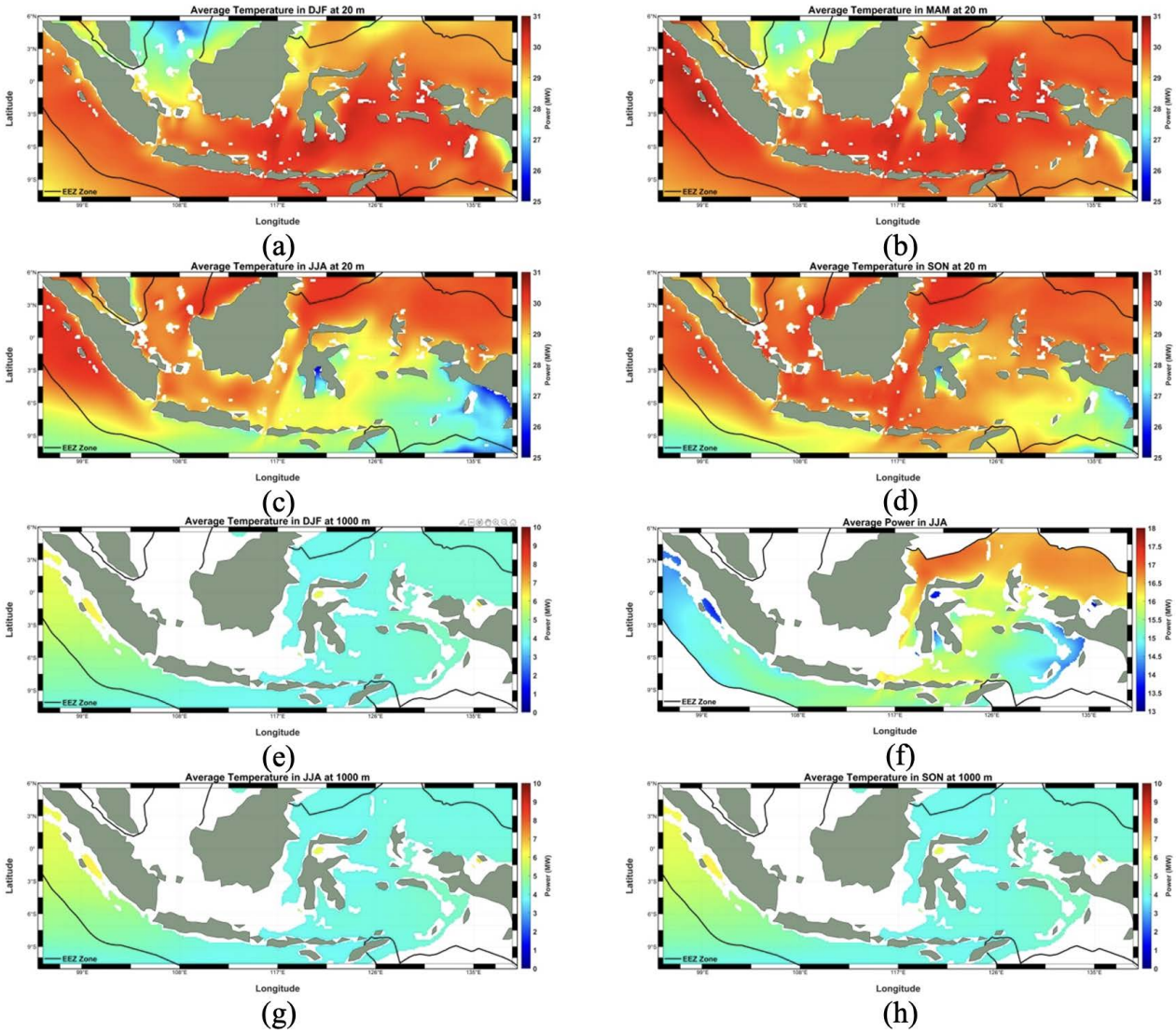

Figure 2. Average 20 m depth temperature in Seasons (a) West, (b) Transition 1, (c) East, and (d) Transition 2. Average 1000 m depth temperature in Seasons (e) West, (f) Transition 1, (g) East, and (h) Transition 2.

Influence of Intraseasonal Variations on Indonesian Sea Surface Temperature

The dominant intraseasonal phenomena that influence surface temperature in Indonesian waters, namely ENSO and IOD. The ENSO phenomenon in the Pacific Ocean and the IOD in the Indian Ocean affect variations in Indonesia's sea surface temperature. Based on historical records of the ENSO phenomenon, it is known that there were 17 times El Nino and 15 times La Nina in the period 1964-2013. Table 5 suggests a potential link between ENSO and Indonesian sea surface temperatures. While the temperature differences between El Niño (Figure 3b) and normal conditions (Figure 3a) appear minimal and La Niña (Figure 3c) conditions show a slight increase compared to normal, further analysis is required to determine the statistical significance of these variations. This is because when El Nino occurs, warm water masses in the Pacific Ocean move eastward or away from Indonesian waters so that the surface temperature of Indonesian waters decreases. Meanwhile, when La Nina occurs, warm water masses are pushed westward or enter Indonesian waters, so that the surface temperature of Indonesian waters increases.

Based on historical records of the IOD phenomenon, it is known that there were 7 times positive IOD and 7 times negative IOD in the period 1964-2013. When a positive IOD (Figure 3f) occurs, the surface temperature of Indonesian waters will be lower than when no IOD phenomenon occurs (Figure 3d). This is because when positive IOD (Figure 3f) occurs, the warm water mass in the Indian Ocean is in the western part of western African waters. Meanwhile, when a negative IOD occurs (Figure 3e), the warm water mass in the Indian Ocean is in the eastern or

western part of Indonesia. This causes the surface temperature of Indonesian waters to increase.

When the El Nino phenomenon occurs, it causes a decrease in average temperature at all peaks of the El Nino phenomenon except in October 1969 and July 1987. The largest decrease in average temperature occurred in October 1965, with an ONI of 2. The temperature decrease varied from -0.08 to -1.43 °C. The largest decrease in average temperature occurred in the Maluku Sea at -1.43 °C. The El Nino phenomenon also causes an increase in temperature in the Indian Ocean area and south of Java at certain times, which is due to an increase in average temperature in the Malacca Strait and Java Sea. The El-Nino phenomenon also caused an increase in average temperature in the Arafura Sea, Banda Sea, and Seram Sea in October 1969, November 1976, December 1979, and July 1987. The average temperature increase varied from 0.05 to 0.68 °C. The largest average temperature increase occurred in the Indian Ocean by 0.68 °C.

When the La-Nina phenomenon occurs, it causes an increase in average temperature at all peaks of the La-Nina phenomenon except in December 1984 and December 1995. The largest increase in average temperature occurred in January 1999, with an ONI of -1.7. The influence of the La-Nina phenomenon on changes in average temperature in western Indonesian waters such as the Indian Ocean and southern Java is not as strong as the El Nino phenomenon. This is shown by the increase and decrease in temperature caused by the La Nina phenomenon in the Indian Ocean and southern Java, which has the same amount at all peak events. The temperature increase that occurred varied in each study area by 0.06 to 0.92 °C. The largest temperature increase occurred in the Maluku Sea by 0.92 °C.

Table 5. Average Indonesian sea temperature at 20 m depth during IOD and ENSO phenomena

Condition	Average Temperature (°C)	Condition	Average Temperature (°C)
Absence of ENSO	29.29	Absence of IOD	29.33
El Nino	29.22	IOD (+)	28.81
La Nina	29.39	IOD (-)	29.31

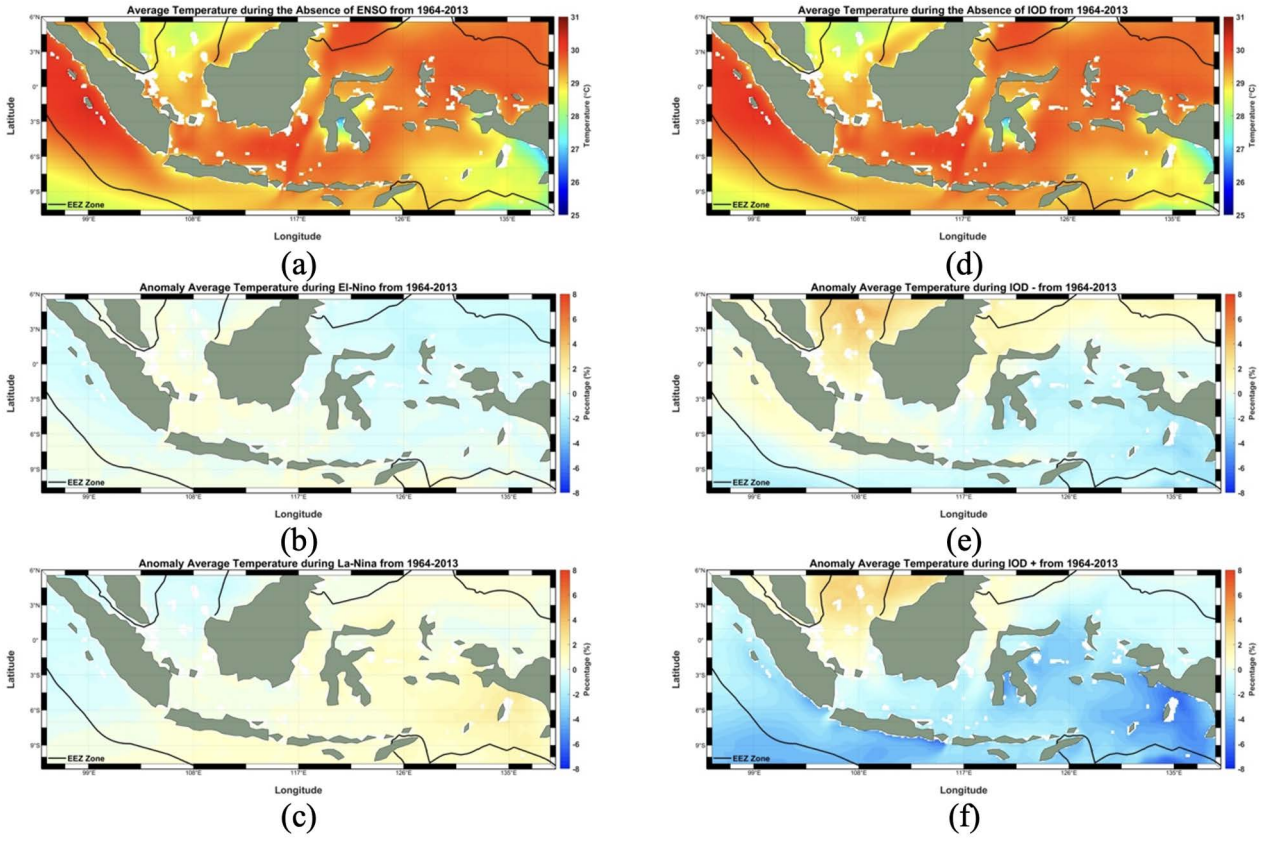

Figure 3. Average 20 m depth temperature during (a) absence of ENSO, (b) El Nino, (c) La Nina, (d) absence of IOD, (e) IOD (-), and (f) IOD (+) from 1964 to 2013.

In addition to the ENSO phenomenon that occurs in the Pacific Ocean, temperature variations in Indonesian waters are also influenced by the IOD phenomenon in the Indian Ocean. During the Positive IOD, the largest decrease in average temperature occurred in the southern region of Java by -1.40 °C. When the Negative IOD phenomenon occurs, it also causes a decrease in temperature, except in the Indian Ocean, Makassar Strait, and Sulawesi Sea. The largest average temperature decrease occurred in the Banda Sea and Seram Sea by -0.66 °C.

When the Positive IOD phenomenon occurs, it causes a decrease in average temperature at all peaks. The largest decrease in average temperature occurred in August 1994, with a DMI of 0.923. The temperature decrease varied from -0.24 to -1.03 °C in each study area. The largest temperature decrease occurred in southern Java at -1.03 °C. However, the Positive IOD phenomenon also caused an increase in average temperature in the Indian Ocean area in July 1983, in the Makassar Strait area in October 2012, in the Sulawesi Sea area in October 2012, and in the Pacific Ocean area in October 2012. The largest temperature increase occurred in the Makassar Strait area by 0.41 °C.

When the Negative IOD phenomenon occurs, it causes an increase in average temperature at all peaks except in September 1992. The largest average temperature increase occurred in October 1996, with a DMI of -0.949. The average temperature increase varied from 0.07 to 0.46 °C. The largest temperature increase occurred in southern Java by 0.46 °C. The Negative IOD phenomenon in September 1992 caused a decrease in average temperature in all study areas except the Indian Ocean and southern Java. The largest decrease in average temperature occurred in the Maluku Sea area by -0.32 °C.

Seasonal Influence on OTEC Potential in EEZ Indonesia

The OTEC power potential is calculated based on the temperature difference between warm surface water (typically at a depth of 20 m) and deep, cold water (usually around 1000 m). While Masutani and Takahashi (2001) suggest a minimum temperature difference of 20°C for OTEC operation, this significant temperature differential is only found in deep sea areas of the Indonesian waters. Indonesia's EEZ area of 3,485,698.72 km² stores potential OTEC resources as shown in Figure 4. The ΔT value in Indonesian waters varies between 22.84°C and 26.77°C. The variation of ΔT is dominantly influenced by the variation of 20 m depth temperature because the variation of 1000 m depth temperature is almost nonexistent.

Indonesia's potential for OTEC varies across regions, with the northern and eastern parts generally favored due to cooler deep waters and a larger temperature gradient compared to the western regions. This gradient, driven by the average temperature difference at a depth of 1000 m, is crucial for OTEC power generation. Based on average power density potential, the regions with the highest OTEC potential are Region 4 (Sulawesi Sea), Region 6 (Banda Sea and Seram Sea), Region 2 (South Java), Region 7 (Maluku Sea), Region 8 (Pacific Ocean), Region 1 (Indian Ocean), Region 5 (Sawu Sea and Arafura Sea), and Region 3 (Makassar Strait). While Figure 4 suggests a higher average total power for Region 1, further investigation into factors beyond temperature difference, such as water flow patterns and current speeds, is needed for a more comprehensive assessment.

The monthly power potential experiences variations due to the monthly ΔT variations. The highest average monthly power potential is in December, reaching 295.65 GW, as shown in Figure 4a. In December, the sun is positioned south of the equator, causing the surface temperature in southern Indonesia to increase. This leads to an increase in the average ΔT and the overall potential for average power. Meanwhile, the lowest average monthly power potential is in August, at 280.09 GW (Figure 4b). This is because the sun, during August, moves northward towards the equator in Indonesia, resulting in a decrease in the overall surface temperature and average ΔT of Indonesian waters.

Seasonal variation is also observed in the ocean's thermal energy potential. The highest average seasonal power potential is during the transitional season I (MAM), at 293.91 GW, as depicted in Figure 4d. Meanwhile, the lowest average seasonal power potential is during the east monsoon season (JJA), shown in Figure 4e, at 284.18 GW. This corresponds to the seasonal variation in the temperature at a depth of 20 m. During the transitional season I, the sun is directly above Indonesia, causing an increase in sea surface temperature and, consequently, an increase in power potential. In contrast, during the east monsoon season, the sun is north of the equator, leading to a decrease in the sea surface temperature in Indonesia and a reduction in the average power potential.

The average power density in each study area is illustrated in Figure 4e. The order of regions with the

highest to lowest average power density potential is Region 4 (Sulawesi Sea), Region 6 (Banda Sea and Seram Sea), Region 2 (South Java), Region 7 (Maluku Sea), Region 8 (Pacific Ocean), Region 1 (Indian Ocean), Region 5 (Sawu Sea and Arafura Sea), and Region 3 (Makassar Strait).

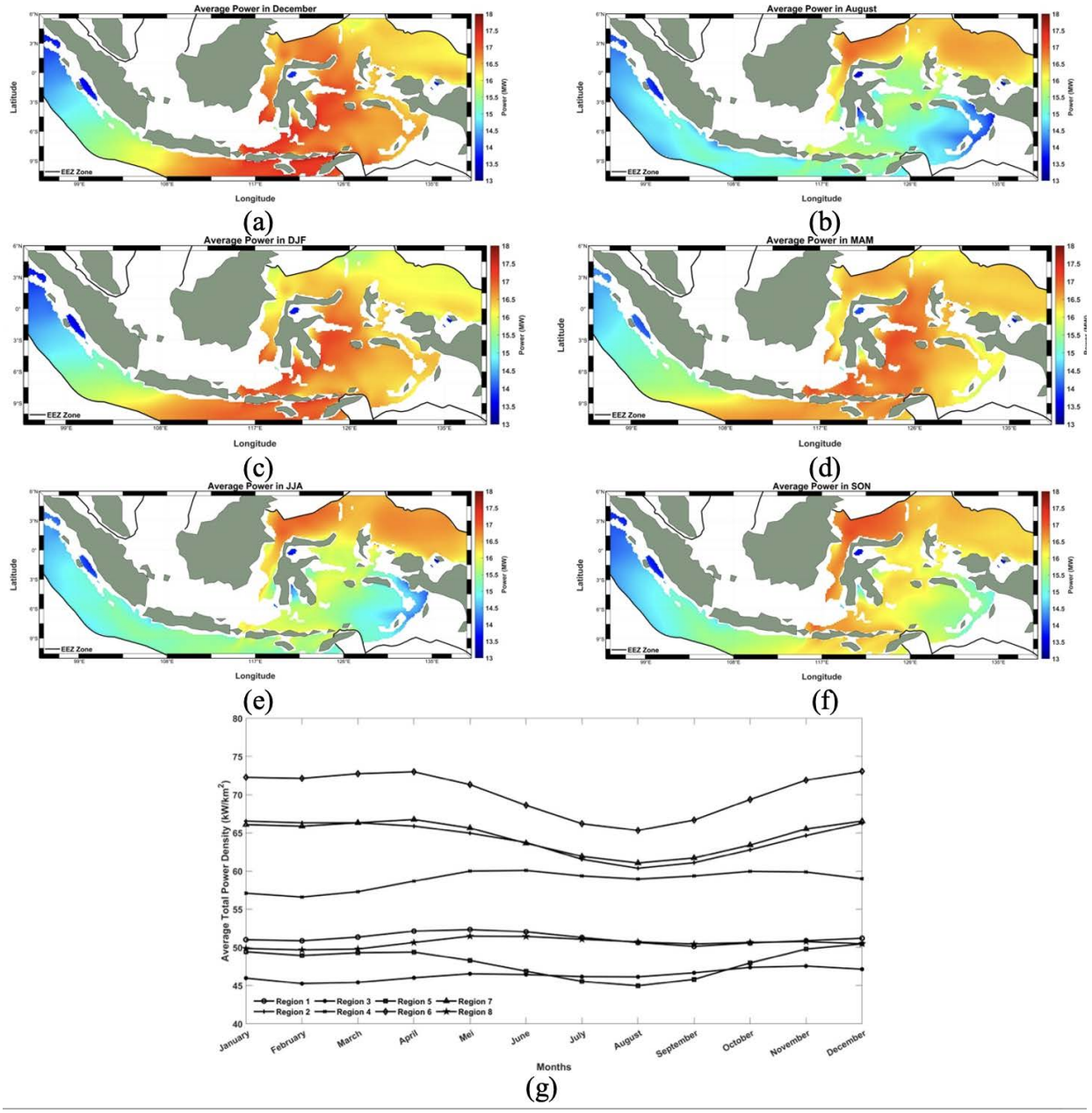

Figure 4. Average power potential of Indonesian Ocean thermal energy in the months of (a) December and (b) August and the seasons of (c) DJF, (d) MAM, (e) JJA, and (f) SON during 1964-2013. (g) The average power density potential of the Indonesian Ocean thermal energy each month in each division of the study area.

The Influence of ENSO and IOD on OTEC Potential in EEZ Indonesia

Changes in ocean temperature variations directly impact the potential for OTEC in Indonesia, as shown in Table 6. OTEC relies on a significant temperature difference between warm surface waters and deep, cold waters. During El Niño events (Figure 5b), when sea surface temperatures generally decrease slightly (as discussed earlier), the temperature difference between surface and deep water also shrinks. This reduction in the temperature gradient leads to a decrease in the total OTEC power potential compared to normal conditions (Figure 5a). Conversely, La Niña events (Figure 5c) are often associated with slightly warmer surface waters, which can increase the temperature difference with

deep water, thus enhancing the overall OTEC potential in Indonesian waters.

The reduction in power potential in each study area varies from -0.07% to -6.48%. The El Niño phenomenon (Figure 5b) causes a more significant decrease in power in the eastern waters of Indonesia, such as in the Sawu Sea and Arafura Sea, Banda Sea and Seram Sea, and Maluku Sea, compared to other regions. The power potential decrease in the Sawu Sea and Arafura Sea reaches -5.40%, followed by -5.64% in the Banda Sea and Seram Sea, and -6.48% in the Maluku Sea. In addition to the reduction in power potential, the El Niño phenomenon also led to an increase in power potential in the Indian Ocean region in December 1979 and July 1987, in South Java in January 1969, December 1979, July 1987, January 1992, December 1994, and December 2009, in the Makassar Strait in January 1992, December 1994, November 2002, and December 2009, in the Sulawesi Sea in November 2002, Sawu Sea and Arafura Sea in December 1979, July 1987, January 1992, December 1994, November 2002, and December 2009, in the Banda Sea and Seram Sea in December 1979, July 1987, December 1994, and December 2009, in the Maluku Sea in October 1969, November 1976, November 1977, December 1979, and December 1994, and the Pacific Ocean in November 2002. The Indian Ocean region in July 1987 experienced the largest increase in power potential compared to other regions, reaching 3.35%.

When a weak El Niño event occurs (ONI: 0.5-0.9) during the west monsoon season, the power decrease is not significant (less than 1%) across all study areas. This is because the seasonal influence is still strong, as seen by the additional power in the southern regions such as the Indian Ocean, Arafura Sea, and Seram Sea. However, during a moderate El Niño event (ONI: 1.0-1.4) in the west monsoon season, a significant power decrease is observed in the Indian Ocean, Banda Sea, Seram Sea, Maluku Sea, and the Pacific Ocean. In the case of a strong El Niño event (ONI: ≥1.5) during the west monsoon

Table 6. Impact of ENSO and IOD Phenomena on Total Power Potential

Condition	Power potential total (GW)	Condition	Power potential total (GW)
Normal	290.28	Normal	290.28
El-Nino	288.23	IOD (+)	281.92
La-Nina	291.72	IOD (-)	292.64

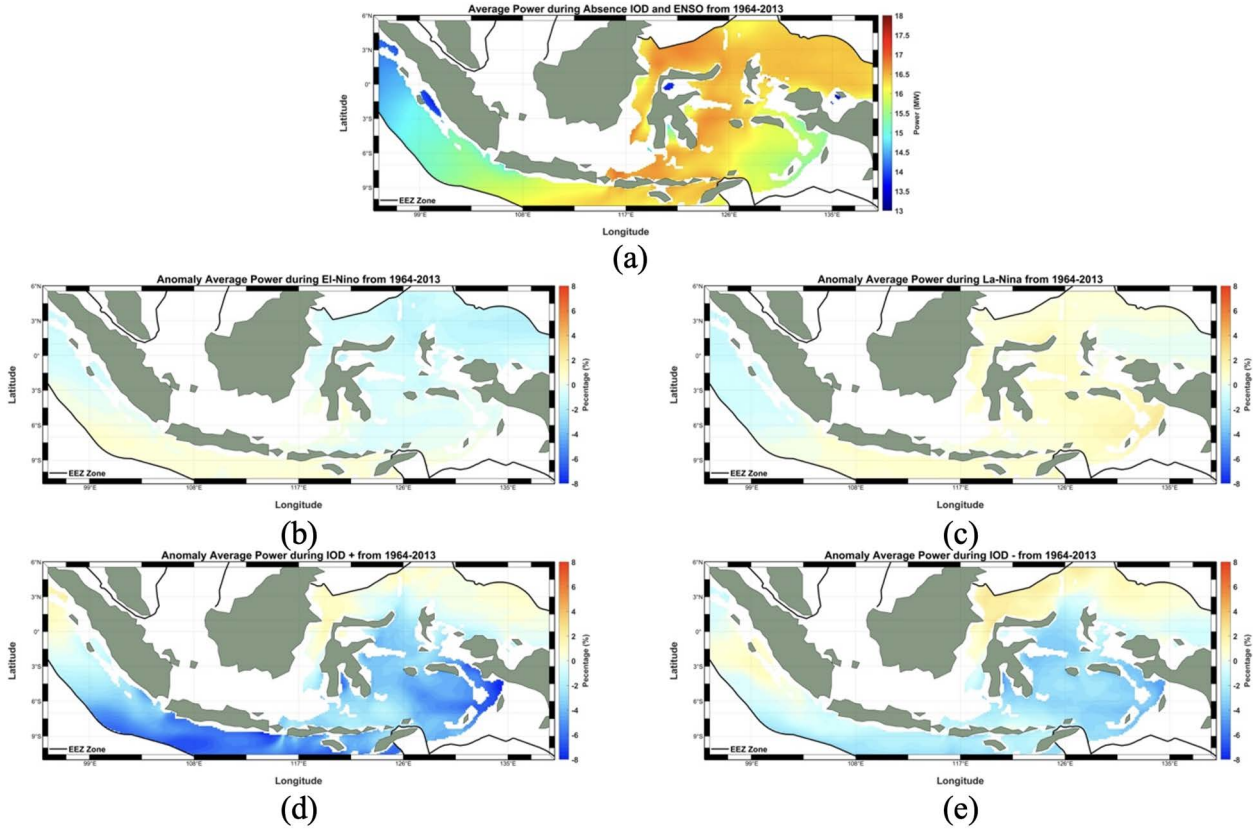

Figure 5. Anomaly of power potential in the study areas during (a) absence of ENSO and IOD, (b) El-Nino, (c) La-Nina, (d) IOD (+), and (e) IOD (-) phenomena.

season, a more substantial power decrease (over 2.5%) occurs in the Makassar Strait, Sulawesi Sea, Sawu Sea and Arafura Sea, Banda Sea and Seram Sea, and Maluku Sea.

The La Niña phenomenon has a minimum impact on power changes in the Indian Ocean (Figure 5c). La Niña causes variable increases in power potential in each study area, ranging from 0.14% to 4.91%. The influence of La Niña on power potential changes is not as significant as that of El Niño, but it leads to substantial increases in potential power in all study areas except the Indian Ocean and the Pacific Ocean. La Niña results in a power increase of 4.72% in South Java, 3.80% in the Makassar Strait, 4.76% in the Sulawesi Sea, 4.80% in the Sawu Sea, and Arafura Sea, 4.91% in the Banda Sea and Seram Sea, and 4.08% in the Maluku Sea.

Similar to El Niño, La Niña does not always cause an increase in power potential in each study area. In fact, during La Niña in December 1970, there was a decrease in power potential across all study areas. The power potential decrease varied from -0.21% to -3.78% in each study area, with the largest decrease occurring in the Pacific Ocean in December 1970 at -3.78%.

OTEC, a technology that utilizes the temperature difference between warm surface and deep, cold ocean waters, presents exciting potential for Indonesia as a renewable energy source. However, its viability is intricately linked to the complex interplay of climate patterns, particularly the ENSO and the IOD. ENSO, with its warm (El Niño) and cool (La Niña) phases, significantly influences OTEC potential through overall sea surface temperature variations. El Niño events, characterized by slightly cooler surface waters, diminish the temperature gradient between surface and deep waters, reducing OTEC potential. Conversely, La Niña events, with their tendency for slightly warmer surface waters, amplify the temperature gradient, enhancing OTEC potential. IOD, another key climate influence, further modulates OTEC potential through the spatial distribution of sea surface temperatures. Positive IOD events, marked by warmer waters in the western Indian Ocean and cooler waters in the east, tend to decrease the temperature gradient in Indonesia, leading to lower OTEC potential (as shown in Table 6). In contrast, Negative IOD events, with cooler western and warmer eastern waters, enhance the temperature gradient, particularly in the eastern Indian Ocean region, increasing OTEC potential (as detailed in Table 7).

Positive Indian Ocean Dipole (IOD) events (Figure 5d) induce varying reductions in OTEC power potential across Indonesia, ranging from -0.10% to -4.44% in different study areas. While the text describes a substantial decrease in the Indian Ocean (-3.92%), Table 7 reveals a smaller decrease for Region 1 within this region (-1.56%). This highlights the importance of spatial variability within regions during Positive IOD events. Further investigation into the specific timeframes and averaging methods used for regional data in Table 7 is recommended for a more nuanced understanding.

Table 7 presents estimations of how ENSO and IOD phenomena influence average power potential changes in each study area. Positive IOD events generally cause larger variations in power potential compared to other phenomena. Based on this table, the South Java region emerges as a potential candidate for OTEC development due to its relatively stable response to both ENSO and IOD events (as evidenced by a smaller range of power changes). Conversely, the Sawu Sea, Arafura Sea, and Maluku Sea exhibit a wider range of power changes due to ENSO and IOD influences, making them less favorable locations for OTEC development.

Negative IOD events (Figure 5e) generally lead to increases in total power potential, with exceptions like September 1992. However, Table 7 also suggests potential decreases in specific regions and months during Negative IOD events. This underscores the complexity of IOD's impact and the need for further

Table 7. Power Potential in Study Areas during ENSO and IOD Phenomena.

Region	Power potential total (GW) (Normal)	Increasing/Decreasing Power Potential (%)			
		El-Nino	La-Nina	IOD (+)	IOD (-)
Region 1	42.95	-0.21	-0.69	-1.56	-0.06
Region 2	17.96	0.77	1.05	-5.71	-1.27
Region 3	7.62	-0.43	0.89	0.54	1.04
Region 4	19.66	-0.98	0.58	0.20	1.35
Region 5	28.39	0.28	0.74	-4.14	-2.03
Region 6	40.98	-0.35	1.07	-4.17	-2.95
Region 7	8.73	-0.74	1.01	-3.33	-3.18
Region 8	52.99	-1.16	0.13	-0.14	0.12

analysis to fully comprehend its influence on OTEC potential. Disentangling the individual contributions of IOD and ENSO, particularly when they co-occur, remains a challenge. Future research endeavors could explore statistical methods to isolate these climate patterns' effects on OTEC potential variations in Indonesia.

CONCLUSSIONS

We obtained that temperature data validation between the model and the observation shows a good agreement with a bias ranging from -0.43°C to 0.09°C and a Root Mean Square Error (RMSE) ranging from 0.42°C to 0.54°C. The monthly average temperature in Indonesian EEZ at a depth of 20 m varies between 24.35°C (in August) and 31.24°C (in December), with a standard deviation of 0.83°C. At a depth of 1000 m, which is used as the reference depth, the average monthly water temperature in Indonesian waters ranges from 2.84°C to 7.88°C, with a standard deviation of 0.09°C that indicates stable temperature with small variability. The average estimation of potential thermal power energy in the Indonesian EEZ, represented by 3,495,698.72 km², is 289.73 GW. This potential power varies in monthly average with a minimum value of 280.09 GW occurring in August and reaching a maximum value of 295.65 GW in December. In 50 years span from 1964 to 2013, we found that the highest seasonal average potential power of ocean thermal energy in Indonesian EEZ is 293.91 GW which occurs during transition season I (March, April, and May). On the other hand, the lowest value, i.e. 284.18 GW, of seasonal average potential power occurs in the east monsoon season (December, January, and February). Furthermore, intra-seasonal variability potential thermal power energy in Indonesian EEZ occurs due to ENSO and IOD. During El-Nino events, the potential power energy decreases to 288.23 GW on a monthly average, whereas at La-Nina events, it increases to 291.72 GW also on a monthly average. In addition, the monthly average of potential thermal power in the same zone decreases to 281.82 GW when positive IOD occurs, and on the contrary, it increases on average to 292.64 GW during negative IOD events. The order of regions with the highest to lowest average power density potential, which are considered potential locations for OTEC development, is as follows: Region 4 (Sulawesi Sea), Region 6 (Banda Sea and Seram Sea), Region 2 (South Java), Region 7 (Maluku Sea), Region 8 (Pacific Ocean), Region 1 (Indian Ocean), Region 5 (Sawu Sea and Arafura Sea), and Region 3 (Makassar Strait).

REFERENCES

Aresti, L., Christodoulides, P., Michailides, C., & Onoufriou, T., 2023. Reviewing the energy, environment, and economy prospects of Ocean Thermal Energy Conversion (OTEC) systems. *Sustainable Energy Technologies and Assessments*, 60, 103459. https://doi.org/10.1016/J.SETA.2023.103459

Bernal, E. M., Garrido, D. C., Perea, G. A., & Escobedo Trujillo, B. A., 2022. Assessment of potential and temperature differential for an ocean thermal energy conversion plant. Case study: Cozumel, Mexico. *2022 IEEE International Conference on Engineering Veracruz, ICEV 2022*. https://doi.org/10.1109/ICEV56253.2022.9959202

Bhuiyan, M. A., Hu, P., Khare, V., Hamaguchi, Y., Thakur, B. K., & Rahman, M. K., 2022. Economic feasibility of marine renewable energy: Review. *Frontiers in Marine Science*, 9, 988513. https://doi.org/10.3389/FMARS.2022.988513/BIBTEX

Chu, W., Calise, F., Duić, N., Østergaard, P. A., Vicidomini, M., & Wang, Q., 2020. Recent Advances in Technology, Strategy and Application of Sustainable Energy Systems. *Energies 2020,* 13(19): 5229. https://doi.org/10.3390/EN13195229

Clemente, D., Rosa-Santos, P., & Taveira-Pinto, F., 2021. On the potential synergies and applications of wave energy converters: A review. *Renewable and Sustainable Energy Reviews*, 135, 110162. https://doi.org/10.1016/J.RSER.2020.110162

Herrera, J., Sierra, S., & Ibeas, A., 2021. Ocean Thermal Energy Conversion and Other Uses of Deep Sea Water: A Review. *Journal of Marine Science and Engineering 2021,* 9(4): 356. https://doi.org/10.3390/ JMSE9040356

Langer, J., Quist, J., & Blok, K., 2020. Recent progress in the economics of ocean thermal energy conversion: Critical review and research agenda. *Renewable and Sustainable Energy Reviews*, 130, 109960. https://doi.org/10.1016/J.RSER.2020.109960

Lubchenco, J., & Haugan, P. M., 2023. Coastal Development: Resilience, Restoration and Infrastructure Requirements. *The Blue Compendium*, 213-277. https://doi.org/ 10.1007/978-3-031-16277-0-7

Masutani, S. M., & Takahashi, P. K., 2001. Ocean Thermal Energy Conversion (otec). *Encyclopedia of Ocean Sciences*, 1993-1999. https://doi.org/10.1006/RWOS.2001.0031

Merchant, C. J., Minnett, P. J., Beggs, H., Corlett, G. K., Gentemann, C., Harris, A. R., Hoyer, J., & Maturi, E., 2019. Global Sea Surface Temperature. *Taking the Temperature of the Earth: Steps towards Integrated Understanding of Variability and Change*, 5-55. https://doi.org/10.1016/B978-0-12-814458-9.00002-2

Nihous, G. C., 2005. An Order-of-Magnitude Estimate of Ocean Thermal Energy Conversion Resources. *Journal of Energy Resources Technology*, 127(4): 328-333. https://doi.org/10.1115/1.1949624

Nihous, G. C., 2007. A Preliminary Assessment of Ocean Thermal Energy Conversion Resources. *Journal of Energy Resources Technology*, 129(1): 10-17. https://doi.org/ 10.1115/1.2424965

Nihous, G., 2018. A Preliminary Investigation of the Effect of Ocean Thermal Energy Conversion (OTEC) Effluent Discharge Options on Global OTEC Resources. *Journal of Marine Science and Engineering 2018,* 6(1): 25. https://doi.org/10.3390/ JMSE6010025

Qu, B., Song, J., Yuan, H., Li, X., Li, N., Duan, L., ... & Lu, X., 2015. Summer carbonate chemistry dynamics in the Southern Yellow Sea and the East China Sea: Regional variations and controls. *Continental Shelf Research*, 111, 250-261.

Rachmayani, R., Ningsih, N. S., Hanifah, F., & Nabilla, Y., 2023. Long-Term Trend and Variability of Volume Transport and Advective Heat Flux through the Boundaries of the Java Sea Based on a Global Ocean Circulation Model (1950–2013). *Water 2023,* 15(4): 740. https://doi.org/ 10.3390/ W15040740

Rajagopalan, K., & Nihous, G. C., 2013. An Assessment of Global Ocean Thermal Energy Conversion Resources With a High-Resolution Ocean General Circulation Model. *Journal of Energy Resources Technology*, 135(4). https://doi.org/10.1115/1.4023868

Rudolph, T. B., Ruckelshaus, M., Swilling, M., Allison, E. H., Österblom, H., Gelcich, S., & Mbatha, P., 2020. A transition to sustainable ocean governance. *Nature Communications 2020*, 11(1): 1-14. https://doi.org/ 10.1038/ s41467-020-17410-2

Serban, M., Li, G. yu, Serban, R. D., Wang, F., Fedorov, A., Vera, S., Cao, Y. peng, Chen, P. chao, & Wang, W., 2021. Characteristics of the active-layer under the China-Russia Crude Oil pipeline. *Journal of Mountain Science*, 18(2): 323-337. https://doi.org/ 10.1007/S11629-020-6240-Y/METRICS

Thomson, R. E., & Emery, W. J., 2014. Data analysis methods in physical oceanography. Newnes.

Topper, M. B. R., Nava, V., Collin, A. J., Bould, D., Ferri, F., Olson, S. S., Dallman, A. R., Roberts, J. D., Ruiz-Minguela, P., & Jeffrey, H. F., 2019. Reducing variability in the cost of energy of ocean energy arrays. *Renewable and Sustainable Energy Reviews*, *112*, 263-279. https://doi.org/10.1016/ J.RSER.2019.05.032

Von Jouanne, A., & Brekken, T. K. A., 2017. Ocean and Geothermal Energy Systems. *Proceedings of the IEEE*, 105(11): 2147-2165. https://doi.org/10.1109 JPROC.2017.2699558

Wang, L., Ma, X., Kong, H., Jin, R., & Zheng, H., 2022. Investigation of a low-pressure flash evaporation desalination system powered by ocean thermal energy. *Applied Thermal Engineering*, *212*, 118523. https://doi.org/ 10.1016/ J.APPLTHERMALENG.2022.118523

Zhang, H. H., Li, M. J., Feng, Y. Q., Xi, H., & Hung, T. C., 2021. Assessment and working fluid comparison of steam Rankine cycle -Organic Rankine cycle combined system for severe cold territories. *Case Studies in Thermal Engineering*, *28*, 101601. https://doi.org/ 10.1016/J.CSITE.2021.101601

SEDIMENT CHARACTERISTICS TO SUPPORT THE REVITALIZATION OF TPPI TUBAN PORT, EAST JAVA, INDONESIA

KARAKTERISTIK SEDIMEN UNTUK MENDUKUNG REVITALISASI PELABUHAN TPPI TUBAN, JAWA TIMUR, INDONESIA

Reno Arief Rachman*, Mardi Wibowo, Aloysius Bagyo Widagdo, Nurkhalis Rahili, Rizaldi Caesar Yuniardi, Hamzah Haru Radityo Suharyanto, Affandy Hamid, Aris Subarkah, Suranto, Hanah Khoirunnisa

Research Center for Hydrodynamics Technology, National Research and Innovation Agency

*Corresponding author: reno001@brin.go.id

(Received 03 February 2024; in revised from 05 February 2024 accepted 31 May 2024)

DOI : 10.32693/bomg.39.1.2024.874

ABSTRACT: TPPI Tuban Port is located in Tuban Regency, East Java. Geologically, the rocks are composed of reef limestone in the Paciran Formation, which is Pliocene–Early Pleistocene. The importance of complying with jetty capacity standards and water conditions in commercial ports is emphasized as the key to maintaining smooth port operations, making port revitalization a necessity. One of the main aspects to consider is the sedimentation problem, closely related to sediment characteristics. A deep understanding of sediment dynamics is essential for designing effective solutions to ensure the sustainability of port operations. This research aims to determine the distribution pattern of bed load characteristics such as water content, specific gravity, gradation, sediment texture, d50 size of sediment grains, and statistical analysis of bed load sediment in the west and rainy seasons, where the influence of sediment from land is very large. so it is hoped that it can support the port revitalization plan. The methods used include taking sediment samples in the field, testing sediment samples in the laboratory, statistical sediment analysis, and descriptive analysis of bed load characteristics using the Gradistat method. Based on the study results, the water content value ranges from 22.446% to 218.289%, and the specific gravity ranges from 2,100 g/m³ to 2.690 g/cm³. Additionally, the grain size varies from 0.080 mm to 0.900 mm, and the average grain size ranges from 261.1 μm to 2657.5 μm. Sediment sorting is dominated by very poorly sorted materials, with statistical analysis indicating a dominance of the very platykurtic type. The lithological type is predominantly sand.

Keywords: bed load, statistics, sediment texture, Tuban, East Java

ABSTRAK: Pelabuhan TPPI Tuban terletak di Kabupaten Tuban, Jawa Timur. Secara geologi batuannya tersusun oleh batugamping trumbu pada Formasi Paciran yang berumur Pliosen-Pleistosen Awal. Pentingnya mematuhi standar kapasitas jetty dan kondisi perairan dalam pelabuhan niaga ditekankan sebagai kunci untuk menjaga kelancaran operasional pelabuhan ,oleh karena itu, revitalisasi pelabuhan dianggap suatu keharusan. Salah satu aspek utama yang perlu diperhatikan adalah permasalahan sedimentasi, yang sangat terkait dengan karakteristik sedimen itu sendiri. Pemahaman mendalam terhadap dinamika sedimen menjadi esensial untuk merancang solusi yang efektif dalam mengatasi masalah ini dan memastikan keberlanjutan operasional pelabuhan. Tujuan penelitian ini adalah untuk mengetahui pola sebaran karakteristik sedimen dasar seperti kadar air, berat jenis, gradasi, tekstur sedimen, ukuran d50 butir sedimen dan analisis statistik sedimen dasar laut pada musim barat/musim hujan mendukung rencana revitalisasi pelabuhan. Metode yang dipakai adalah pengambilan sampel sedimen di lapangan, pengujian sampel sedimen di laboratorium, analisis sedimen secara statistic dan analisis deskriptif

karakteristik sedimen dasar menggunakan metode Gradistat. Berdasarkan hasil kajian diketahui nilai kadar air 22,446 % - 218,289 %, berat jenis 2,100 g/m3 – 2,690 g/cm3, ukuran butir 0,080 mm – 0,900 mm, ukuran rerata butir 261,1 µm - 2657,5 µm, sortasi sedimen didominasi very poorly sorted (terpilah sangat buruk), analisis statistik sedimen didominasi tipe very platykurtic, jenis lithologi didominasi oleh pasir.

Kata Kunci: sedimen dasar, statistik, tekstur sedimen, Tuban, Jawa Timur

INTRODUCTION

Shipping stands as a cornerstone of transportation in Indonesia, particularly given its status as a maritime nation with expansive seas. Beyond serving public transportation needs, shipping plays a crucial role in facilitating trade activities, notably in sectors such as coal, oil, and gas. This assertion aligns with the findings by Saepuloh et al. (2017), who delineate shipping into two categories: commercial and non-commercial. Commercial shipping, as highlighted in their study, handles the bulk of imported and exported goods, along with large cargo volumes. Additionally, ensuring seamless shipping operations entails addressing various infrastructure needs, including robust port facilities.

As described by Notteboom et al. (2022) a port serves as a pivotal transit area and gateway facilitating the movement of goods and people to and from the sea. In Indonesia, ports are not solely under governmental ownership but also have partnerships with various companies, particularly those involved in the oil and gas processing sector. Ports owned by these partner entities primarily facilitate the transportation of raw materials to or from industrial sites. For instance, PT Trans-Pacific Petrochemical Indotama (TPPI) operates a port for such purposes.

To ensure the capacity and seamless operations of companies, commercial ports must adhere to specific standards, particularly concerning jetty capacity and water conditions such as currents and waves. Business Continuity Management (BCM) becomes imperative in maintaining operational continuity and safeguarding against disruptions that could potentially halt business operations, particularly in critical sectors like ports (Budiyanto, 2022). This necessity underscores the importance of port rejuvenation or revitalization efforts.

In the planning of port revitalization, a crucial aspect that requires study is the sedimentation process. All marine structures inherently disturb the balance of sediment transport along the shoreline (longshore current), potentially resulting in alterations to sediment supply, so that these marine structures can either diminish, halt, or augment sediment supply (Diposaptono, 2011; Melisa et al., 2020).

The sedimentation process in ports is intricately linked to dredging activities during the operational stage, as dredging significantly impacts a port's competitiveness. Dredging can enhance port efficiency by 3-10%, reduce port costs by 1-24%, and increase port operator income by 3-19% (Rosyidi, 2015). For instance, the annual cost of dredging to mitigate silting at Baai-Bengkulu Island Harbor amounts to Rp. 28-30 billion (Supiyati et al., 2011). The sedimentation rate at Pulau Baai Harbor parallels the construction pace of a 390-meter-long breakwater from the beach. Despite the design expectation of reaching a distance of 400 meters after 10 years, in reality, sand deposits reached the end of the breakwater within just 3 years (Hamdani, 2013). Combining sediment management and (bio) remediation in ports has the potential to reduce dredging need and remediate contaminated mud, potentially improving port competitiveness (Polrot et al., 2021).

Understanding underwater conditions, especially seabed sediment, is crucial in planning the revitalization of coastal structures (Pasaribu et al., 2021; Permana et al., 2012; Siry, 1990). Sediment transport along coastlines leads to various issues such as shallowing and beach erosion, underscoring the significance of studying sediment transport predictions (Triatmodjo, 1999; Umar et al., 2020). Sediment transport around coastal areas encompasses both onshore-offshore and longshore transport (Triatmodjo, 1999; Thunyaphun et al., 2023). Tidal fluctuations, a primary cause of current patterns and sediment movement in sheltered coastal regions, significantly influence sediment transport, particularly in estuaries, bay mouths, or protected straits (Wahyudi and Jupantara, 2004; Ali et al., 2017; Pu et al, 2022). Tidal currents not only affect wave height, which carries sediment to and from the coast, but also impact current speed and direction, facilitating substantial sediment transport (Wahyudi and Jupantara, 2004; Ali et al., 2017; Pu et al, 2022). In contrast, for open beaches, wave energy plays a significant role alongside tidal currents in the

sedimentation process (Purba et al., 2022). According to (Rifardi, 2012), the most dominant factors influencing sedimentation are currents and waves (Ansari et al., 2020; Dwinanto et al., 2017).

Tides and river estuary discharge are among the key factors influencing sediment distribution (Andayani et al., 2020; Dwianti et al., 2017). Understanding the distribution of sediment fractions is crucial for analyzing the shallowing process. Factors such as distribution, cohesiveness, density, and grain size play dominant roles in sediment transport (Rachman and Wibowo, 2019). Sediment characteristics, including grain size, sediment type, and classification parameters, along with sediment distribution, are significant marine dynamic factors influencing sediment deposition and defining the sedimentation environment (Liu et al., 2023; Rifardi, 2008). The distribution and heterogeneity of sediment gradation serve as indicators of sediment flow behavior in an area (Anggraini et al., 2020; Junaidi and Wigati, 2011; Nugroho and Basit, 2014; Rachman et al., 2021).

Sedimentation in seawater results not only from the deposition of suspended sediment material but also from the movement of bed load in the area. The settling speed of cohesive sediment is influenced by various factors including the concentration of suspended sediment, salinity, and the diameter of underlying sediment particles (Rachman and Wibowo, 2022). An alternative method for studying sedimentation environments and determining sediment transport direction involves determining statistical parameters such as mean grain size, standard deviation, skewness, and kurtosis, which are commonly utilized (Affandi and Surbakti, 2012; Muhardi et al., 2022). This study aims to ascertain the distribution pattern of seabed sediment characteristics during the west season, particularly significant due to the substantial influence of sediment from land during this period. These characteristics are pivotal for further sedimentation studies, serving as crucial input data for both analytical and numerical modeling of sedimentation velocity. Additionally, they are integral for numerical studies regarding the revitalization of the TPPI Tuban port.

The research is conducted in the waters surrounding TPPI Tuban Port, East Java, where a port has been established. Thus far, there has been limited research conducted on sedimentation and sediment characteristics at this location. Therefore, as an initial investigation, this study focuses on examining the characteristics of the bed load.

To analyze the characteristics of bed loads, the Gradistat statistical method will be employed. This method, proposed by (Blott, 2010; Blott and Pye 2001) in collaboration with *Kenneth Pye Associates Ltd*., operates within the Microsoft Excel program. The calculation methods utilized include the *Method of Moments* (mathematical) and the *Folk and Ward* approach (graphical). Gradistat serves as an alternative to computational numerical modeling software for sediment analysis. One of its key advantages is its accessibility and cost-effectiveness, as it does not require licensing fees and can be easily implemented, leveraging the familiarity of Microsoft Excel.

METHODS

The research implementation comprises several stages: (1) Field sampling of bed load. (2) Laboratory analysis of soil water content in bed loads, utilizing the SNI 1965:2019 method, which follows the Test Method for Determining Water Content for Soil and Rock (BSN, 2019). (3) Determination of soil specific gravity in bed load, employing the SNI 1964:2008 method for testing soil specific gravity (BSN, 2008a). (4) Analysis of soil gradation in bed loads, utilizing the SNI 3423:2008 method for testing soil grain size analysis (BSN, 2008b). (5) Analysis of sediment characteristics using the Gradistat method.

Sediment sampling employs tools such as a sediment grabber, plastic sampler, and permanent marker. Soil mechanics testing involves the use of various equipment, including scales, ceramic cups, pycnometers, measuring cups, measuring tubes, desiccators (cooling devices), ovens, thermometers, hydrometers, electric furnaces, porcelain cups, suspension stirrers, stopwatches, and sieve shakers. Additionally, distilled water and reagent fluids are utilized as materials for soil mechanics testing.

Sediment sampling was conducted using a purposive sampling method, covering the waters surrounding TPPI Tuban. In July 2020, a total of 30 samples were collected (refer to Figure 1 and Table 1) for subsequent laboratory testing, which took place in August 2020.

The analysis of the distribution characteristics of seabed sediment in the waters of TPPI Tuban employs the Gradistat version 8 method. This analysis focuses on discussing statistical grain size distribution for unconsolidated soil types, utilizing sieving and laser granulometer methods (Blott, 2010; Blott and Pye 2001). The aim is to provide a descriptive and systematic account of the bed load

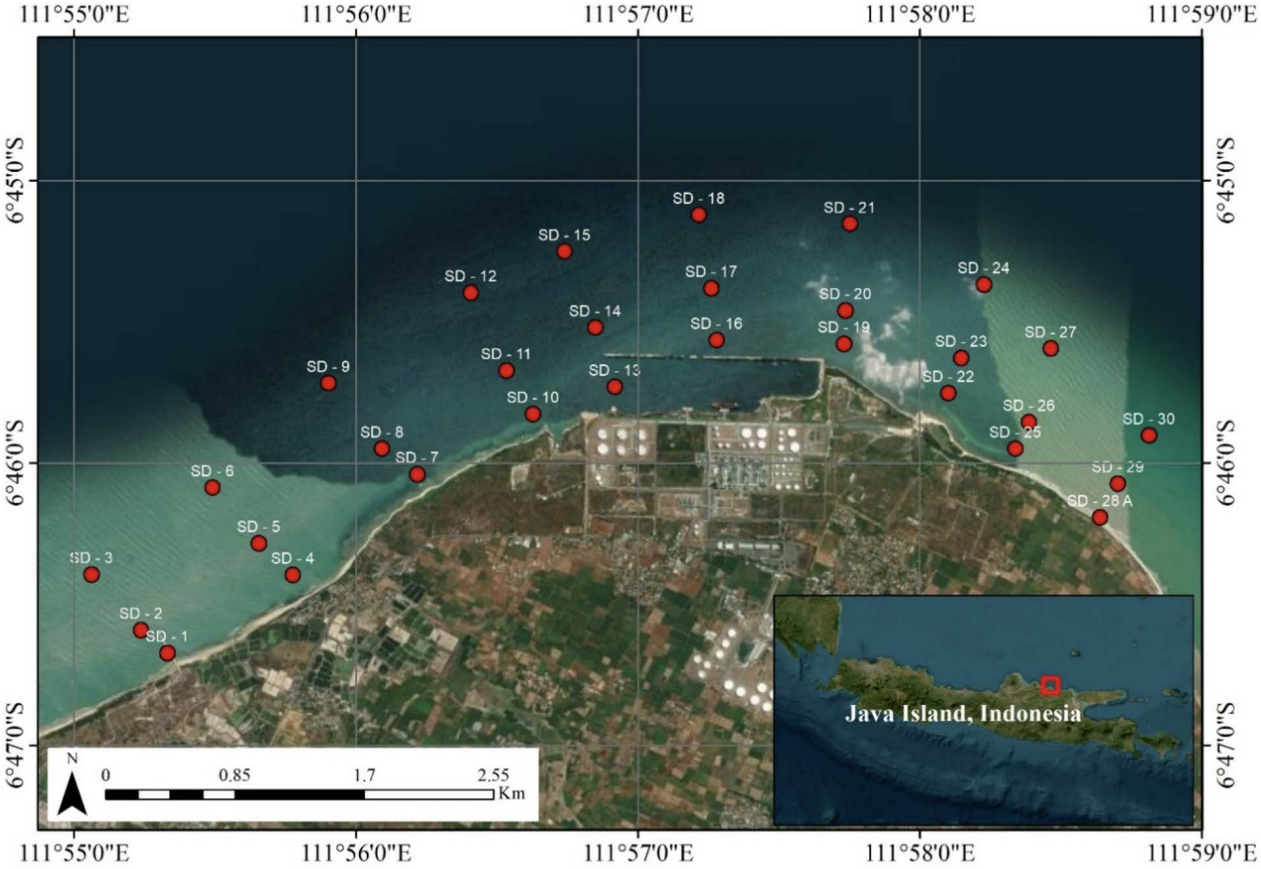

Figure 1. Bed load sampling location

Table 1. Bed load sampling coordinate point (converted to UTM zone 49S)

No	Code	Depth (m)	Date	Time (WIB)	X	Y
1	SD - 1	2	09/07/2020	9:51	601906.695	9250707.637
2	SD - 2	4.5	09/07/2020	9:58	601735.72	9250857.686
3	SD - 3	5	09/07/2020	10:05	601412.357	9251222.999
4	SD - 4	3	09/07/2020	9:04	602727.634	9251218.114
5	SD - 5	3	09/07/2020	9:36	602506.428	9251423.533
6	SD - 6	5	09/07/2020	9:29	602204.507	9251786.426
7	SD - 7	3	09/07/2020	9:10	603541.419	9251872.062
8	SD - 8	6	09/07/2020	9:15	603312.992	9252039.359
9	SD - 9	5	09/07/2020	9:21	602963.538	9252466.708
10	SD - 10	3	09/07/2020	9:00	604299.911	9252263.903
11	SD – 11	5	09/07/2020	8:57	604126.515	9252547.897
12	SD – 12	6	09/07/2020	8:49	603893.979	9253056.07
13	SD – 13	7	08/07/2020	10:15	604834.053	9252438.394
14	SD – 14	5	09/07/2020	8:35	604706.085	9252825.663
15	SD – 15	7	08/07/2020	8:41	604506.894	9253324.24
16	SD – 16	5	08/07/2020	10:46	605499.414	9252743.067
17	SD – 17	5.5	08/07/2020	10:51	605466.717	9253081.615
18	SD – 18	7	08/07/2020	10:57	605384.255	9253560.898
19	SD – 19	4	08/07/2020	10:39	606330.98	9252717.593
20	SD – 20	5	08/07/2020	10:35	606340.94	9252934.49
21	SD – 21	5	08/07/2020	10:28	606370.651	9253499.366
22	SD – 22	5.5	08/07/2020	9:39	607011.835	9252394.443
23	SD – 23	6.5	08/07/2020	9:38	607098.072	9252623.107
24	SD – 24	8.5	08/07/2020	9:42	607246.764	9253101.934
25	SD – 25	5	08/07/2020	12:22	607449.553	9252031.248
26	SD – 26	5.7	08/07/2020	9:28	607538.065	9252205.081
27	SD – 27	7.5	08/07/2020	9:22	607681.995	9252683.917
28	SD – 28	3	08/07/2020	11:59	608001.467	9251582.005
29	SD – 29	4	08/07/2020	9:18	608118.666	9251801.07
30	SD – 30	5	08/07/2020	9:15	608321.84	9252115.31

characteristics, ensuring a factual and accurate portrayal of the observed phenomena and their interrelationships ((Nazir, 1983; Rachman and Wibowo, 2019). Understanding the statistics of bedload particle motions is of great importance (Zi et al., 2023)

RESULTS AND DISCUSSIONS

Based on the results of analyses conducted at the Geotechnical and Soil Mechanics Laboratory, BTIPDP-BPPT, the distribution patterns and the characteristics of bed load sediments such as water content, specific gravity, gradation, sediment texture, d50 size of sediment grains, and statistical analysis of seabed sediments in the waters of TPPI Tuban are as follows:

Soil Water Content

Soil water content represents the comparison between the mass (weight) of water or wet content within the soil and the dry mass (weight) of the soil, typically expressed as a percentage (BPPT, 2021). The soil's capacity to retain water can be measured by weight or volume. Factors like temperature and humidity impact the lower limits of water content and matric potential in soil, affecting its ability to retain water (Tianyu et al., 2022). In addition to soil properties, climate factors significantly impact the soil's water retention capability, including temperature, humidity, and wind speed (Salam, 2020). Soil texture plays a crucial role in determining water-holding capacity, with coarse-textured soils generally having lower capacity compared to fine-textured soils. Consequently, silt soils tend to retain moisture more effectively than sandy soils (Salam, 2020; Caroline et al., 2023; Chunliu et al., 2023).

The soil water content in the research area varies from 22.446% to 218.289% (refer to Table 2). The highest water content, recorded at 218.289%, is observed at point SD-13 within the anchor pool of TPPI Tuban, while the lowest, at 22.446%, is found at point SD-1 in the waters off Pier Beach, west of TPPI Tuban.

Soil Specific Gravity

The specific gravity of sedimentary soil represents the ratio of sediment particle size to the volume weight of water (Ponce, 1989; Rashid et al., 2017; Mira, 2021). Specific gravity is necessary for computing the soil's void ratio and determining the grain-size distribution in hydrometer analysis (Mir, 2021). Generally, sediment has a specific gravity estimated at around 2.65 g/cm3, unless it contains heavy materials like magnetite, in which case the specific gravity can reach around 5.18 g/cm3 (Hambali and Apriyanti, 2016). In the study area, the specific gravity of bed loads ranges from 2.1 g/cm3 to 2.69 g/cm3 (refer to Table 3). These sediments are classified as light, likely due to their composition containing silicate minerals (SiO2) and a significant amount of organic minerals such as peat or humus, which have low specific gravity (Hardiyatmo, 2002; Volkov et al., 2021). The distribution pattern of sediment specific gravity appears consistent, although sediment with the lowest specific gravity is found north of the Tuban TPPI breakwater (SD-17) at 2.1 g/cm3, while the highest is in the waters of Sumur Pawon Beach (SD-25) at 2.69 g/cm3. This variation is attributed to the dominant influence of sediment rich in humus/peat during sampling.

Table 2. Bed load water content

Sample Code	**SD-1**	**SD-2**	**SD-3**	**SD-4**	**SD-5**	**SD-6**	**SD-7**	**SD-8**	**SD-9**	**SD-10**
Water Content (%)	22.446	50.259	50.30	24.355	37.32	205.946	34.192	34.20	39.1	39.942
Sample Code	**SD-11**	**SD-12**	**SD-13**	**SD-14**	**SD-15**	**SD-16**	**SD-17**	**SD-18**	**SD-19**	**SD-20**
Water Content (%)	205.061	176.482	218.289	212.911	213.1	213.866	190.17	169.335	168.219	155.465
Sample Code	**SD-21**	**SD-22**	**SD-23**	**SD-24**	**SD-25**	**SD-26**	**SD-27**	**SD-28**	**SD-29**	**SD-30**
Water Content (%)	171.746	168.444	128.065	108.218	59.06	69.434	130.553	112.657	104.312	136.536

Table 3. Bed load specific gravity

Sample Code	SD-1	SD-2	SD-3	SD-4	SD-5	SD-6	SD-7	SD-8	SD-9	SD-10
Specific Gravity (g/cm^3)	2.439	2.524	2.53	2.657	2.621	2.200	2.542	2.55	2.3	2.299
Sample Code	SD-11	SD-12	SD-13	SD-14	SD-15	SD-16	SD-17	SD-18	SD-19	SD-20
Specific Gravity (g/cm^3)	2.164	2.371	2.267	2.355	2.4	2.470	2.100	2.347	2.309	2.28
Sample Code	SD-21	SD-22	SD-23	SD-24	SD-25	SD-26	SD-27	SD-28	SD-29	SD-30
Specific Gravity (g/cm^3)	2.414	2.473	2.512	2.455	2.690	2.529	2.675	2.669	2.501	2.439

Gradation and Sediment Texture

Grain size analysis is a method used to determine the distribution of soil grain sizes, specifically for soil samples without grains larger than 2 mm. The analysis involves sediment examination with a hydrometer for particles smaller than sieve no. 10 (0.0075 mm), while particles retained on sieve no. 200 (0.0075 mm) are analyzed using a sieve (BPPT, 2021).

According to the d50 value of the grain size (refer to Table 4), the majority of seabed sediments in the study area are classified as very fine sand (12 samples), fine sand (7 samples), medium sand (1 sample), and silt (10 samples).

The level of sediment grain gradation, indicating variations in grain size, is determined by the d90/d10 value, where a higher d90/d10 value signifies better sediment gradation or more diverse grain sizes. In the study area, all seabed sediments are classified as well-graded, as their d90/d10 values are below 3 (Hardiyatmo, 2002) (refer to Table 5).

The analysis of sediment grain size reveals that the lithology of the majority of seabed sediment in the study area consists mainly of sand with a minor presence of silt (refer to Figures 3 and 4, and Table 4). Sand fraction dominates the sediment, ranging from 11.8% to 92.2%, followed by the mud fraction ranging from 0.3% to 25.2%, and the gravel fraction ranging from 7.5% to 77.3% (refer to Table 6). These findings align with previous research conducted in areas surrounding the study location, which indicated that the bed load in Tuban TPPI waters is predominantly composed of sand with a d50 size ranging from 0.09 to 0.35 mm (Wibowo, 2018). This sand dominance is likely attributed to the presence of small currents in areas with finer-grained bed loads. Such currents tend to transport fine sediment particles over distances, resulting in their deposition in locations farther from the source (Rifardi, 2008; Mengual at al, 2020). The consistency between the results of this study and previous research underscores the reliability of the findings.

Specifically, the sand fraction is primarily composed of very fine sand. Detailed composition and percentage data of gravel, sand, silt, and mud from each sediment sample are provided in Table 6, Figure 2, Figure 3, and Figure 4.

Table 4. D50 Bed load

Sample Code	SD-1	SD-2	SD-3	SD-4	SD-5	SD-6	SD-7	SD-8	SD-9	SD-10
D50 (mm)	0.140	0.095	0.095	0.140	0.140	0.350	0.089	0.089	0.090	0.090
Sample Code	SD-11	SD-12	SD-13	SD-14	SD-15	SD-16	SD-17	SD-18	SD-19	SD-20
D50 (mm)	0.140	0.100	0.150	0.095	0.095	0.100	0.150	0.330	0.210	0.100
Sample	SD-21	SD-22	SD-23	SD-24	SD-25	SD-26	SD-27	SD-28	SD-29	SD-30
D50 (mm)	0.290	0.140	0.400	0.100	0.900	0.250	0.500	0.080	0.090	0.350

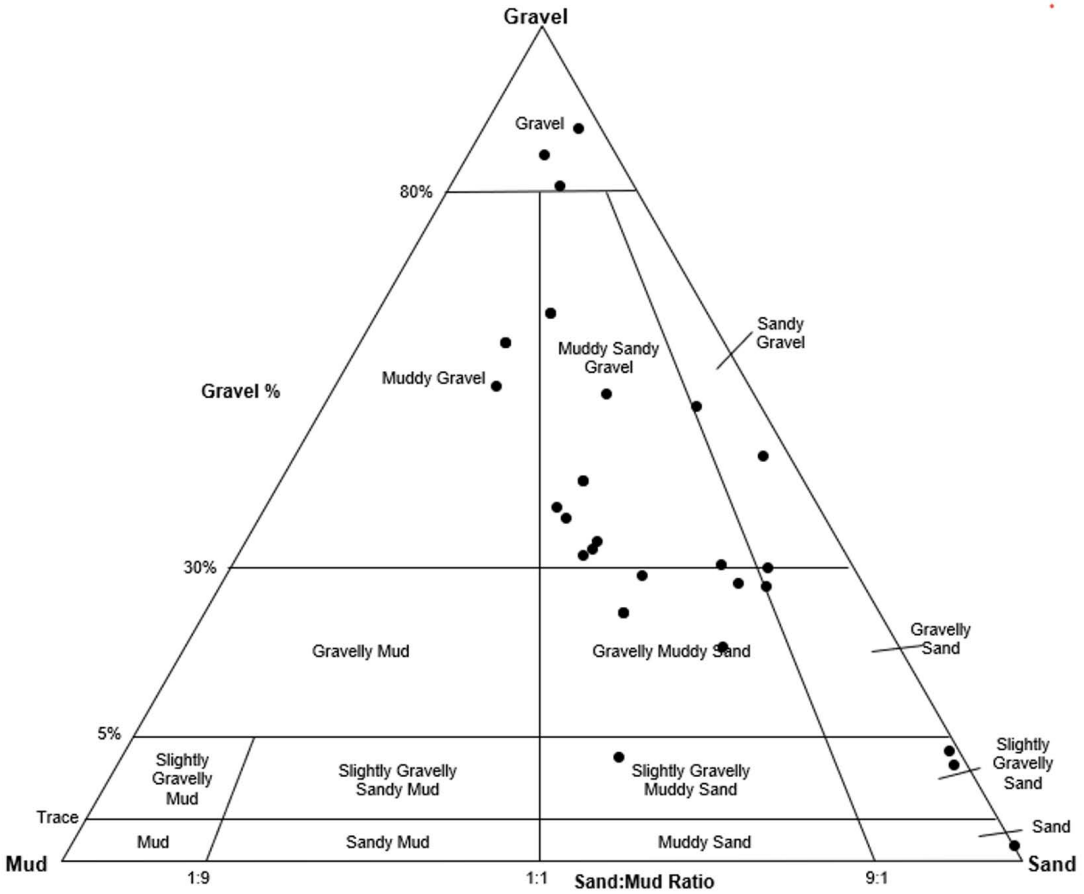

Figure 2. Sediment grain size classification based on sheppard's triangle (1954)

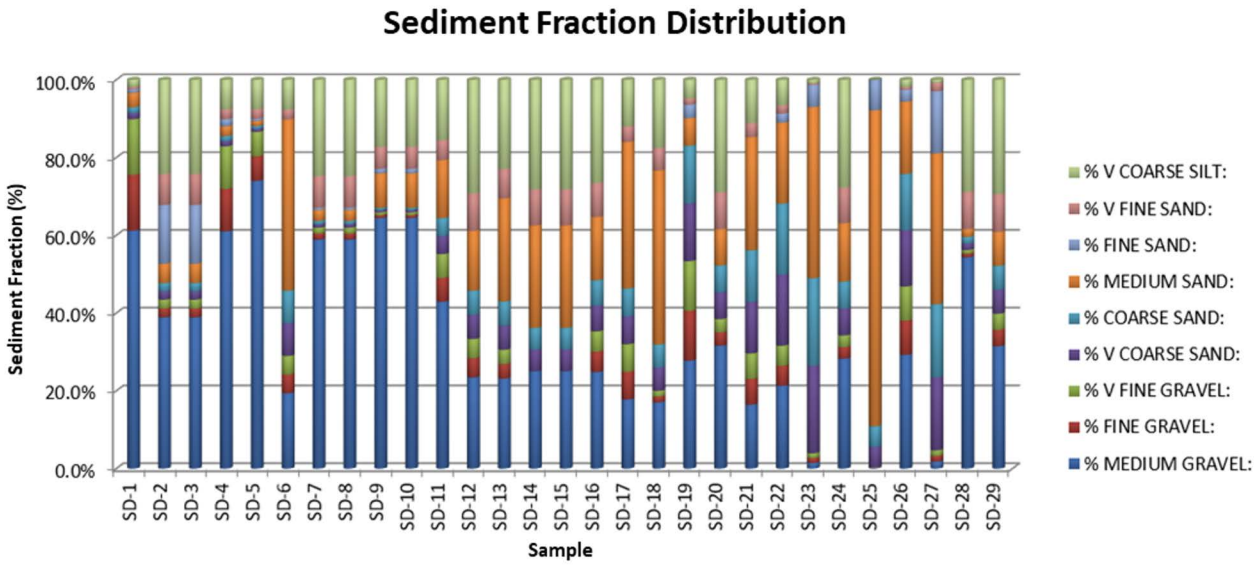

Figure 3. Bed load fraction distribution graph

Statistical Analysis of Sediment Grains

Statistical analysis serves to describe the frequency distribution of grain sizes, typically expressed through four parameters: mean, sorting, skewness, and kurtosis. The mean represents the arithmetic average of various grain sizes within a sediment sample. Sorting, indicated by the standard deviation, illustrates the width of the distribution around the mean. Skewness measures the asymmetry of the distribution, while kurtosis indicates the peak or flatness compared to a normal distribution (Dyer, 1996; Oyedotun, 2022). The equations and methods employed for statistical analysis of sediment grains

and classification in this research follow the Folk and Ward Method (Blott, 2010; Blott and Pye, 2001; Folk and Ward, 1957; Raj and Nilanjana, 2021). The results of the statistical values of sediment grain size measurement are presented in Table 5.

Average Sediment Grain Size (Mean)

The average grain size serves as an index to measure grain size distribution within a sample, representing the weighted percentage of each fraction. This value is indicative of the predominant grain size within the sample and can provide insights into the energy dynamics driven by water flow or wind in the area (Folk and Ward, 1957; Friedman, 1967; Sakai and Hotta, 2023).

The average grain size of sediments in the study area ranges from 261.1 µm to 2657.5 µm, categorizing the sediment as very fine sand (refer to Table 6). The presence of sand-sized bed loads indicates strong currents capable of forming sand sediment deposits in the area (Nybakken, 1992; Phillipe et al., 2022) Similarly, (Rifardi, 2012) notes that dominance of coarse sediment grains suggests significant flow strength anchoring the sediment, while dominance of fine/small sediment indicates weaker flow energy responsible for sediment transport.

Sediment Grain Sorting

Sorting is an indicator of sediment grain uniformity, reflects the level of uniformity of sediment grains (Rachman et al., 2021). A smaller sorting value indicates better sorting, resulting in more uniform sediment grain sizes, whereas a larger sorting value suggests poorer sorting and less uniform grain sizes (Rifardi, 2012; Blott, 2010; Blott and Pye, 2001; Campmans & Wijnberg, 2022). Sorting provides insights into particle size limits, sediment type, flow characteristics, and sediment transport duration from the sediment source. In the research area, sorting varies from moderately sorted (1 sample) to very poorly sorted (23 samples). Well-sorted sediment grains indicate a stable current environment with relatively uniform grain size deposition, while poorly sorted grains suggest an unstable current environment with varying grain sizes. This variability implies fluctuations in current strength, with periods of strong currents followed by weaker currents under different conditions.

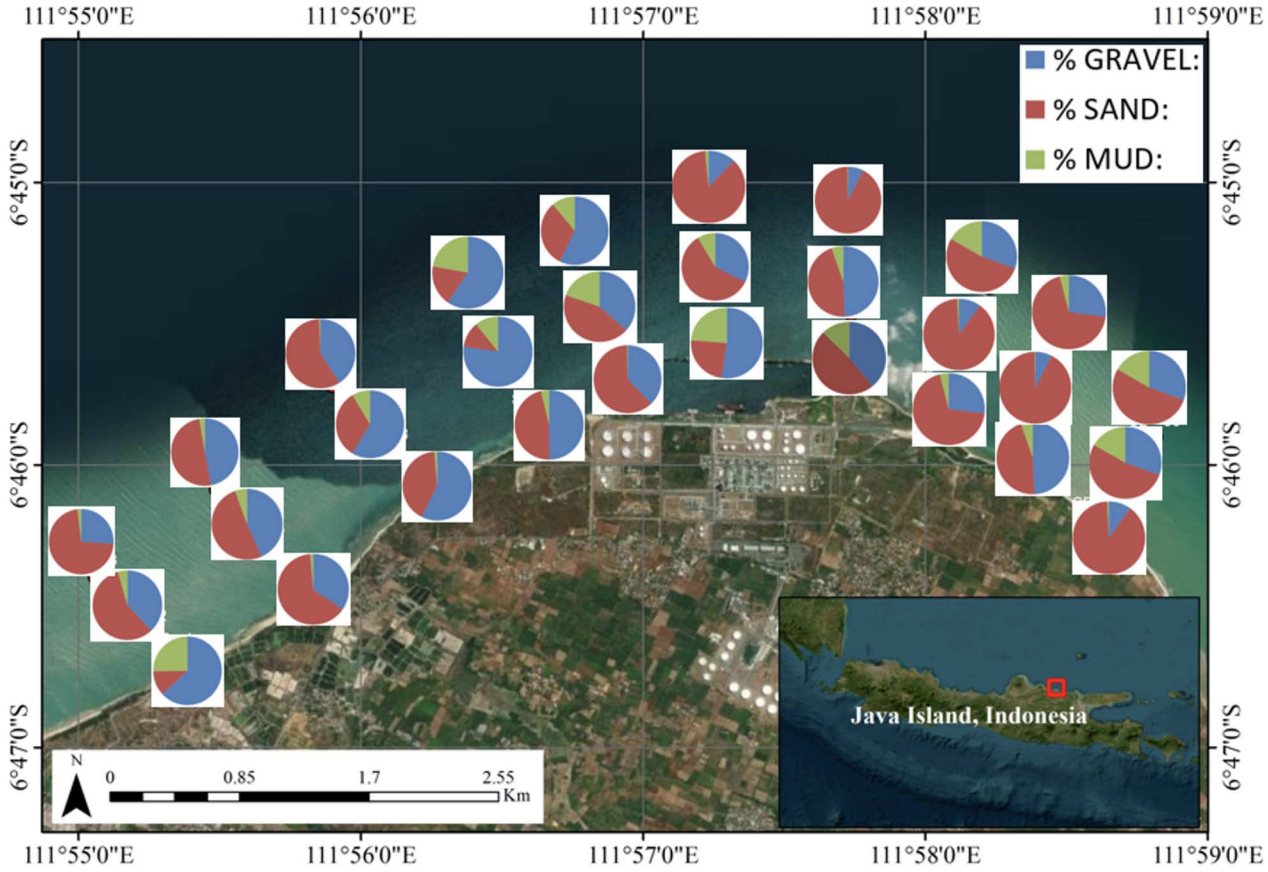

Figure 4. Distribution map of bed load fractions at each sampling location

Based on the sorting analysis of sediment grains in the research area, they are classified as moderately well sorted at 2 locations, moderately sorted at 1 location, poorly sorted at 4 locations, and predominantly very poorly sorted at 23 locations (refer to Table 6). This indicates stable current strength in the waters, with consistent conditions of stable currents that do not fluctuate over time. This stability may be influenced by river discharge entering the sea waters around the research area.

Dominance of Sediment Grain Size (Skewness)

The skewness characterizes the predominant direction of grain size distribution within a population, indicating whether it leans towards coarse-grained or fine-grained sediment, or exhibits symmetry (Rifardi, 2008; Khalil, 2023). A positive skewness value suggests a tendency towards fine grained sediment, while a negative skewness value indicates a tendency towards coarse-grained sediment. Skewness is influenced by wave and current characteristics, making it a valuable indicator of their strength in the deposition process. Based on statistical analysis results, the bed load in the study area predominantly exhibits positive skewness, with 21 out of 30 samples showing positive values, while only 9 samples exhibit negative values (refer to Table 6). Positive values indicate fine skewed to very fine skewed or symmetrical distributions, while negative values indicate very coarse skewed to coarse skewed distributions. This suggests that the aquatic environment in the study area is characterized by a predominance of fine-grained sediment and relatively weak currents.

Sediment Grain Size Distribution (Kurtosis)

The kurtosis measures the peak of the distribution curve and is indicative of the spread of the normal distribution (Rifardi, 2008; Perera et.al., 2023). A mesokurtic distribution curve is moderately peaked, neither too sharp nor too flat. A leptokurtic curve is sharply peaked, indicating a dominant sediment size in the distribution, while a platykurtic curve is flat, suggesting uniform sediment size distribution. Based on statistical analysis results, nearly all bed load samples in the study area exhibit very platykurtic distribution (24 samples) (refer to Table 6). This indicates dominance of a specific sediment grain size, namely very fine sand sediment, in the study area.

Table 5. Results of bed load texture analysis

	SD-1	SD-2	SD-3	SD-4	SD-5	SD-6	SD-7	SD-8	SD-9	SD-10
TEXTURAL GROUP:	Gravel	Muddy Sandy Gravel	Muddy Sandy Gravel	Gravel	Gravel	Gravelly Muddy Sand	Muddy Gravel	Muddy Gravel	Muddy Gravel	Muddy Gravel
(d90 / d10):	0.200	-0.669	-0.669	-0.742	-0.570	-1.067	-0.391	-0.391	-0.296	-0.296

	SD-11	SD-12	SD-13	SD-14	SD-15	SD-16	SD-17	SD-18	SD-19	SD-20
TEXTURAL GROUP:	Muddy Sandy Gravel	Muddy Sandy Gravel	Muddy Sandy Gravel	Gravelly Muddy Sand	Gravelly Muddy Sand	Muddy Sandy Gravel	Muddy Sandy Gravel	Gravelly Muddy Sand	Muddy Sandy Gravel	Muddy Sandy Gravel
(d90 / d10):	-0.946	-1.058	-1.168	-0.877	-0.877	-1.030	-1.068	-1.231	-0.545	-0.998

	SD-21	SD-22	SD-23	SD-24	SD-25	SD-26	SD-27	SD-28	SD-29	SD-30
TEXTURAL GROUP:	Gravelly Muddy Sand	Sandy Gravel	Slightly Gravelly Sand	Muddy Sandy Gravel	Slightly Gravelly Sand	Sandy Gravel	Slightly Gravelly Sand	Muddy Gravel	Muddy Sandy Gravel	Slightly Gravelly Muddy Sand
(d90 / d10):	-1.189	-0.638	-2.656	-0.906	2.383	-0.503	-3.369	-0.147	-0.841	3.613

Table 6. Results of statistical analysis of sediment granules

Sample Code		SD-1	SD-2	SD-3	SD-4	SD-5	SD-6	SD-7	SD-8	SD-9	SD-10
FOLK AND WARD METHOD (Description)	MEAN:	5409.4	434.0	434.0	4091.8	4706.2	1035.9	1161.6	1161.6	1196.7	1196.7
	SORTING:	1.573	5.363	5.363	2.601	1.777	5.433	4.651	4.651	4.155	4.155
	SKEWNESS:	-2.738	-0.003	-0.003	-1.809	-5.931	0.481	-1.917	-1.917	-2.145	-2.145
	KURTOSIS:	0.618	0.294	0.294	1.087	-75.655	0.864	0.330	0.330	0.539	0.539
FOLK AND WARD METHOD (Description)	MEAN:	Fine Gravel	Medium Sand	Medium Sand	Fine Gravel	Fine Gravel	Very Coarse Sand	Very Coarse Sand	Very Coarse Sand	Very Coarse Sand	Very Coarse Sand
	SORTING:	Moderately Well Sorted	Very Poorly Sorted	Very Poorly Sorted	Poorly Sorted	Moderately Sorted	Very Poorly Sorted	Very Poorly Sorted	Very Poorly Sorted	Very Poorly Sorted	Very Poorly Sorted
	SKEWNESS:	Very Fine Skewed	Symmetrical	Symmetrical	Very Fine Skewed	Very Fine Skewed	Very Coarse Skewed	Very Fine Skewed	Very Fine Skewed	Very Fine Skewed	Very Fine Skewed
	KURTOSIS:	Very Platykurtic	Very Platykurtic	Very Platykurtic	Mesokurtic	Very Platykurtic	Platykurtic	Very Platykurtic	Very Platykurtic	Very Platykurtic	Very Platykurtic
Percentage	Gravel	89.9%	43.4%	43.4%	82.9%	86.6%	29.0%	62.0%	62.0%	65.9%	65.9%
	Sand	8.3%	32.3%	32.3%	9.5%	5.8%	63.3%	13.3%	13.3%	16.8%	16.8%
	Mud	1.9%	24.2%	24.2%	7.6%	7.6%	7.7%	24.8%	24.8%	17.3%	17.3%
Sample Code		SD-11	SD-12	SD-13	SD-14	SD-15	SD-16	SD-17	SD-18	SD-19	SD-20
FOLK AND WARD METHOD (Description)	MEAN:	1341.0	603.4	606.8	519.7	519.7	638.1	665.4	585.1	2332.7	726.8
	SORTING:	6.471	7.394	7.370	6.596	6.596	7.327	6.298	7.706	4.213	7.401
	SKEWNESS:	-0.928	0.078	0.120	0.096	0.096	0.032	0.116	0.239	-0.355	-0.140
	KURTOSIS:	0.434	0.360	0.400	0.454	0.454	0.344	0.647	1.407	0.693	0.319
FOLK AND WARD METHOD (Description)	MEAN:	Very Coarse Sand	Coarse Sand	Coarse Sand	Coarse Sand	Coarse Sand	Coarse Sand	Coarse Sand	Coarse Sand	Very Fine Gravel	Coarse Sand
	SORTING:	Very Poorly Sorted	Very Poorly Sorted	Very Poorly Sorted	Very Poorly Sorted	Very Poorly Sorted	Very Poorly Sorted	Very Poorly Sorted	Very Poorly Sorted	Very Poorly Sorted	Very Poorly Sorted
	SKEWNESS:	Very Fine Skewed	Symmetrical	Coarse Skewed	Symmetrical	Symmetrical	Symmetrical	Coarse Skewed	Coarse Skewed	Very Fine Skewed	Fine Skewed
	KURTOSIS:	Very Platykurtic	Very Platykurtic	Very Platykurtic	Very Platykurtic	Very Platykurtic	Very Platykurtic	Very Platykurtic	Leptokurtic	Platykurtic	Very Platykurtic
Percentage	Gravel	55.2%	33.3%	30.6%	25.0%	25.0%	35.3%	32.0%	20.0%	53.4%	38.5%
	Sand	29.3%	37.4%	46.5%	46.8%	46.8%	38.2%	56.0%	62.5%	41.8%	32.6%
	Mud	15.6%	29.2%	23.0%	28.2%	28.2%	26.5%	12.0%	17.5%	4.8%	28.9%
Sample Code		SD-21	SD-22	SD-23	SD-24	SD-25	SD-26	SD-27	SD-28	SD-29	SD-30
FOLK AND WARD METHOD (Description)	MEAN:	1140.7	1458.8	573.8	584.6	330.6	1883.5	494.5	1105.9	628.4	104.9
	SORTING:	5.578	4.655	2.083	6.773	1.437	4.298	2.273	4.407	6.446	2.936
	SKEWNESS:	0.232	-0.027	0.282	-0.006	0.217	0.032	0.304	-2.098	-0.222	0.593
	KURTOSIS:	0.970	0.687	0.771	0.312	2.039	0.559	0.835	0.348	0.303	0.923
FOLK AND WARD METHOD (Description)	MEAN:	Very Coarse Sand	Very Coarse Sand	Coarse Sand	Coarse Sand	Medium Sand	Very Coarse Sand	Medium Sand	Very Coarse Sand	Coarse Sand	Very Fine Sand
	SORTING:	Very Poorly Sorted	Very Poorly Sorted	Poorly Sorted	Very Poorly Sorted	Moderately Well Sorted	Very Poorly Sorted	Poorly Sorted	Very Poorly Sorted	Very Poorly Sorted	Poorly Sorted
	SKEWNESS:	Coarse Skewed	Symmetrical	Coarse Skewed	Symmetrical	Coarse Skewed	Symmetrical	Very Coarse Skewed	Very Fine Skewed	Fine Skewed	Very Coarse Skewed
	KURTOSIS:	Mesokurtic	Platykurtic	Platykurtic	Very Platykurtic	Very Leptokurtic	Very Platykurtic	Platykurtic	Very Platykurtic	Very Platykurtic	Mesokurtic
Percentage	Gravel	29.6%	31.6%	3.9%	34.2%	0.3%	46.8%	4.7%	56.2%	39.9%	4.3%
	Sand	59.2%	61.8%	95.0%	38.0%	99.7%	51.2%	94.5%	14.9%	30.7%	56.8%
	Mud	11.1%	6.6%	1.0%	27.7%	0.0%	1.9%	0.8%	28.9%	29.4%	38.9%

CONCLUSIONS

The sediment texture characteristics of most of the bed load in the study area is classified as very fine sand. Statistically, the fraction is dominated by sand, which ranges from 11.8% to 92.2%. The sediment gradation varies, with some portions classified as good due to grain size variations. The average sediment grain size falls within the range of 261.1 µm to 2657.5 µm. Overall, the sorting is predominantly very poorly sorted, indicating an environment dominated by fine-grained sediment and relatively weak currents. The sediment distribution curve is classified as very platykurtic, suggesting dominance of a specific grain size, particularly very fine sand sediment. These findings indicate that the bed load in these waters has good soil bearing capacity, making it highly suitable for port revitalization.

ACKNOWLEDGEMENTS

We extend our sincere gratitude to the management and staff of the PRTH-BRIN Hydrodynamic Technology Research Center, the BTIPDP-BPPT 2020 Topo-Hydro Survey Laboratory survey team, and the members of the BTIPDP-BPPT 2020 Geotechnical and Soil Mechanics Laboratory. Special thanks also go to all the contributors involved in the Port Infrastructure and Coastal Dynamics Technology Services activities, particularly the Current and Sediment Hydrooceanographic Survey team of PT. TPPI Tuban, for their invaluable efforts during the 2020 fiscal year.

REFERENCES

Affandi, A. K., and Surbakti, H., 2012. Distribusi Sedimen Dasar di Perairan Pesisir Banyuasin, Sumatera Selatan. *Maspari Journal*, 4(1): 33–39.

Ali, M. N., Hariadi, and Satriadi, A., 2017. Analisa Pengaruh Arus Terhadap Sebaran Sedimen Dasar di Pantai Ujungnegoro Batang, Jawa Tengah. *Jurnal Oseanografi*, 6(1): 288–294.

Andayani, D., Suryoputro, A. A. D., Atmodjo, W., Satriadi, A., and Subardjo, P., 2020. Studi Tranpor Sedimen di Perairan Muara Sungai Bodri, Kabupaten Kendal. *Indonesian Journal of Oceanography*, 2(3): 1–10.

Anggraini, R. R., Yanuhar, U., and Risjani, Y., 2020. Characteristic Of Sediment At Lekok Coastal Waters, Pasuruan Regency, East Java. *Jurnal Ilmu Dan Teknologi Kelautan Tropis*, 12(1): 235–246. https://doi.org/10.29244/jitkt.v12i1.28705

Ansari, A., Apriansyah, and Risko., 2020. Distribusi Sedimen Dasar di Perairan Muara Mempawah Kalimantan Barat Distribution Sediment of Bedload at the Estuary Waters Mempawah, West Borneo. *Jurnal Laut Khatulistiwa*, 3(2): 48. http://jurnal.untan.ac.id/index.php/lk

Blott, S. J., and Pye, K., 2001. Gradistat: A Grain Size Distribution and Statistics Package for The Analysis of Unconsolidated Sediments. *Earth Surface Processes and Landforms*, 26(11): 1237–1248. https://doi.org/10.1002/esp.261

Blott, S. J., 2010. Gradistat: A Grain Size Distribution and Statistics Package for the Analysis of Unconsolidated Sediments by Sieving or Laser Granulometer. In *Earth Surface Processes and Landforms*.

BPPT., 2021. *Standar Petunjuk Pengujian Mekanika Tanah. Edisi-4, Revisi-0, ND:SPP.BTIPDP.LUG.01.02*.

BSN., 2008a. *SNI 1964:2008 Cara Uji Berat Jenis Tanah*.

BSN., 2008b. *SNI 3423:2008 Cara Uji Analisis Ukuran Butir Tanah*.

BSN., 2019. SNI 6989.3:2019 Cara Uji Padatan Tersuspensi Total (Total Suspended Solids) Secara Gravimetri. In BSN (Ed.), *Badan Standarisasi Nasional*. Badan Standarisasi Nasional. http://lib.atk.ac.id/index.php?p=show_detail&id=7467&keywords=

Budiyanto, E.H., 2022. *Konsep Pengembangan Manajemen Kontinuitas Bisnis Dengan Pendekatan Baru di Sektor Penyedia Jasa Pelabuhan*.

Campmans, G.H.P., & Wijnberg, K.M. 2022. Modelling the vertical grain size sorting process in aeolian sediment transport using the discrete element method. *Aeolian Research*, 57: 100817. https://doi.org/10.1016/j.aeolia.2022.100817

Caroline, A.P., Rodrigo, P.M., Quirijn, de, J.L., Fabrício, A.P., Paulo, I.G., 2023. Particle arrangement and internal porosity of coarse fragments affect water retention in stony

soils. *European Journal of Soil Science*, https://doi.org/10.1111/ejss.13382.

Chunliu, Y., Jianhua, W., Peiyue, L., Yuanhang, W., Ningning, Y., 2023. Evaluation of Soil-Water Characteristic Curves for Different Textural Soils Using Fractal Analysis. *Water*, https://doi.org/10.3390/w15040772

Diposaptono, S., 2011. *Mengantisipasi Bencana Gempa Bumi, Tsunami, Banjir, Abrasi, Pemanasan Global dan Semburan Lumpur Sidoarjo : Sebuah Kumpulan Pemikiran*. Penerbit Buku Ilmiah Populer.

Dwianti, R. F., Widada, S., and Hariadi., 2017. Distribusi Sedimen Dasar Di Perairan Pelabuhan Cirebon. *Jurnal Oseanografi*, 6(1): 228–235. http://ejournal-s1.undip.ac.id/index.php/jose.50275

Dwinanto, A. W., Purba, N. P., Harahap, S. A., Mega, D., and Syamsudin, L., 2017. Pola Arus Dan Transpor Sedimen Pada Kasus Pembentukan Tanah Timbul Pulau Puteri Kabupaten Karawang. *Jurnal Perikanan Dan Kelautan*, VIII(2): 152–160.

Dyer, K. R., 1996. *Coastal and Estuarine Sediment Dynamics*. John Wiley and Sons Ltd.

Folk, R. L., and Ward, W. C. W., 1957. Brazos River Bar : A Study in The Significance of Grain Size Parameters. *Journal of Sedimentary Petrology*, 27(1): 3–26.

Friedman, G., 1967. Dynamics Processes and Statistical Parameters Compared for Size Frequency Distribution of Beach and Riversands. *Journal of Sedimentary Petrology*, 37: 327–354.

Hambali, R., and Apriyanti, Y., 2016. Studi Karakteristik Sedimen dan Laju Sedimentasi Sungai Daeng – Kabupaten Bangka Barat. *Jurnal Fropil*, 4(2): 165–174.

Hamdani., 2013. Kajian Teknologi Sand by Passing Penanggulangan Sedimentasi dan Erosi Pantai Bengkulu (Pelabuhan Pulau Baai. *Jurnal Media Komunikasi Teknik Sipil*, 19(1): 77–87.

Hardiyatmo, H. C., 2002. *Mekanika Tanah I*. Gadjah Mada University Press.

Junaidi, and Wigati, R., 2011. Analisis Parameter Statistik Butiran Sedimen Dasar Pada Sungai Alamiah (Studi Kasus Sungai Krasak Yogyakarta. *Wahana Teknik Sipil*, 16(2): 46–57.

Khalil, R., 2023. Grain-Size Analysis of Middle Cretaceous Sandstone Reservoirs, the Wasia Formation, Riyadh Province, Saudi Arabia. *Sustainability*, 15(10): 7983. http://doi.org/10.3390/su15107983

Liu, C., Fu, S., Li, Z., Zhang, Z., and Zeng, J., 2023. Effects of Sediment Characteristics on The Sediment Transport Capacity of Overland Flow. *International Soil and Water Conservation Research*, 11(1): 75–85. https://doi.org/10.1016/j.iswcr.2022.06.003

Melisa, W., Hariyadi, Widada, S., Indrayanti, E., Sugianto, D. N., Usmunarti, D. H., and Yusuf, M., 2020. Studi Pengaruh Longshore Current Terhadap Abrasi di Pantai Moro, Kabupaten Kendal, Jawa Tengah. *Indonesian Journal of Oceanography*, 02(04): 1–10.

Mengual, B., Hir, P., Rivier, A., Caillaud, M., & Grasso, F., 2020. Numerical modeling of bedload and suspended load contributions to morphological evolution of the Seine Estuary (France). *International Journal of Sediment Research*. https://doi.org/10.1016/j.ijsrc.2020.07.003.

Mir, B., 2021. Specific Gravity of Soil Solids. *Manual of Geotechnical Laboratory Soil Testing*. https://doi.org/10.1201/9781003200260-3.

Muhardi, M., Nurrahman, Y. A., Risko, R., Muliadi, M., Rahayu, K., and Susiati, H., 2022. Statistical Parameters Analysis Of Sediment Grain Size From Raya River Bengkayang Regency, West Borneo. *Bulletin Of The Marine Geology*, 36(2). https://doi.org/10.32693/bomg.36.2.2021.726

Nazir, M., 1983. *Metode Penelitian*. Ghalia Indonesia.

Notteboom, T., Pallis, A., and Rodrigue, J.-P., 2022. *Port Economics, Management and Policy*.

Nugroho, S. H., and Basit, A., 2014. Sebaran Sedimen Berdasarkan Analisis Ukuran Butir Di Teluk Weda, Maluku Utara. *Jurnal Ilmu Dan Teknologi Kelautan Tropis*, 6(1): 229–240. http://itk.fpik.ipb.ac.id/ej_itkt61

Nybakken, J. W., 1992. *Biologi Laut: Suatu Pendekatan Ekologis*. PT Gramedia.

Oyedotun, T. D. T., 2022. Compositional and Multivariate Statistical Analyses for Grain-size Characterisation of Intertidal Sedimentary Facies in an Estuarine Environment. *Geology, Ecology, and Landscapes*, 6(3): 224–230. https://doi.org/10.1080/24749508.2020.1814186.

Pasaribu, R., Irwan, A., and Pattirane, C., 2021. Perencanaan Bangunan Pelindung Pantai Untuk Pencegahan Abrasi Di Pantai Utara Karawang. *Jurnal Kelautan Nasional*, 16(3): 223–236.

Perera, U.L.H.P., Ratnayake, A.S., Weerasingha, W.A.D.B., 2023. Grain size distribution of modern beach sediments in Sri Lanka. *Anthropocene Coasts,* 6(10). https://doi.org/10.1007/s44218-023-00025-7

Permana, H., Hariadi, and Rochaddi, B., 2012. Kajian Kondisi Arus dan Sedimen Dasar Pada Saat Musim Timur di Perairan Semarang-Demak. *Journal of Oceanography*, 1(1): 121–128. Link: https://ejournal3.undip.ac.id/index.php/joce/article/view/4139/4021.

Phillipe, R., Tobias, B., Pereira, R., Fábio, Veríssimo, G., 2022. Bedload Sediment Transport Estimation in Sand-Bed Rivers Comparing Traditional Methods and Surrogate Technologies. Applied Sciences 13(1), https://doi.org/10.3390/app13010005

Polrot, A., Kirby, J., Birkett, J., & Sharples, G., 2021. Combining sediment management and bioremediation in muddy ports and harbours: A review. *Environmental pollution*, 289 pp. 117853. https://doi.org/10.1016/j.envpol.2021.117853.

Ponce, V. M., 1989. *Engineering Hydrology Principles and Practice*. Prentice-Hall Inc.

Pu, J., Chen, Y., Su, M., Mei, J., Yang, X., Yu, Z., & Yao, P., 2022. Residual Sediment Transport in the Fine-Grained Jiangsu Coast under Changing Climate: The Role of Wind-Driven Currents. *Water*. https://doi.org/10.3390/w14193113.

Purba, J. R., Setiyono, H., Atmodjo, W., Muslim, and Widada, S., 2022. Pengaruh Kondisi Oseanografi Terhadap Pola Sebaran Sedimen Dasar di Perairan Mangunharjo, Kota Semarang. *Indonesian Journal of Oceanography*, 01: 77–87. https://doi.org/10.14710/ijoce.v%vi%i.13214

Rachman, R. A., and Wibowo, M., 2019. Kajian Karakteristik Sedimen Dasar Laut untuk Mendukung Rencana Pembangunan Pelabuhan Patimban. *Jurnal Geologi Kelautan*, 17(2): 99–111. http://www.mgi.esdm.go.id

Rachman, R. A., and Wibowo, M., 2022. Kajian Sedimen Tersuspensi di Muara Sungai Jelitik untuk Mendukung Pengembangan Kawasan Ekonomi Khusus Sungailiat, Kabupaten Bangka. *Buletin Oseanografi Marina UNDIP*, 11(3): 255–262.

Rachman, R. A., Wibowo, M., Wiguna, E. A., Nugroho, S., Madyani, and Santoso, B., 2021. Kajian Karakteristik Sedimen Dasar di Perairan Sungailiat untuk Mendukung Pengembangan Pelabuhan Perikanan Nusantara Sungailiat, Kab. Bangka. *Buletin Oseanografi Marina UNDIP*, 10(2): 112–122.

Raj, K.B., and Nilanjana, D.C., 2021. Sediment Grain Size Analysis and Mining Intensity: Estimation by GRADISTAT, G-STAT and LDF Techniques. https://doi.org/10.1007/978-3-030-72296-8_4

Rashid, A. S. A., Kalatehjari, R., Hashim, N. A., Yunus, N. M., and Noor, N. M., 2017. Determination of Soil Specific Gravity by Using Partially Vacuum and Shaking Methods. *Journal of The Institution of Engineers (India): Series A*, 98(1–2): 25–28. https://doi.org/10.1007/s40030-017-0201-7

Rifardi., 2008. *Tekstur Sedimen (Sampling dan Analisis)*. UNRI Press.

Rifardi., 2012. *Ekologi Sedimen Laut Modern*. UNRI Press.

Rosyidi, H., 2015. *Analisis Dampak Pengerukan Alur Pelayaran Pada Daya Saing Pelabuhan, Studi Kasul: Pelabuhan Tanjung Perak Surabaya*.

Saepuloh, A., Pebrina, D., Utami, E. N., Kurniawan, H., Ramadhan, M., Oktaviani, N., Saely, S., and Sutrisno., 2017. *Analisis Mengenai Dampak Lingkungan (AMDAL) Studi Kasus Proyek Infrastruktur Pelabuhan*.

Sakai, Y., & Hotta, N., 2023. Laboratory investigation of the effects of grain size on the dynamics of debris flows: Measurement of pore fluid pressure in an open channel. *E3S Web of Conferences*. https://doi.org/10.1051/e3sconf/202341501022.

Salam, A. K., 2020. *Ilmu Tanah* (2nd ed., Vol. 2). Global Madani Press. www.globalmadani.sch.id

Siry, H. Y., 1990. Studi Sebaran Sedimen Dasar Dan Pendangkalan Di Pelabuhan Minyak (Oil Wharves) Pt Caltex Pacific Indonesia Dumai, Riau Pascapengerukan 1990 Study And Distribution In Oil Ports Shallowing Sediments (Oil Wharves) Pt Caltex Pacific Indonesia Dumai, Riau 1990 Post-Dredging. *Widyariset*, 14(3): 643–650.

Supiyati, Suwarsono, and Setiawan, I., 2011. Angkutan Sedimen Penyebab Pendangkalan Pelabuhan Pulau Baai Bengkulu Dengan Model Diskritisasi Dinamika Oseanografi. *Jurnal Dinamika Teknik Sipil*, 11(2): 172–180.

Thunyaphun, T., Umeda, S., & Yuhi, M., 2023. Sediment Budget and Net Sediment Transport on a Coast Dominated by Waves and Offshore Currents: A Case Study on the Ishikawa Coast and Its Surrounding Areas in Japan. *Journal of Marine Science and Engineering*. https://doi.org/10.3390/jmse11030621.

Triatmodjo, B., 1999. *Teknik Pantai* (8th Edition 2016). Beta Offset.

Tianyu, H., Jiangjun, L., Lubo, L., 2022. Impact of Hydrochar Amendment on the Water Retention Capability of Agricultural Soil. https://doi.org/10.1061/9780784484258.015

Umar, H., Baeda, A. Y., Husain, F., and Taufiqurrahman., 2020. Study of Longshore Sediment Transport on Erosion and Sedimentation Beaches in South Sulawesi. *IOP Conference Series: Materials Science and Engineering*, 875(1). https://doi.org/10.1088/1757-899X/875/1/012075

Volkov, D. S., Rogova, O. B., and Proskurnin, M. A., 2021. Organic Matter and Mineral Composition of Silicate Soils: FTIR Comparison Study by Photoacoustic, Diffuse Reflectance, and Attenuated Total Reflection Modalities. *Agronomy*, 11(9). https://doi.org/10.3390/agronomy11091879

Wahyudi, and Jupantara, 2004. Studi Simulasi Sedimentasi Akibat Pengembangan Pelabuhan Tanjung Perak Surabaya. *Jurnal Teknologi Kelautan*, 8(2): 74–85.

Wibowo, M., 2018. Study Of Sedimentation In The Water Of Patimban Port Development Plan Using Computation Modeling. *Jurnal Kelautan Nasional*, 13(1): 1–14. https://doi.org/10.15578/jkn.v1i1.6270.

Zi, NW, Limin Z, Xu, Guang, F., 2023. Theoretical analysis for bedload particle deposition and hop statistics. *Journal of Fluid Mechanics*, 954 Available from: https://doi.org/10.1017/jfm.2022.959

STUDY OF HEAVY METAL LEAD (PB) CONTENT IN THE CORAL REEF ENVIRONMENT OF PANJANG ISLAND, BANTEN

STUDI KANDUNGAN LOGAM BERAT TIMBAL (PB) PADA LINGKUNGAN TERUMBU KARANG DI PERAIRAN PULAU PANJANG, BANTEN

Ahmad Al Fauzan[1], Dwi Amanda Utami[2], Rima Rachmayani[1], Ayu Utami Nurhidayati[2]

[1] Oceanography Study Program - Institut Teknologi Bandung, Jl. Ganesha No. 10, 40132 Bandung, Indonesia

[2] Research Center for Climate and Atmosphere - National Research and Innovation Agency Republic of Indonesia, Jl. Cisitu Sangkuriang, 40135 Bandung, Indonesia

*Corresponding author: aalfauzan@students.itb.ac.id

(Received 12 November 2023; in revised from 20 November 2023; accepted 12 February 2024)

DOI : 10.32693/bomg.39.1.2024.862

ABSTRACT: Rapid industrial expansion in Banten has triggered a surge in pollution, impacting areas like Panjang Island in Banten Bay. Pollution on Panjang Island stems primarily from industrial operations and shipping activities. This study investigates the distribution of lead (Pb) metal concentrations in Panjang Island's coral reef environment, focusing on sediment and surface water. It also examines how seasonal variations, influenced by ocean currents, affect Pb concentration distribution. Data were gathered using purposive sampling, collecting sediment samples, surface water samples, and oceanographic data. Pb levels in both sediments and surface water underwent analysis at the National Research and Innovation Agency (BRIN) laboratory, employing atomic absorption spectrophotometry (AAS). Our findings indicate that during the transitional II season, Pb concentrations in sediment ranged from 4.2 to 17 mg/kg, while the westerly season showed Pb concentrations spanning 3.8 to 23.4 mg/kg. Surface water during these seasons exhibited Pb concentrations varying from 0 to 0.03 mg/l. Notably, at several monitoring stations, surface water Pb concentrations exceeded the threshold set by Regulation No. 22 of 2021, suggesting potential harm to the coral reef ecosystem surrounding Panjang Island. Elevated Pb concentrations were observed during the transitional II season in the island's western part and the westerly season in the eastern part. These disparities appear to be influenced by the direction of ocean currents, highlighting their role in shaping Pb distribution in Panjang Island's waters.

Keywords: Lead (Pb), sediment, surface water, transitional II season, westerly season, Panjang Island

ABSTRAK: *Perkembangan industri yang cepat di Banten telah menyebabkan peningkatan polusi yang signifikan. Pulau Panjang yang terletak di Teluk Banten merupakan salah satu pulau yang terkena dampaknya. Aktivitas industri dan lalu lintas kapal secara signifikan berkontribusi pada polusi di Pulau Panjang. Tujuan dari penelitian ini adalah untuk menentukan distribusi konsentrasi logam timbal (Pb) dalam sedimen dan air permukaan di lingkungan terumbu karang Pulau Panjang, serta untuk menilai pengaruh musim (arus laut) terhadap distribusi konsentrasi Pb. Pengumpulan data dilakukan menggunakan metode pengambilan sampel yang melibatkan sampel sedimen, sampel air permukaan, dan parameter arus laut. Pb dalam sedimen dan air permukaan dianalisis di laboratorium Badan Riset dan Inovasi Nasional (BRIN) menggunakan metode Spektrofotometri Serapan Atom (SSA). Berdasarkan hasil penelitian menunjukkan bahwa selama musim transisi II, kandungan logam Pb dalam sedimen berkisar antara 4,2 - 17 mg/kg, sementara musim barat menunjukkan kandungan Pb berkisar antara 3,8 hingga 23,4 mg/kg. Di air permukaan, konsentrasi Pb selama musim transisi II dan musim barat berkisar antara 0 - 0,03*

mg/l. Beberapa stasiun menunjukkan konsentrasi Pb di air permukaan melebihi ambang batas yang ditetapkan oleh PP. No. 22 tahun 2021, dengan potensi merugikan terhadap kondisi terumbu karang di perairan Pulau Panjang. Konsentrasi Pb yang lebih tinggi di perairan Pulau Panjang selama musim transisi II di bagian barat dan selama musim barat di bagian timur. Perbedaan ini tampak dipengaruhi oleh arah pergerakan arus laut yang berperan dalam membentuk sebaran Pb di perairan Pulau Panjang.

Kata Kunci: *Timbal, sedimen, permukaan air, musim peralihan II, musim barat, Pulau Panjang*

INTRODUCTION

Heavy metals, characterized by their density exceeding 5 g/cm³ (Holleman and Wiberg, 1985), encompass around 40 elements, including lead (Pb), cadmium (Cd), chromium (Cr), iron (Fe), and silver (Ag), among others. These metals can originate from natural processes like rock weathering and atmospheric deposition, but human activities such as industrialization and urbanization contribute significantly to heavy metal contamination. They are most prevalent in soils and aquatic ecosystems (Sharma and Agrawal, 2005), often entering marine waters via rivers or atmospheric deposition. The movement of heavy metals is influenced by various factors such as pH, sediment, organic matter, temperature, and other metal concentrations (Falah *et al*., 2020). While trace amounts of heavy metals are essential for metabolic processes, excess amounts can be toxic (Philips, 1980), especially the highly toxic mercury (Hg), Cd, and Pb (Waldhicuk, 1974).

Banten has witnessed rapid industrial growth, resulting in increased waste production, including solid, gas, and liquid waste. Industrial waste has the potential to contribute to the contamination of Banten Bay's waters with heavy metals (Afiyatillah *et al*., 2022). Moreover, activities at the port and industries, particularly ship-related operations, have the potential to release heavy metal waste, including lead (Pb) (Rizkiana *et al*., 2017). Panjang Island, located near industrial areas and ship traffic routes, is a key site with pollution primarily linked to industrial activities and shipping (Falah *et al*., 2020). Notably, lead (Pb) is present in ship paints and fuels, further contributing to its presence in the waters (Rizkiana *et al*., 2017).

Lithology of Panjang is primarily characterized by limestone coral reefs, formed through the accumulation of coral colonies, shell fragments, and mollusks (Rusmana and Suwitodirjo, 2005). The coral reef ecosystem is highly sensitive to environmental changes, encompassing both physical and chemical alterations in the surrounding environment (Guzman and Jimenez, 1992; Al-Rousan et al., 2007). Notably, anthropogenic pollution poses a significant threat to the health of the coral reefs. A recent investigation revealed a notable presence of persistent organic pollutants originating from the burning of plastic waste on the beaches of Panjang Island which can give negative impact for coral reefs health in the island (Utami *et al*., 2023).

Furthermore, given its proximity to industrial areas, there is a growing concern that Panjang Island may be affected by heavy metal pollution resulting from industrial activities. Heavy metals can become integrated into the coral framework through various processes, subsequently impacting coral health and overall ecosystem stability (David, 2003; Al-Rousan et al., 2007). Of particular concern is the elevated presence of Pb, which has been associated with detrimental effects on coral ecosystems. Elevated levels of Pb can induce physiological stress, reduce reproductive success, alter population dynamics, and contribute to coral bleaching (Harland and Brown, 1989; Falkowski *et al*., 1990; Mitchelmore et al., 2007; Sabdono, 2009). The multifaceted impact of heavy metal contamination underscores the need for comprehensive assessments and mitigation strategies to safeguard the ecological integrity of Panjang Island's coral reefs.

Studies on nearby Tunda Island found heavy metal Pb contamination in coral reefs, raising concerns about Panjang Island's coral reef ecosystem. Elevated dissolved heavy metal concentrations in seawater or sediments disrupt aquatic ecosystems, including coral reefs (Razi *et al*., 2023). Given these concerns, it is essential to study heavy metal Pb concentrations in Panjang Island's coral reef environment, considering oceanographic factors such as ocean currents, to assess its current state and potential impact to the coral reef environment. This research aims to determine heavy metal Pb concentrations in sediment and surface water samples, clarifying distribution patterns influenced by oceanographic phenomena around Panjang Island, Banten.

METHODS AND MATERIALS

The study area in this research is Panjang Island, Banten, situated between 6°25'18" to 6°28'12" S and 106°22'9" to 106°25'36" E in the Java Sea (Figure 1). The research focuses on four specific regions: west, north, east, and south, along with measurements conducted on the mainland at Grenyang Port and Gope Beach. Grenyang Port, serving as a transit hub to Panjang Island, represents a potential pollution source from the Bojonegara industrial district west of Panjang Island. Gope Beach, at a river mouth in Banten Bay, indicates potential pollution from river discharge into Banten Bay.

The research employs two main types of data: primary and secondary. Primary data, collected in September 2022 (transitional II season) and February 2023 (westerly season), comprises field data from sediment samples, surface water samples, and oceanographic parameters. These samples were processed at the Geological Engineering Laboratory of the National Research and Innovation Agency (BRIN) and the Chemistry Laboratory of BRIN. Secondary data supports the primary data and includes ocean currents, sourced from Marine Copernicus, and validated with field data collected using drifters (data collected on September 28-29, 2022, and February 8, 2023).

The sample collection process comprised two main categories: sediment and surface water sampling. Sediment sampling involved traversing transects across Panjang Island, including the near coast, reef flat, and reef front in the eastern, southern, western, and northern regions. A total of 12 locations were sampled in both seasons using grab samplers. The sediment samples were collected using an Eckman grab sampler and stored in polyethylene bags. Similarly, surface water sampling followed a transect approach to understand the spatial distribution of Pb metal in the coral reef environment. During the transitional II season, surface water samples were taken from areas near the coast of Panjang Island and the reef front. Additional samples were collected at Grenyang Port and Gope Beach to identify potential sources of pollution in Banten. In the westerly season, surface water sampling expanded to include the reef flat, resulting in a total of 10 and 14 samples, respectively. The water sample then collected using 500 ml polyethylene water sample bottles. The samples were preserved with concentrated HNO_3 with a pH of <2

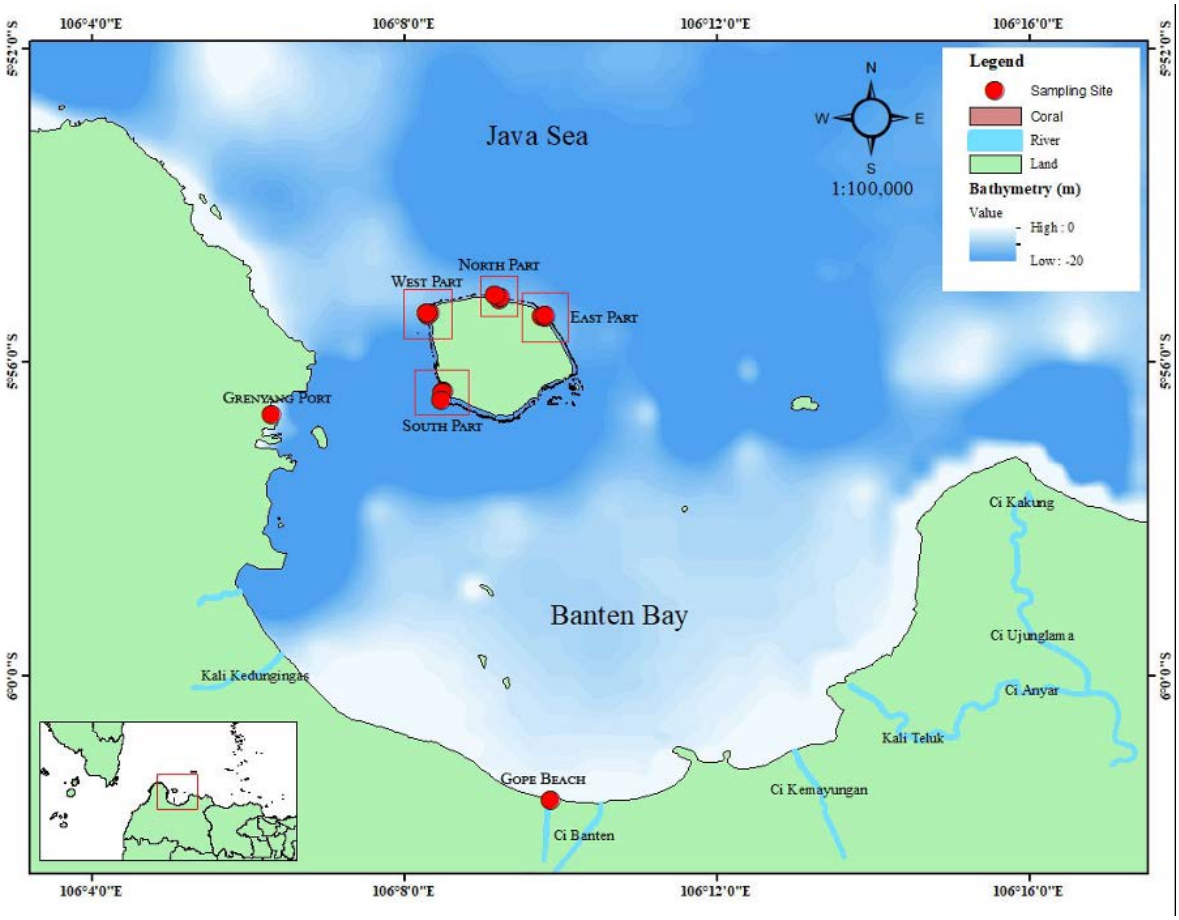

Figure 1. Sampling site location

before being stored in a cool place protected from sunlight.

In the laboratory, sediment samples underwent drying, sieving, sub-sampling, and destruction to enable elemental analysis using atomic absorption spectrophotometry (AAS). Surface water samples were processed similarly, with the addition of dilution and filtration steps. The instrument to measure Pb content in the sediment and water samples were using Shimadzu AA-7000 series Atomic Absorption Spectrophotometers featuring dual atomizer. During laboratory analysis, each sediment sample was divided into three sub-samples to ensure triplicate measurements for quality control. The sub-samples for AAS analysis typically weighed around 0.5000 to 0.5010 grams. Subsequently, the sample destruction process was carried out, transforming the sediment sample into a form that could be measured, enabling the analysis of its elemental content (Asmorowati *et al*., 2020). The sample destruction process commenced by mixing the sediment sample with a solution containing 10 ml of HF, 1 ml of HNO_3, and 1 ml of H_2SO_4. Prior to heating, the sediment sample and the solution were thoroughly mixed to achieve homogeneity. After the heating process, the sample was cooled until all vapors had dissipated. The subsequent step involved mixing the dried and cooled sample with 25 ml of concentrated HCL until homogenous. The mixture was then heated using a hot plate at a temperature of 360°C for 5 minutes and subsequently cooled until no vapor was present. The following step consisted of diluting the sediment sample with distilled water (aquabidest) and filter paper of Whatman Grade 41. During this process, the sample was filtered to remove any impurities. The dilution process was considered complete when the solution reached a volume of 100 mL within a measuring flask. For surface water samples, the preparation involved taking 50 ml of surface water and adding 1 ml of HNO_3. The mixture was then heated until the water sample was reduced to 20 ml. The shrunken sample was transferred into a 50 ml measuring flask using filter paper, and aquabidest was added to reach the flask's capacity. The sample was then shaken within the measuring flask. After that process, sample analysis with AAS can be carried out. In this study the analysis AAS using AA-7000 machine, this type followed the calibration curve quantification method using Pb standard solutions of varying concentrations, namely 0.08, 0.06, 0.04, 0.02, 0.1, and 0.5 ppm.

The Pb concentrations were then compared to quality standards, namely the Sediment Quality Guidelines (SQG) and seawater quality standards as per Regulation No. 22 of 2021 (Indonesian State Gazette). Subsequently, the relationship between Pb concentrations and oceanographic parameters (ocean currents) was qualitatively assessed. The pollution index method is a technique for determining the condition of a water body based on the calculation of quality indices, namely the average index (I_R), which indicates the average pollution level of all parameters in one observation period, and the individual index (I_m), which identifies the dominant parameter responsible for the decrease in water quality during one observation period (Desmawati, 2014). The water quality index using the pollution index method is calculated using the following equation.

$$IP_j = \sqrt{\frac{\left(\frac{C_i}{L_{ij}}\right)_m^2 + \left(\frac{C_i}{Li_{ij}}\right)_R^2}{2}} \quad \text{..... (1)}$$

Where:

IP_j : Pollution Index for parameter j

C_i : Concentration of the field test results for parameter.

L_{ij} : Concentration of the parameter according to the water quality standards for parameter j

$\left(\frac{C_i}{Li_{ij}}\right)_m^2$: Maximum of C_i/L_{ij} Value

$\left(\frac{C_i}{Li_{ij}}\right)_R^2$: Average of C_i/L_{ij} value

The evaluation of the IP values is as follows:

$0 \leq IP_j \leq 1$: Goods condition.

$1 < IP_j \leq 5$: Slightly polluted.

$5 < IP_j \leq 10$: Moderately polluted.

$IP_j > 10$: Heavily polluted.

RESULTS

Condition of the ocean current

Drifter measurements were conducted across the western, northern, eastern, and southern regions of Panjang Island during both the transitional II season in September and the westerly season in February. The transitional II season typically spans from September to November and is characterized by the persistence of the easterly monsoon, marked by eastward-blowing winds. This meteorological

pattern is reflected in the prevailing westward to north-westward ocean currents observed during the drifter measurements. These current measurements were timed to coincide with the transition from high tide to low tide, particularly during the full moon phase, as shown in Figure 2 (left).

the northern waters, the dominant seaward current moves eastward, with speeds ranging from 0.2 to 0.5 m/s. In the eastern waters, the dominant seaward current moves north-westward, with speeds ranging from 0.1 to 0.3 m/s. In the southern waters, the dominant seaward current moves south-eastward,

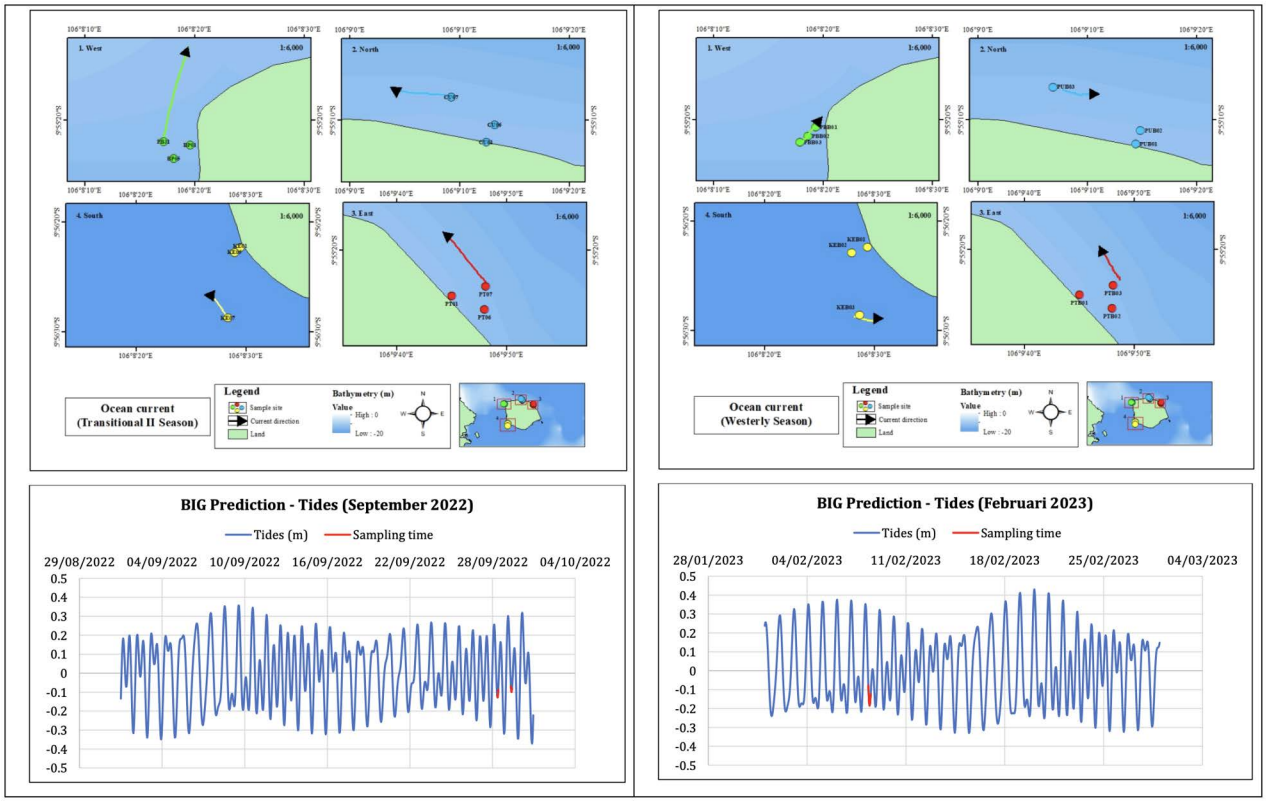

Figure 2. Top: Ocean current during transitional II season (left) and westerly season (right) at Panjang Island (field measurement); 1. West part; 2. North part; 3. East part; 4. South part.
Bottom: Tides from BIG Prediction in September 2022 (left) and February 2023 (right)

The current rose diagrams derived from the drifter data collected during transitional II season as shown in Figure 3 (left), including the four distinct areas—west, north, east, and south—revealed specific current patterns in each location. In the western waters surrounding Panjang Island, the dominant ocean current flows northward, with speeds ranging from 0.2 to 0.5 m/s. In the northern region, the predominant current flows westward, with speeds ranging from 0.1 to 0.2 m/s. In the eastern waters, the dominant current flows north-westward, with speeds ranging from 0.1 to 0.5 m/s. In the southern waters, the dominant current flows north-westward, with speeds ranging from 0.1 to 0.2 m/s.

Figure 3 (right) displays the current rose diagrams in westerly season for the same four areas—west, north, east, and south—revealed the following: in the western waters of Panjang Island, the dominant seaward current moves north-eastward, with current speeds ranging from 0.1 to 0.4 m/s. In with speeds ranging from 0.2 to 0.5 m/s.

Moreover, by relying on secondary data from Marine Copernicus, we established that the dominant currents in the waters surrounding Panjang Island consistently flow westward throughout the year, from March 2022 to February 2023 (Figure 4). A high level of congruence is evident when comparing this secondary data with the field measurements, as presented in Table 1. This alignment holds true for both the transitional II and westerly seasons, where minor discrepancies exist in seawater current velocity and direction. During the transitional II season in September, the current velocity exhibits a variance of 0.118 m/s, while the westerly season shows a difference of 0.083 m/s. Additionally, the current direction closely matches the field measurements and Marine Copernicus data in both seasons.

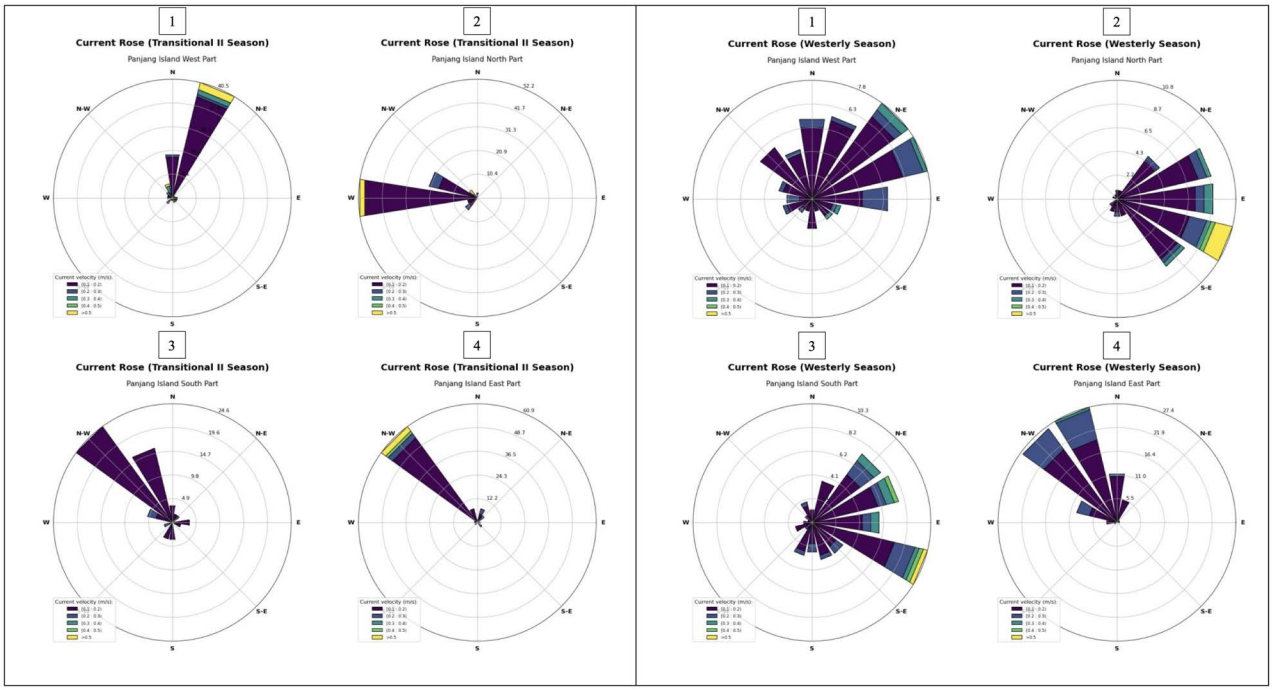

Figure 3. Current rose during transitional II season (left) and westerly season (right) at Panjang Island (field measurement); 1. West part. 2. North part. 3. East part. 4. South part

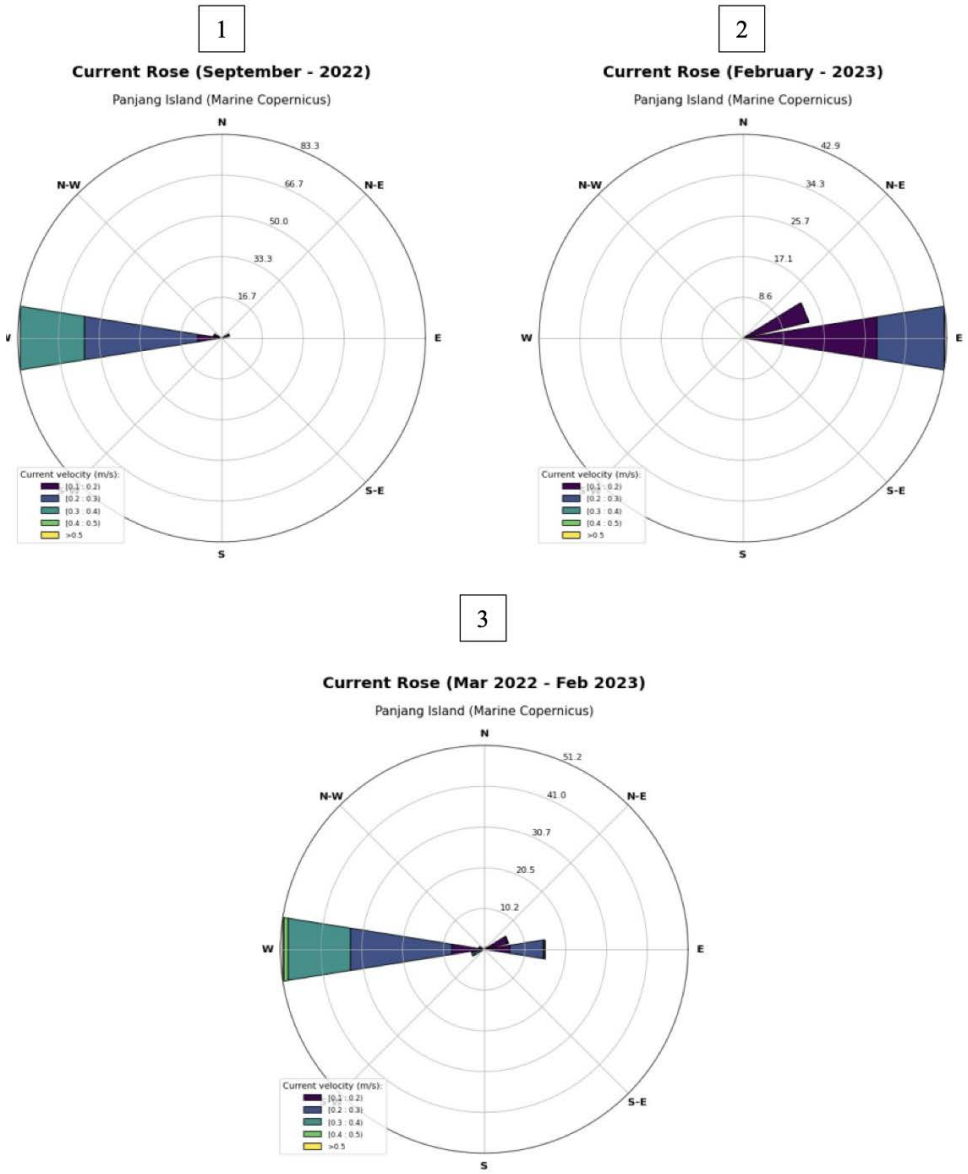

Figure 4. Current rose at Panjang Island (Marine Copernicus). 1: September 2022. 2: February 2023.

Table 1. The comparison of ocean current data between field measurements and Marine Copernicus

Time (DD-MM-YYYY)	Current velocity (m/s)		Current direction (^{o})		Difference	
	Drifter (North part)	Marine Copernicus	Drifter (North part)	Marine Copernicus	Current velocity (m/s)	Current direction (^{o})
29-09-2022	0.187	0.305	262.7 (West)	263.8 (West)	0.118	1.1
08-02-2023	0.113	0.197	115.2 (East)	73.9 (East)	0.083	41.3

Concentration of Pb in sediment and water surface

In this study, the concentrations of Pb metal were assessed in sediment and surface water samples (Table 2). The laboratory results indicated that during both the transitional II and westerly seasons, the concentrations of Pb in sediment generally remained below the thresholds defined by the Sediment Quality Guidelines (SQG) (Table 3). Specifically, during the transitional II season, the maximum Pb concentration recorded was 16.9 mg/kg, with an average of 10.3 mg/kg. In the westerly season, the maximum concentration was 23.4 mg/kg, with an average of 11.4 mg/kg. In contrast, the concentrations of Pb in surface water at various stations during both seasons exceeded the water quality standards set by Regulation No. 22 of 2021 ((Indonesian State Gazette, 2021). As shown in Table 4, during the transitional II season, Pb concentration reached a peak of 0.029 mg/l, with an average of 0.016 mg/l. Similarly, during the westerly season, it reached a

Table 2. The concentration of Pb in sediment and water surface on transitional II season and westerly season.

Sample Site	Transitional II Season		Westerly Season	
	Concentration of Lead (Sediment) (mg/kg)	Concentration of Lead (Surface Water) (mg/l)	Concentration of Lead (Sediment) (mg/kg)	Concentration of Lead (Surface Water) (mg/l)
PEL.G	-	0.029	-	0.010
PGP	-	0.016	-	Nd
CU01/PUB01	15.3	0.016	9.5	Nd
CU06/PUB02	7.2	-	5.7	Nd
CU07/PUB03	15.3	0.009	23.4	Nd
PT01/PTB01	7.5	Nd	3.8	0.029
PT06/PTB02	4.2	-	6.2	Nd
PT07/PTB03	8.5	Nd	20.5	0.005
KE01/KEB01	12.4	0.002	11.4	Nd
KE05/KEB02	8.1	-	12.4	Nd
KE07/KEB03	8.8	0.023	11.4	Nd
BP01/PBB01	11.2	0.016	10.0	Nd
BP05/PBB02	7.8	-	9.5	Nd
PB31/PBB03	16.9	0.016	13.3	Nd

Nd : not detected

Table 3. Statistic descriptive of concentration of Pb in sediment during transitional II season and westerly season

	Transitional II Season	Westerly Season
Sample Size (n)		12
Maximum	16.9	23.4
Minimum	4.2	3.8
Average	10.3	11.4
Sediment Quality Guideline		
ANZECC/ARMCANZ Guidelines		50
CCME		30.2

maximum of 0.029 mg/l, with an average of 0.014 mg/l.

When analyzing the spatial distribution of Pb metal concentrations in sediments, we observed that during the transitional II season, the reef flat area exhibited lower Pb metal concentrations (ranging from 4.2 mg/kg to 8.1 mg/kg) compared to the areas near the coast (ranging from 7.5 mg/kg to 15.3 mg/kg) and the reef front (ranging from 8.5 mg/kg to 16.9 mg/kg). However, the concentration values fluctuated when comparing the coastal areas with the reef front. In the western and southern coastal areas, the concentrations were higher than those in the reef front, while in the northern and eastern parts, the reef front had higher concentrations than the coastal areas during the transitional II season, we observed fluctuations. There were areas with higher Pb metal concentrations near the coastal areas in the northern part (0.016 mg/l), while in the southern part, the reef front had higher Pb metal concentrations (0.023 mg/l). In the western part of the water, the Pb metal concentrations remained relatively stable (Figure 7). In contrast, during the westerly season, the concentrations of heavy metals were higher in the coastal areas (0.029 mg/l) compared to the reef front (0.005 mg/l). During the westerly season, measurements were also taken in the reef flat area, and no Pb metal was detected at any of the stations (Figure 8).

Table 4. Statistic descriptive of concentration of Pb in sediment on transitional II season and westerly season

	Transitional II Season	Westerly Season
Sample Size (n)	10	14
Maximum	0.029	0.029
Minimum	Nd	Nd
Average	0.016	0.014
PP No. 22 of 2021		0.008

(Figure 5). Conversely, during the westerly season, Pb metal concentrations in the reef flat area were lower (ranging from 5.7 mg/kg to 12.4 mg/kg) compared to the areas near the coastal area (ranging from 3.8 mg/kg to 11.4 mg/kg) and the reef front (ranging from 11.4 mg/kg to 23.4 mg/kg). In the southern part, the Pb metal content in the reef flat area was higher than both the reef front and the coastal areas. However, when comparing the coastal areas with the reef front, the concentrations were higher in the reef front compared to the coastal areas, except in the southern part, where they were equal in both the reef front and coastal areas (Figure 6).

Additionally, when examining the spatial distribution of Pb metal concentrations in water

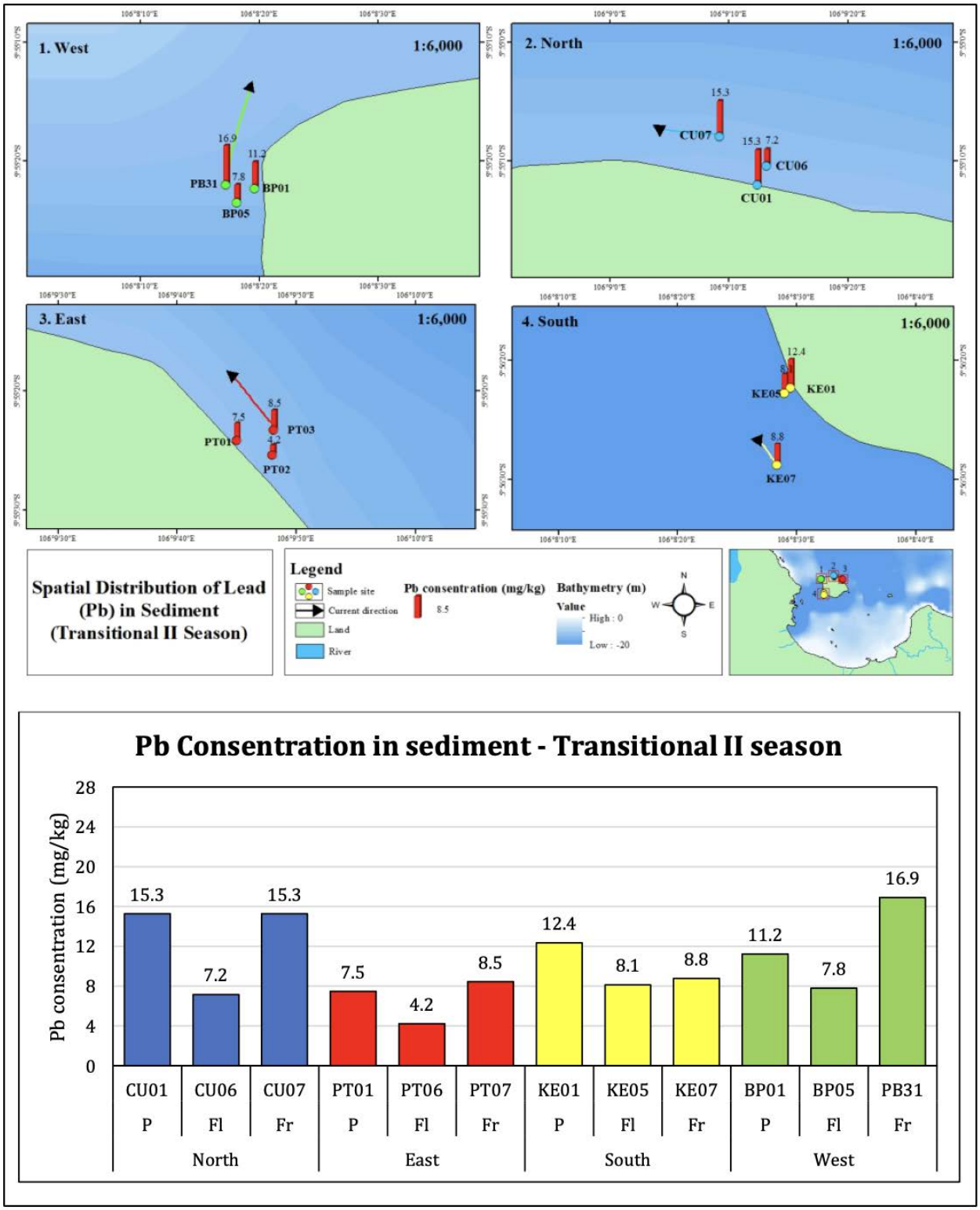

Figure 5. Top: Spatial distribution of Pb in sediment during transitional II season. Bottom: Pb consentration in sediment during transitional II season in all sampling site. P: Near of coastal areas. Fl: Reef flat. Fr: Reef front

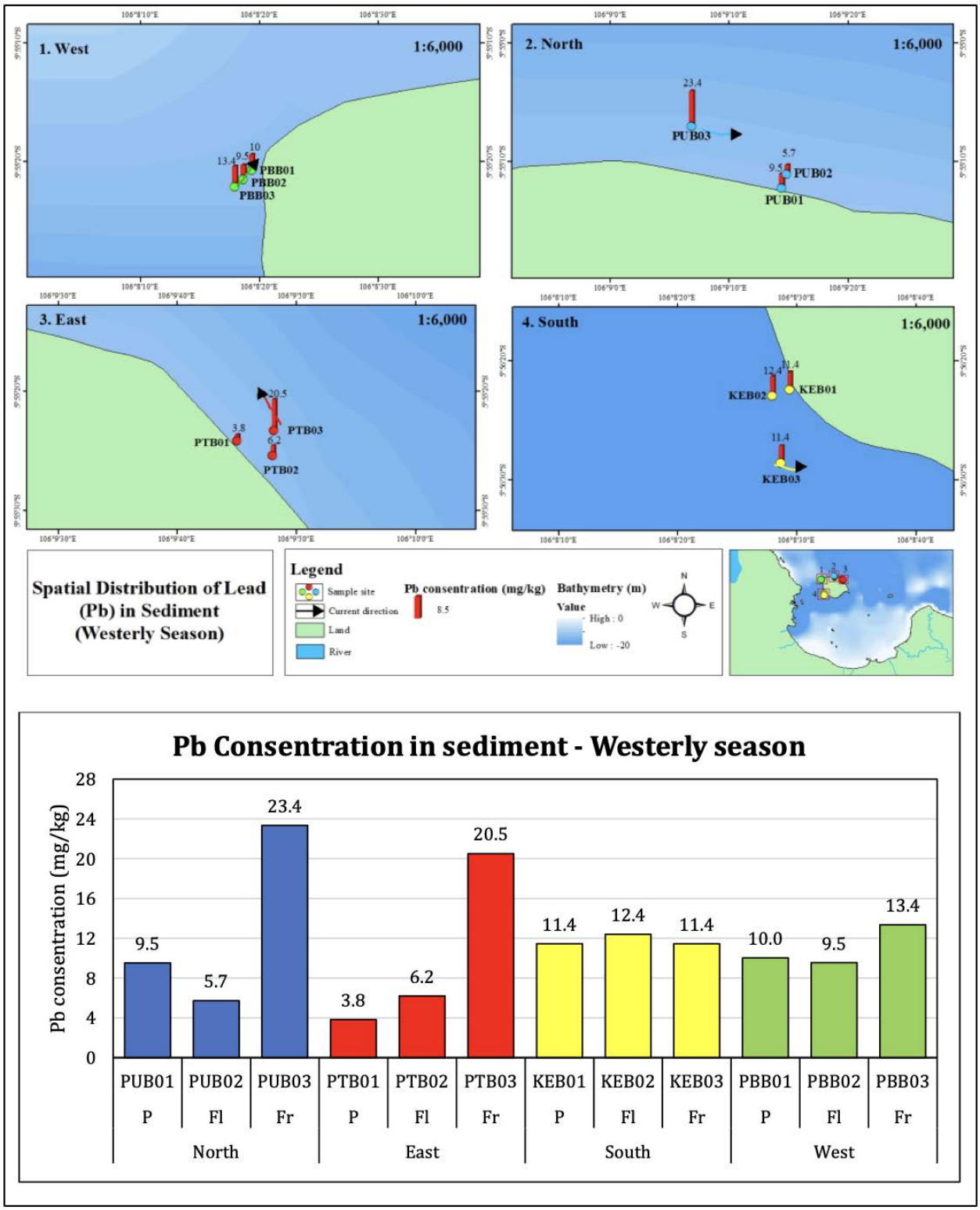

Figure 6. Top: Spatial distribution of Pb in sediment during westerly season. Bottom: Pb consentration in sediment during westerly season in all sampling site. P: Near of coastal areas. Fl: Reef flat. Fr: Reef front

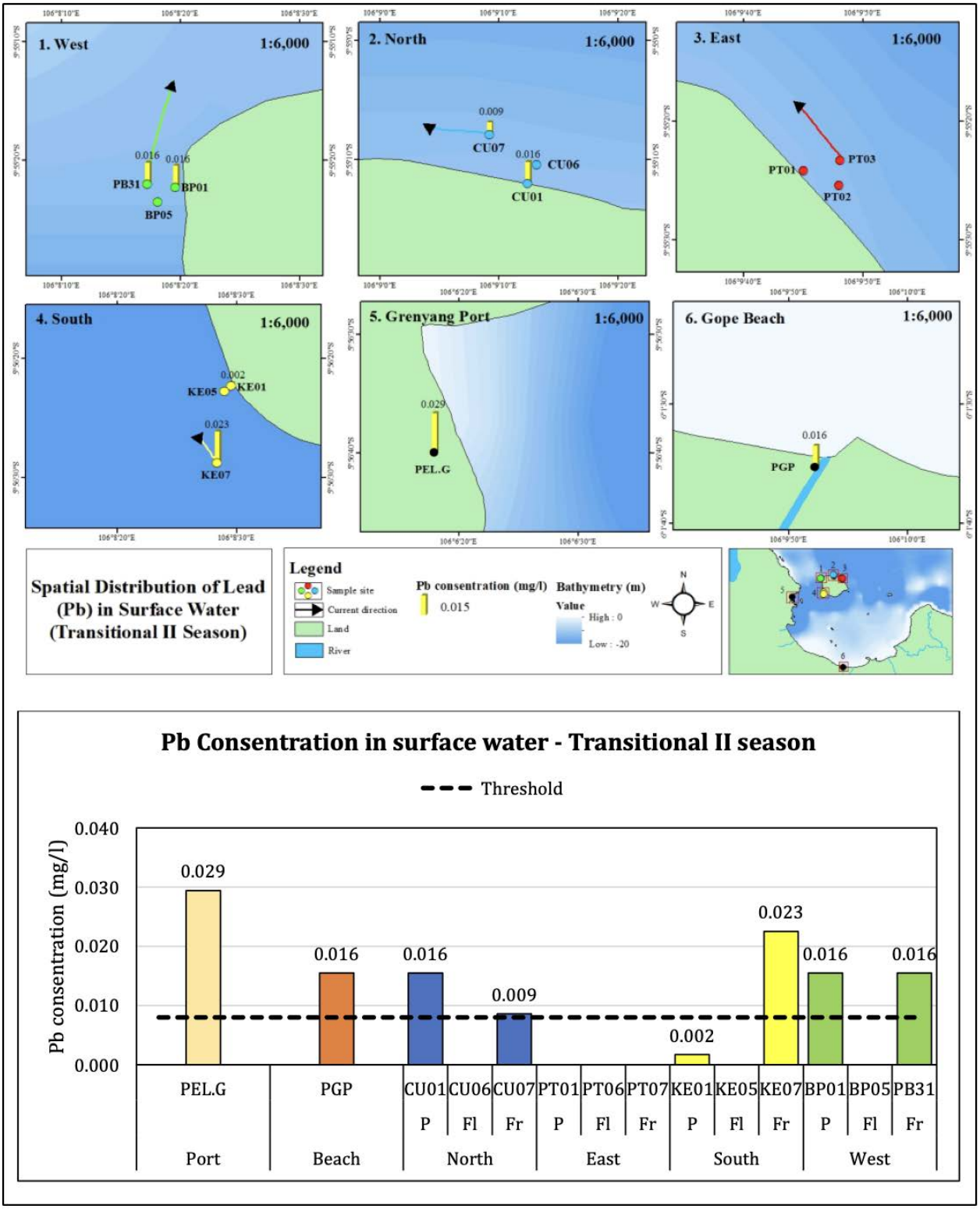

Figure 7. Top: Spatial distribution of Pb in surface water during transitional II season. Bottom: Pb in surface water consentration during transitional II season in all sampling site. P: Near of coastal areas. Fl: Reef flat. Fr: Reef front

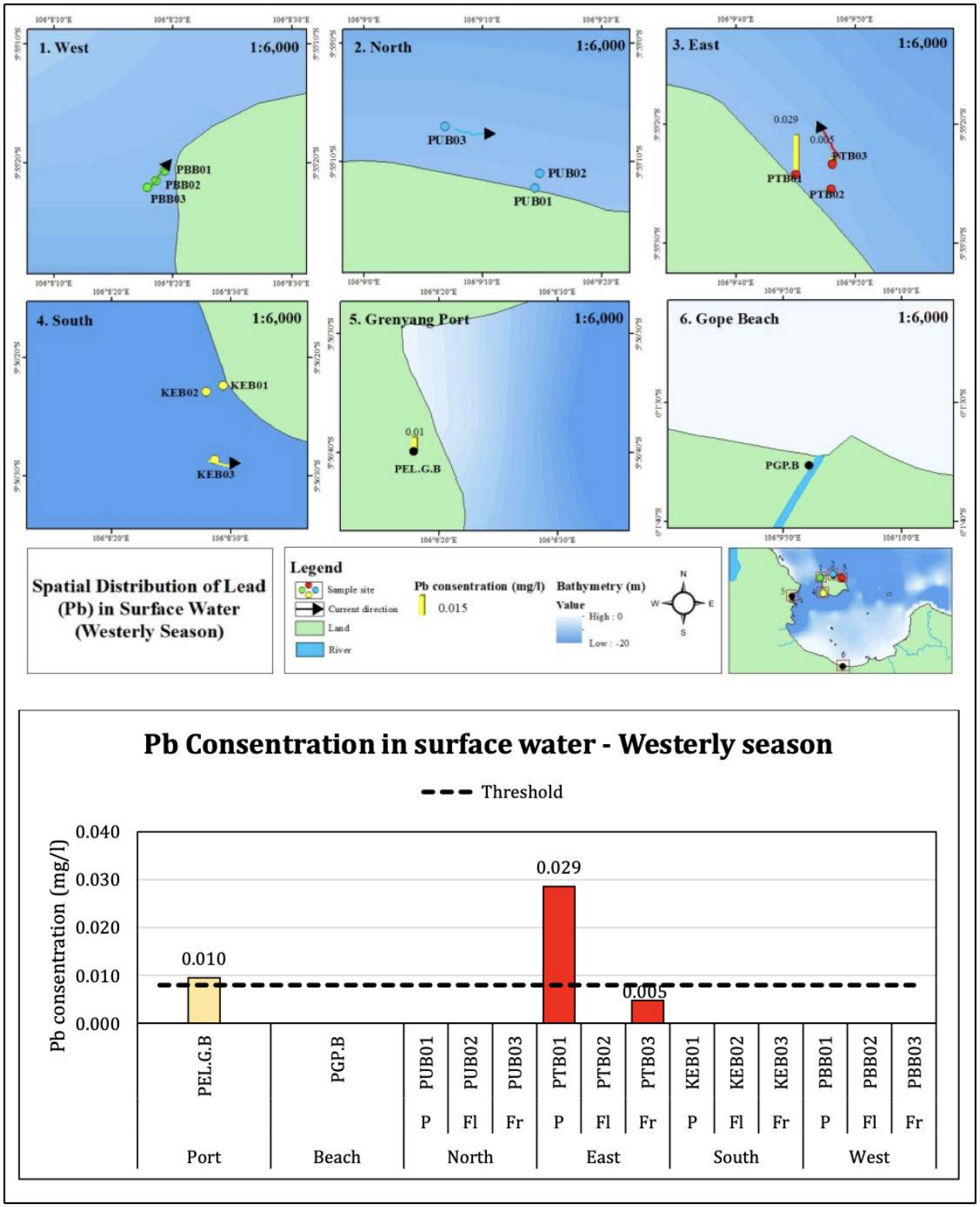

Figure 8. Top: Spatial distribution of Pb in surface water during westerly season. Bottom: Pb in surface water consentration during westerly season in all sampling site. P: Near of coastal areas. Fl: Reef flat. Fr: Reef front

IP Method

Based on the pollution index calculation results for the transitional II season, all measurement stations exhibited a condition of slightly polluted with IP scores ranging around 4 (Table 5). Meanwhile, during the westerly season, Gope Beach experienced a moderately polluted condition with an IP score of 6, while other stations remained in a slightly polluted condition with IP scores ranging from 3 to 4 (Table 5).

Table 5. IP Method on sample siteduring transitional II season and westerly season for water sample

Sample Site	Transitional II Season		Westerly Season	
	IP Score	Condition	IP Score	Condition
PEL.G	4.2	Slightly Polluted	3.6	Slightly Polluted
PGP	4.2	Slightly Polluted	6.2	Moderately Polluted
CU01/PUB01	4.3	Slightly Polluted	4.2	Slightly Polluted
CU06/PUB02			4.2	Slightly Polluted
CU07/PUB03	4.2	Slightly Polluted	4.3	Slightly Polluted
PT01/PTB01	4.4	Slightly Polluted	4.5	Slightly Polluted
PT06/PTB02			4.3	Slightly Polluted
PT07/PTB03	4.2	Slightly Polluted	4.1	Slightly Polluted
KE01/KEB01	4.1	Slightly Polluted	4.5	Slightly Polluted
KE05/KEB02			3.9	Slightly Polluted
KE07/KEB03	4.3	Slightly Polluted	3.8	Slightly Polluted
BP01/PBB01	4.3	Slightly Polluted	4.0	Slightly Polluted
BP05/PBB02			3.9	Slightly Polluted
PB31/PBB03	4.3	Slightly Polluted	4.3	Slightly Polluted

DISCUSSIONS

This study focuses on evaluating the concentration of Pb metal in both sediment and surface water and its implications for the coral reef ecosystem in the vicinity of Panjang Island, Banten. The laboratory results show that, in general, Pb metal concentrations in sediment are higher than those in surface water. This discrepancy can be attributed to the gradual accumulation of metals in sediment over time, possibly due to the binding of metals with hydroxides and organic matter within the sediment (Suryono, 2016). Sediments play a crucial role in aquatic ecosystems as the primary repository and origin of heavy metals (Peng *et al*., 2009). Metals in a dissolved state can find their way into water sources through various pathways and may gather in sediments through processes such as adsorption, precipitation or coprecipitation, and biological interactions. This leads to significantly higher concentrations of heavy metals in sediments, often exceeding those observed in the water above (by order of magnitude). Nevertheless, alterations in the environmental physicochemical conditions, such as changes in pH, redox potential (Eh), dissolved oxygen levels, can trigger the release of heavy metals stored in sediments back into the overlying water (Peng *et al*., 2009).

Despite the higher concentrations of Pb in the sediment, they remain below the established threshold values outlined in the sediment quality guidelines during both the transitional II and westerly

seasons. In contrast, several surface water stations exceeded the water quality standards mandated by Government Regulation No. 22 of 2021 (Indonesian State Gazette, 2021). These findings suggest potential repercussions for the condition of coral reefs around Panjang Island, Banten, a conclusion further supported by this study's outcomes. Utilizing the Pollution Index (IP) method, we determined that the waters surrounding Panjang Island, Banten, experienced lightly polluted conditions during both the transitional II and westerly seasons (Table 5).

The geochemical processes governing the distribution of Pb metal in both sediment and the water column are complex and influenced by various factors. This study also aims to shed light on the possible influence of seawater quality parameters on the variability of Pb metal concentrations. This hypothesis is grounded in existing literature, which suggests that Pb metal concentrations in both sediment and water are generally associated with various seawater quality parameters, including temperature, salinity, pH, and dissolved oxygen (Fauziah *et al*., 2012; Rompas, 2010; Effendi, 2003; Putri *et al*., 2014). However, it's essential to acknowledge that the limited dataset in this study may not provide definitive evidence for the relationships between Pb metal and these seawater quality parameters, as described in existing literature. Some of these relationships are as follows: temperature can affect the solubility of substances in water. In general, as temperature increases, the solubility of most substances, including Pb compounds, tend to increase. This can result in higher concentrations of dissolved Pb in the water. Higher temperatures can increase metal concentrations in the water column, while lower temperatures promote metal accumulation in sediments (Fauziah *et al*., 2012). Changes in salinity can impact the solubility and speciation of Pb. Increasing salinity can reduce the solubility of Pb compounds, leading to decreased concentrations of dissolved Pb in the water column. Reduced salinity levels can lead to higher Pb accumulation in aquatic environments (Rompas, 2010). pH influences the speciation of Pb in water. At lower pH values, lead is more soluble and can remain in the water column. At higher pH, it maybe precipitated or adsorbed onto sediment which result in elevated pH levels that typically correspond to a decreased heavy metal concentrations in water bodies (Effendi, 2003). Dissolved oxygen is a key factor in determining the redox conditions of the water column and sediment. In oxygen-rich (aerobic) conditions, Pb is more likely to form insoluble precipitation, reducing its mobility. Conversely, in oxygen-depleted (anaerobic) conditions, Pb may be more soluble and mobile. Low dissolved oxygen levels can result in increased heavy metal accumulation in sediments (Putri *et al*., 2014).

Furthermore, our study reveals distinctions in the distribution of Pb metal concentrations within sediment and surface water. These variations are prominently evident across different locations, including the coastal areas, reef flats, and reef fronts surrounding Panjang Island's waters in the western, northern, eastern, and southern regions. The observed difference can be explained by the main source of Pb metal, which primarily comes from Banten rather than Panjang Island. As a result, there is a higher accumulation of metals in the reef front, as it serves as the initial point of contact for pollutants originating from Banten. Additionally, there are indications that human activities, particularly shipping operations on Panjang Island, contribute to elevated Pb metal concentrations in the coastal areas.

An intriguing observation from both seasons is that during the transitional II season, Pb in surface water was undetectable in the eastern region, while during the westerly season, only the eastern region exhibited detectable levels of the heavy metal Pb. These findings align with the patterns observed in sediment. During the transitional II season, the predominant ocean current movement is westward, suggesting the likely accumulation of Pb metal in the western waters of Panjang Island, Banten. Conversely, during the westerly season, Pb metal accumulates in the eastern waters of Panjang Island, Banten, due to the dominance of eastward-moving ocean currents. Additionally, the waters around Panjang Island intersect with several river estuaries, such as Cibanten, Cibeureun, Cengkok, and Ciruas (Juniardi *et al*., 2021). These estuaries may contribute to human activities on the mainland that elevate Pb metal concentrations in Panjang Island's waters. Moreover, rainfall patterns can influence Pb metal concentrations in surface water (Rochyatun *et al*., 2006). Rainfall during the night before data collection can lead to undetectable Pb metal concentrations during the westerly season. According to Darmono (1995), the metal content in water varies based on environmental and climatic conditions. During the rainy season, metal content tends to be lower due to dilution processes, while during the dry season, metal content tends to be higher as metals become more concentrated.

Gope Beach was selected to represent potential pollutant sources originating from river inflow into the Banten Bay region, while Grenyang Port was chosen to detect potential sources of pollution arising from shipping activities. The measurement data indicate indications of Pb metal originating from both shipping activities and the mainland during both seasons. Pb metal was detected at Grenyang Port, and during the transitional II season, it was found at Gope Beach. Examination of the conditions at Gope Beach also reveals that Pb metal can originate from human activities on the mainland, corroborating the findings of Juniardi et al. (2021). When comparing Grenyang Port and Gope Beach, it is evident that Pb metal concentrations are higher at Grenyang Port. This is attributed to Grenyang Port's location in the Bojonegara industrial area, where numerous shipping activities occur, resulting in a higher likelihood of elevated Pb metal concentrations (Falah *et al*., 2020). This assertion is further supported by Liyubayina (2018), who reported the existence of 44 types of industrial activities in Bojonegara Regency, some of which are situated in coastal areas. One of the significant waste products generated by port and industrial activities, such as the use of ship lubricants, is heavy metal waste, which has the potential to be an environmental pollutant.

CONCLUSIONS

The study on Pb metal content in the coral reef environment of Panjang Island waters, Banten, has yielded several key findings:

(1) In sediment samples, Pb concentrations during the transitional II season ranged from 4.2 to 16.9 mg/kg, while in the westerly season, they varied from 3.8 to 23.4 mg/kg. For surface water samples, Pb concentrations during the transitional II season ranged from 0 to 0.029 mg/l, and in the westerly season, they also spanned from 0 to 0.029 mg/l. According to the pollution index method, the overall state of Panjang Island waters in Banten can be classified as lightly polluted during both the transitional II and westerly seasons.

(2) The spatial distribution of Pb concentrations exhibited fluctuations during both seasons (transitional II and westerly). Some areas had elevated Pb concentrations near the coast, while others showed higher concentrations at the reef front. Generally, Pb concentrations in the reef flat area were lower in comparison to the reef front and nearshore regions. This pattern is primarily attributed to the main Pb source in Panjang Island waters, which originates from the mainland. This allows Pb to accumulate on the reef front, as it serves as the initial point of contact for Pb arriving from the mainland. When higher concentrations are detected near the coast, it may indicate human activities on Panjang Island are contributing to heightened Pb levels in coastal areas.

(3) Ocean current movements provide valuable insights into the distribution of Pb concentrations in Panjang Island waters, Banten. During the transitional II season, Pb concentrations in sediment and surface water tended to be higher in the western part of Panjang Island waters, suggesting that pollution originates from river inflows in Banten Bay (eastern part of Panjang Island, Banten). Conversely, in the westerly season, Pb concentrations tended to be higher in the eastern part of Panjang Island waters, indicating a pollution source from the Bojonegara industrial area (western part of Panjang Island, Banten).

These findings provide valuable insights into the distribution of Pb metal in the waters surrounding Panjang Island and its potential environmental impact. They serve as a foundational basis for further research and management strategies aimed at preserving the health and sustainability of the coral reef environment around Panjang Island.

ACKNOWLEDGEMENTS

The author would like to express sincere gratitude to the National Research and Innovation Agency (BRIN) for the invaluable opportunity to serve as a research assistant, particularly within the research group specializing in paleo climate and environmental studies. Furthermore, the author extends heartfelt appreciation to the Oceanography program study for their invaluable contributions, which included sharing profound insights into oceanographic knowledge and providing essential support with field equipment throughout the research endeavors.

REFERENCES

Afiyatillah, G., Sulistiono, Hariyadi, S., Simanjuntak, Riani, E., Rostika, R., and Kleinertz, S., 2022. Heavy Metals (Hg, Cd,

Pb, Cu) in Greenback Mullets (*Planiliza subviridis*) Valenciennes, 1836) from Bojonegara coastal waters, Banten Bay, Indonesia. *Jurnal Ilmu Kelautan*, 27(2): 169-180.

Al-Rousan, S.A., Al-Shloul, R. N., Al-Horani, F. A., and Abu-Hilal, A.H.A., 2007. Heavy Metal Contents in Growth Bands of Porites Corals: Record of Anthropogenic and Human Developments from The Jordanian Gulf of Aqaba. *Journal Marine Pollution Bulletin,* 54(12): 1912-1922.

Asmorowati, D.S., Sumarti, S.S., and Kristanti, I.I., 2020. Perbandingan Metode Destruksi Basah dan Destruksi Kering untuk Analisis Timbal dalam Tanah di Sekitar Laboratorium Kimia FMIPA UNNES. *Indonesian Journal of Chemical Science*, 9(3):169-173.

Darmono, 1995. *Logam Dalam Sistem Biologi Makhluk Hidup*, Jakarta, UI Press.

David, C.P., 2003. Heavy Metal Concentrations in Growth Bands of Corals: A Record of Mine Tailings Input Through Time (Marinduque Island, Philippines). *Journal Marine Pollution Bulletin*, 46(2): 187–196.

Desmawati, E., 2014. *Sistem Informasi Kualitas Air Sungai di Wilayah Sungai Seputih Sekampung*. Tesis Magister Teknik Universitas Lampung, Bandar Lampung.

Effendi, H., 2003. *Telaah Kualitas Air Bagi Pengelolaan Sumberdaya dan Lingkungan Perairan*. Penerbit Kanisius, Yogyakarta.

Falah, F., Chrisna, A.S., and Ita. R., 2020. Logam Berat (Pb) pada *Lamun Enhalus acoroides* (*Linnaeus F.*) Royle 1839 (*Magnoliopsida: Hydrocharitaceae*) di Pulau Panjang dan Pulau Lima Teluk Banten. *Journal of Marine Research*, 9(2): 193-200.

Falkowski, P.G., Jokiel, P.L., and Kinzie, R.A, 1990. Irradiance and Corals, in Dubinsky, Z. (ed.), Ecosystems of the World. *Journal. Coral Reefs*, 25(1): 89-107.

Fauziah, A.R., Rahardja, B.S., and Cahyoko, Y., 2012. Korelasi ukuran kerang darah (Anadara granosa) dengan konsentrasi logam berat Merkuri (Hg) di muara Sungai Ketingan, Sidoarjo Jawa Timur. *Journal Marine and Coastal Sci*, 1(1): 34-44.

Guzman, H.M., and Jimenez, C.E., 1992. Contamination of Coral Reefs by Heavy Metals Along the Caribbean Coast of Central America (Costa Rica and Panama). *Journal Marine Pollution Bulletin,* 24(11): 554-561.

Harland, A.D., and Brown B.E., 1989. Metal tolerance Metal Tolerance in the scleractinian coral *Porites lutea*. *Journal Marine Pollution Bulletin,* 20(7): 353-357.

Holleman, A.F., and Wiberg, E., 1985. *Lehebuch du Anoranischen chemie*. Water de Gruyter, Berlin, 868p.

Indonesian State Gazette, 2021. Government Regulation no. 22 of 2021 on Environmental Protection, Organisation and Management. Republic of Indonesia.

Juniardi, E., Sulistiono, and Haryadi, S., 2021. Heavy metals (Pb and Cd) contents in the seawater and sediment in Panjang and Pamujaan Besar Islands, Banten Bay, Indonesia.
IOP Conf. Series: Earth and Environmental S cience.

Liyubayina, V., 2018. Analisis dampak reklamasi Teluk Banten Terhadap kondisi lingkungan dan sosial ekonomi. *J. Planesa*, 9(1): 37-46.

Mitchelmore, C.L., Verde, E.A., and Weis, V.M., 2007. Uptake and Partitioning of Copper and Cadmium in The Coral *Pocillopora damicornis. Journal Aquatic Toxicology,* 85(1): 48-56.

Peng, J.F., Song, Y.H., Yuan, P., Cui, X.Y., Qiu, G.L, 2009. The remediation of heavy metals contaminated sediment. *Journal of Hazardous Materials*. 161(2-3):633–640.

Philips, J.D.H., 1980. Proposal for monitoring studies on the contamination of the east seas by trace metal and organoclorine. *South China Sea Fisheries Development and Coordinating Programe*, Manila.

Rusmana, E., Suwitodirdjo, K., and Suharsono, 2005. Peta Geologi Lembar Serang, Jawa. Pusat Survei Geologi, Kementerian Energi dan Sumber Daya Mineral https://geologi.esdm.go.id/geomap/pages/preview/peta-geologi-lembar-anyer-jawa-barat accessed at 2023-06-11.

Putri, Z.L., Wulandari, S.Y., and Masluka, L., 2014. Studi Sebaran Kandungan Logam Berat Timbal (Pb) dalam Air dan Sedimen Dasar di Perairan Muara Sungai Manyar Kabupaten

Gresik, Jawa Timur. *Jurnal Oseanografi*, 3(4): 589 – 595.

Razi, N. M., Fildzah, F., Dhani, D. N., Nasir, M., Rizki, A., & Firdus, F., 2023. Literatur Review: Pencemaran Logam Berat di Pelabuhan Indonesia. *Jurnal Laot Ilmu Kelautan*, 5(1), 48-61.

Rizkiana, L., Sofyatuddin, K. and Nurfadilla., 2017. Analisis Timbal (Pb) pada Sedimen dan Air Lauti Di Kawasan Pelabuhan Nelayan Gampong Deah Glumpang Kota Banda Aceh. *Jurnal Ilmiah Mahasiswa Kelautan dan Perikanan Unsyiah*, 2(1): 89-96.

Rochyatun, E., Kaisupy, M., and Rozak, A., 2006. Distribusi Logam Berat dalam Air dan Sedimen di Perairan Muara Sungai Cisadane. *Makara*, 10(1): 35-40.

Rompas, M. R., 2010. *Toksikologi Kelautan*. Walaw Bengkulen, Jakarta.

Sabdono, A., 2009. Heavy Metal Levels and Their Potential Toxic Effect on Coral *Galaxea fascicularis* from Java Sea, Indonesia. *Journal Research Environmental Science*, 3(1): 96-102.

Sharma, R.K. and Agrawal, M., 2005. Biological Effects of Heavy Metals: An Overview. *Journal of Environmental Biology*, 26: 301-313.

Suryono, C. A., 2016. Akumulasi Logam Berat Cr, Pb dan Cu dalam Sedimen dan Hubungannya dengan Organisme Dasar di Perairan Tugu Semarang. *Jurnal Kelautan Tropis*, 19(2): 143-149.

Utami, D.A., Reuning, L., Schwark, L. et al., 2023. Plastiglomerates from uncontrolled burning of plastic waste on Indonesian beaches contain high contents of organic pollutants. *Sci Rep 13*, 10383. https://doi.org/10.1038/s41598-023-37594-z

Waldichuk, M., 1974. Some Biology Concentration in Metal Pullution. In F.J.Verberg (eds). Pollution and Physioology of Marine Organism. *Academic Press*. 1-15.

TIDAL HARMONIC ANALYSIS AND PREDICTION TO SUPPORT EARLY WARNING FOR COASTAL FLOODING

ANALISIS HARMONIK DAN PREDIKSI PASANG SURUT UNTUK MENDUKUNG PERINGATAN DINI BANJIR PESISIR

Randi Firdaus[1], Nurul Tazaroh[1], Oky Surendra[1], Eko Prasetyo[1], Riris Adriyanto[1]

[1] Center for Marine Meteorology, Indonesia Agency for Meteorology Climatology and Geophysics (BMKG), Jl. Angkasa 1, No. 2 Kemayaoran, Jakarta 10610

*Corresponding author: randi.firdaus@bmkg.go.id

(Received 15 November 2023; in revised from 20 November 2023; accepted 25 March 2024)

DOI : 10.32693/bomg.39.1.2024.863

ABSTRACT: The Indonesian Maritime Continent (IMC) is the largest archipelago that vulnerable to climate change especially sea level rise. Some coastal areas frequently experience coastal flooding affecting the activities and infrastructures. Thus, an accurate tide prediction in this region plays a pivotal role in providing the early warning, mitigation, and adaptation to frequent coastal flooding. BMKG, through the Center for Marine Meteorology has done undertaken efforts to provide an accurate tidal prediction information by developing the tidal information system call the Indonesian Tidal Information System (INATIS). Tidal harmonic analysis (THA) using the least-square method was applied to sea level data from 49 Marine Automatic Weather System (MAWS) stations collected between 2020-2021 to generate tidal predictions for the period of 2022-2023. Accuracy was assessed based on Mean Absolute Error (MAE) and the Mean Absolute Percentage Error (MAPE). MAWS stations with prediction accuracy above 80% visualized on publicly accessible online platform of the BMKG website using the open-source Looker Studio. Verification of the tidal predictions showed an average prediction accuracy of 93.21% with a MAE of 0.11 m. The high accuracy of INATIS demonstrates its potential as a reference for coastal flood early warning systems.

Keywords: tidal prediction, tidal accuracy, Ina-TIS, least-square method

ABSTRAK*: Benua Maritim Indonesia (BMI) merupakan kepulauan terbesar di dunia yang rentan terhadap perubahan iklim utamanya kenaikan tinggi muka laut. Beberapa wilayah pesisir secara reguler mengalami banjir pesisir (ROB) yang berdampak terhadap berbagai aktivitas dan infrastruktur pesisir. Sehingga informasi prediksi pasang surut yang akurat sebagai acuan peringatan dini banjir pesisir sangat diperlukan. BMKG melalui Pusat Meteorologi Maritim yang menurut Undang-Undang ditugaskan untuk menyampaikan informasi pasang surut telah melakukan berbagai upaya untuk memberikan informasi pasang surut yang akurat salah satunya melalui pengembangan sistem informasi yang diberi nama dengan INATIS (Indonesian Tidal Information System). Analisis harmonik pasang surut (THA) menggunakan metode kuadrat terkecil (least square) diterapkan pada data tinggi muka laut di 49 stasiun Marine Automatic Weather System (MAWS) pada periode 2020-2021 digunakan untuk menghasilkan prediksi pasang surut pada periode 2022-2023. Akurasi prediksi pasang surut dievaluasi menggunakan kriteria galat mutlak rata-rata (MAE) dan persentase akurasi galat mutlak rata-Rata (MAPE). Stasiun MAWS yang memiliki hasil akurasi prediksi >80% selanjutnya ditampilkan pada laman online menggunakan platform open-source looker studio yang bisa diakses publik pada laman BMKG. Hasil verifikasi prediksi pasang surut menunjukkan bahwa nilai persentase rata-rata akurasi prediksi sebesar 93,21% dan MAE sebesar 0,11 m. Nilai akurasi yang tinggi pada INATIS*

ini menunjukkan hasil prediksi yang bisa menjadi acuan dalam membuat peringatan dini banjir pesisir.

Kata Kunci: *prediksi pasut, akurasi pasut, Ina-TIS, metode kuadrat terkecil*

INTRODUCTION

The sea level rise is regarded as a crucial indicator of climate change, exerting significant influence across various sectors of human life, particularly within coastal communities. Sea levels have experienced a substantial increase over the past decade, and projections indicate continued elevation in the future (Storto et al., 2019). Research conducted by Widlansky et al. (2020) has revealed that a 2°C rise in sea surface temperature can enhance the global variability of sea levels by 4-10%. Concurrently, studies by Frederikse et al. (2020) demonstrate that sea levels have been rising at a rate of 1.56 mm per year during the 20th century. This situation rise threatens approximately 23% of the world's population residing in vulnerable coastal regions, susceptible to extreme coastal flooding events (Small & Nicholls, 2003).

Climate change and land subsidence combine to cause coastal flooding, damaging infrastructure and threatening coastal livelihoods. Losses can reach millions of dollars (Dasgupta et al., 2009). Indonesian coastal regions, including the northern coast of Java and the eastern coast of Sumatra, routinely experience coastal flooding. According to Ward et al. (2011), extreme coastal flooding events in Jakarta with return periods of 100 and 1000 years could cause total losses of 4 and 5.2 million Euros, respectively.

Hence, the provision of tidal prediction information becomes paramount importance for early warning systems and coastal flooding mitigation efforts. Tidal prediction information also benefits maritime activities, facilitating ship loading and unloading operations, planning port construction, meeting recreational needs such as fishing and surfing, and indirectly enhancing the productivity of fisheries for local fishermen (Su & Jiang 2023). Sea level data is also utilized for verifying events such as tsunami waves, tropical cyclones, or meteo-tsunamis. Globally, observational data from tide gauges, in conjunction with satellite data, have been employed for projecting global sea level rise under various scenarios.

Tides, short-term sea level fluctuations, are primarily caused by the gravitational forces of the moon and sun interacting with the Earth's shape and bodies of water. This oceanographic phenomenon is relatively predictable due to the cyclical nature of these forces (Egbert & Ray, 2017). Various methods for predicting tides have been developed. The harmonic analysis method is one of the most common approaches, known for its accuracy in generating tidal predictions (Li et al., 2019). Other approaches are also frequently employed, such as numerical modeling (Haditiar et al., 2020), as well as the application of machine learning and artificial intelligence (Riazi, 2020; Granata & Di Nunno 2021).

According to Law No. 31 of 2009 on Meteorology, Climatology, and Geophysics, BMKG (Indonesia's Meteorology, Climatology, and Geophysics Agency) has the responsibility to conduct observations of tidal movements in the ocean. BMKG, through the Maritime Meteorological Center, has employed various approaches to provide tidal prediction information. Previously, BMKG developed the Coastal Flooding Prediction System, known as the Indonesian Coastal Inundation Forecasting Demonstration Project (INA-CIFDP), utilizing numerical methods (Riama et al. 2021). The expansion of weather and oceanography monitoring networks, including sea level sensors, has enable to the development of a tidal prediction system using harmonic analysis methods, making use of observational data known as the BMKG-Indonesian Tidal Information System (INATIS). This web-based system utilizes harmonic analysis and observational data to provide tidal predictions accessible to the public.

METHODS

The data used in this research comprises of sea level data collected over a period of two years (2021-2022), recorded by water level sensors within the Marine Automatic Weather Station (MAWS) instruments at 49 MAWS stations located in various locations (Figure 1). A MAWS is an automated observatory equipped with various of weather and ocean sensors. Typically, at each MAWS stations, there are at least two types of water level sensors, including bubbler sensors (pressure-based) and radar sensors. Additionally, tide staffs serve as reference points for the raw data (Figure 2).

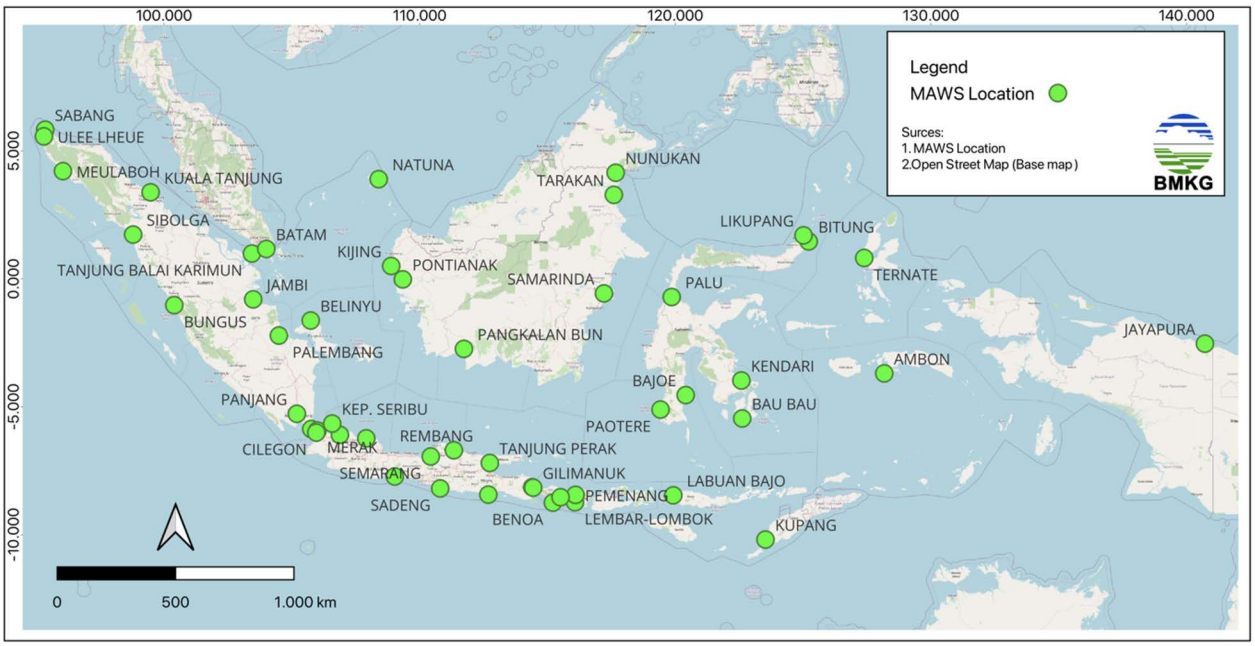

Figure 1. Study location (distribution of BMKG's Marine Automatic Weather Station for sea level

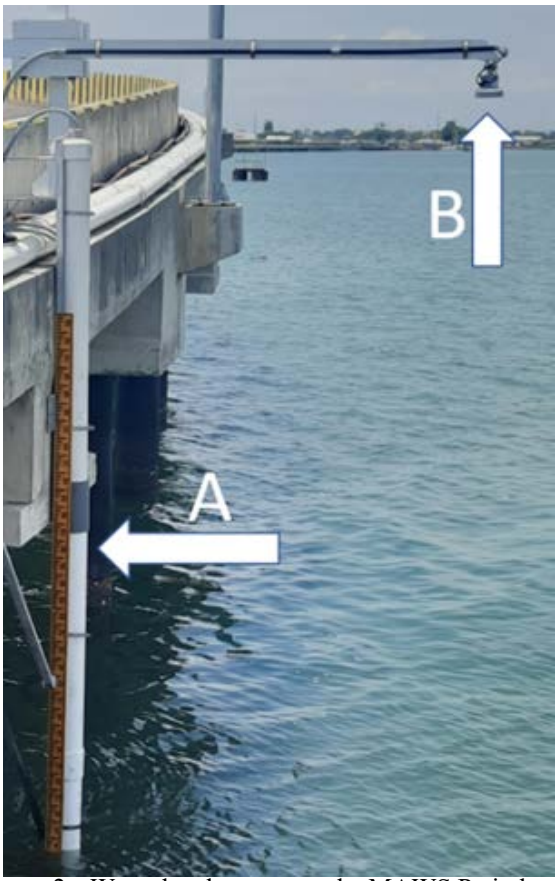

Figure 2. Water level sensors at the MAWS Patimban: a. bubler sensor, b. radar sensor

Water level data from MAWS stations was collected at either 1-minute or 10-minute intervals. The data has undergone a quality control (QC) process (IOOS, 2016) that is programmed into the MAWS system, as shown in Table 1. Despite the presence of the QC system, further data conditioning was conducted prior to harmonic analysis. Data conditioning includes the removal of noise and spikes through the application of high-frequency filtering, filtering data based on favorable QC flags (i.e., QC flag 1), and ensure consistent time intervals (without gaps).

Table 1. QC flag for MAWS

Flag	Description
0	No QC was performed
1	Good data
2	Probably good data
3	Probably bad data that are potentially correctable
4	Bad data
5	Value changed
6	Not used
7	Not used
8	Interpolated value
9	Missing value

Harmonic Analysis

The sea level recorded by MAWS water level sensors at any time represents a superposition (summation) of several waves with specific frequencies (referred to as tidal components), along with a residual component (Parker, 2007), as expressed by Equation (1).

$$h(t) = H_0 + \sum_{i=1}^{n} f_i H_i \cos(\alpha_i t + \{V_0 + u\}_i - \kappa_i) + h_r(t) \quad (1)$$

Here, in Equation (1), $h(t)$ represents the water surface elevation at time t with respect to a specific datum, n is the number of tidal components, H_0 is the mean sea level above the datum, H_i is the amplitude of the i-th tidal component, while $\alpha_i t + \{V_0 + u\}_i - \kappa_i$ represents the phase of the i-th tidal component, and h_r is the residual sea level component.

Tidal Harmonic Analysis (THA) employs the least-squares (LS) method to determine the amplitude and phase of predetermined tidal harmonic components with known frequencies (Thomson and Emery 2014). The LS method is employed to minimize the variance of time series data, and this can be expressed as Equation (2) (Pawlowicz *et al.* 2002).

$$E = \sum_{i=1}^{n} |x(t_i) - y(t_i)|^2 \qquad (2)$$

Equation (1) is substituted to Eq. (2), results in Equation 3 as follow.

$$e^2 = \sum_{i=1}^{n} {h_r}_i^{\,2} = \sum_{i=1}^{n} \{h_i - [H_0 + \sum_{i=1}^{n} f_i H_i \, cos \, cos \, (\alpha_i t + \{V_0 + u\}_i - \kappa_i)\,]\}^2 \qquad (3)$$

The least-squares harmonic analysis method can be employed for the analysis of up to hundreds of tidal components. Harmonic analysis is conducted using the T_Tide software package in MATLAB, as provided by Pawlowicz et al. (2002).

We applied the THA to nearly two years of water level time series data. While Parker (2007) suggests a standard length of 369 days for THA, 365 days of data often sufficient for the least-square in practice. The amplitude and phase values obtained from THA can be utilized for tidal prediction throughout 2023 using Equation (1). This one-year prediction window is conducted due to the limitation of THA which only resolve two years tidal constituent for 2 years data.

An example of tidal components resulting from harmonic analysis at the MAWS Bajoe station is presented in Figure 3. With a length of data of about 400 days, it can result in about 70 tidal constituents in total, with 58 constituents being significant (the value of signal-to-noise (SNR) ratio> 1). Detailed information about the first 20 highest amplitude of significant harmonic constituent with its description is shown in Table 3. The five highest tidal amplitudes in Table 3 are M2, K1, O1, S2, and N2, with an amplitude (in m) of 0.57, 0.33, 0.20, 0.16, and 0.12, respectively. The next step is the 58 significant constituents (in this case) will be used to predict the tidal for the next one year.

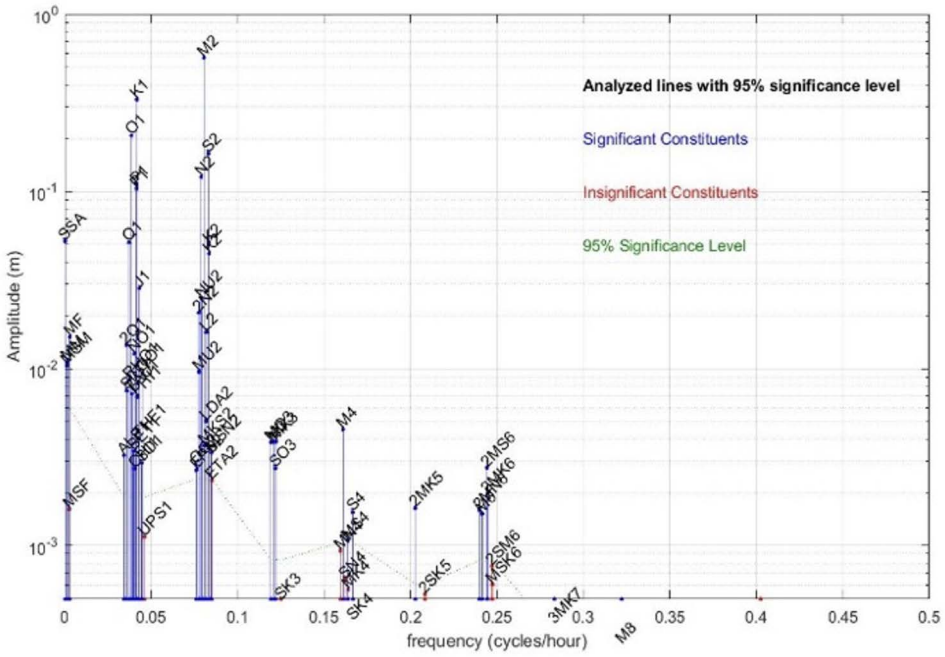

Figure 3. An Example of tidal harmonic analysis in Bajoe station. The significant harmonic constituents at significant level of 95% were note by the blue line.

Table 2. The first 20th highest significant tidal constituent in Bajoe station for about 400 days harmonic analysis

No	Tidal Constituent	Amplitude (m)	Phase (degree)	SNR	Description
1	M2	0.5715	137.66	6.90E+04	Principal lunar semidiurnal
2	K1	0.3302	185.06	5.00E+04	Lunar diurnal
3	O1	0.2069	168.4	2.00E+04	Lunar diurnal
4	S2	0.1622	192.97	5.50E+03	Principal solar semidiurnal
5	N2	0.1216	114.99	3.10E+03	Larger lunar elliptic semidiurnal
6	P1	0.1093	192.13	5.40E+03	Solar diurnal
7	SA	0.0734	54.29	1.80E+02	Solar annual
8	Q1	0.051	166.44	1.20E+03	Larger lunar elliptic diurnal
9	K2	0.048	189.94	4.90E+02	Lunisolar semidiurnal
10	J1	0.0275	204.74	3.40E+02	Smaller lunar elliptic diurnal
11	NU2	0.0263	116.89	1.50E+02	Larger lunar evectional
12	S1	0.025	213.69	2.80E+02	Solar diurnal
13	2N2	0.0211	92.21	93	Lunar elliptical semidiurnal 2nd order
14	L2	0.017	171.83	61	Smaller lunar elliptic semidiurnal
15	MF	0.0168	34.58	9.4	Lunisolar fortnightly
16	2Q1	0.0136	163.39	85	Larger elliptic diurnal
17	NO1	0.0133	154.88	80	Smaller lunar ellipti
18	SSA	0.0105	271.05	3.7	Solar semiannual
19	MM	0.0104	359.58	3.6	Lunar monthly
20	T2	0.0099	170.66	21	Larger solar elliptic

Tidal prediction verification

Verification of prediction results is conducted by comparing them with observational data. The criterion used for this verification is the Mean Absolute Percentage Error (MAPE) as defined in Equation (4) (Zhang et al., 2023).

$$MAPE = \left(\frac{\sum_{i=1}^{n} \frac{|h-h'|}{h}}{n}\right) \times 100\% \qquad (4)$$

Where h represents the observed water surface elevation, h' represents the predicted tidal elevation, and n is the number of data points used in the calculation.

Therefore, the accuracy percentage can be obtained from Equation (5).

$$Accuracy(\%) = 100\% - MAPE \qquad (5)$$

The accuracy criteria modified from MAPE criteria by Lewis (1962) is showed in Table 2.

Table 3. Prediction's accuracy criteria

Accuracy (%)	Interpretation
>90	Highly accurate
80-90	Good
50-80	Reasonable
<50	Weak and inaccurate

Verification is conducted monthly, allowing for an assessment of the variation in the performance of tidal predictions each month. Tidal prediction verification at one of the MAWS stations in Bajoe for January 2023 is illustrated in Figure 4.

Web-based visualization

MAWS stations with accuracy values exceeding 80% are visualized on the open-source web-based platform, Looker Studio (latest name from Google Data Studio). Looker Studio is primarily designed for creating interactive analytical reports, yet can also be utilized to create a user interface for tidal prediction with various data display options such as graphs, maps, tables, diagrams, and more (Snipes 2018). Looker Studio is an intuitive platform that does not require specific programming language skills in the implementation. In this study, the tide prediction data for the year 2023 is displayed on Looker Studio to avoid the heaviness of loading on the website. At the end of each year, the dashboard will be updated with prediction data for the following year. In general, the research flowchart is presented in Figure 5.

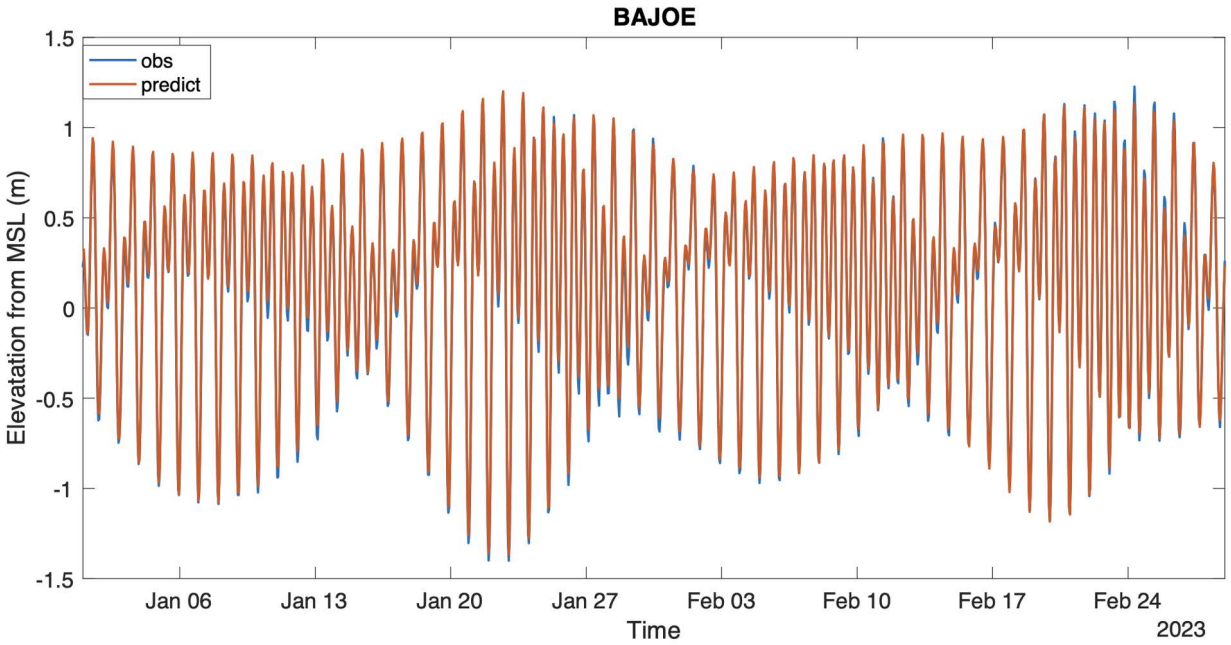

Figure 4. Verification of tidal prediction (red line) and observation (blue line) data in BAJOE station for January-February 2023.

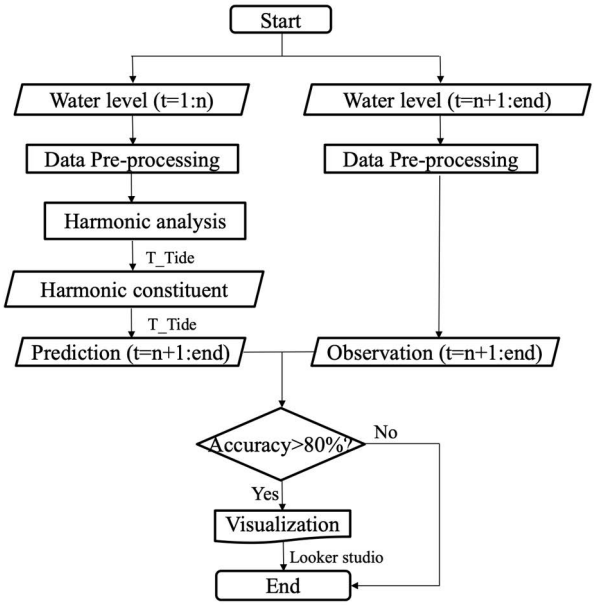

Figure 5. Research's flowchart

RESULTS AND DISCUSSIONS

Tidal prediction accuracy

The average accuracy percentage of tidal prediction results and the mean absolute bias (MA) against observational data from January 2022 to April 2023 is displayed in Figure 6. The average of accuracy percentage of tidal predictions during this period is 93.21%, with the highest percentage at the Bajoe station (98.26%) and the lowest at the Belinyu station (79.6%) (Figure 6). According to Lewis (1962) criteria, the overall accuracy percentage is classified as highly accurate, makes the predictions in a suitable reference for the early warning of coastal floods. The Mean Absolute Error (MAE) ranges from 0.049 to 0.43 m. A lower MAE signifies a more accurate prediction. The MAE values generally aligns with the Mean Absolute Percentage Error (MAPE). The highest MAE value is observed at the Belinyu station (0.43 m), whereas the lowest MAE value is recorded at the Bajoe station (0.049 m) (Figure 6). Some locations with accuracy values below 85% and high value of MAE (such as the Belinyu station) are associated with the observational data quality and data availability issues. Data at these locations often contain significant noise that can no longer be eliminated. Moreover, data availability also significantly impacts the accuracy percentage. In some of these locations, there are lengthy data gaps during certain periods. According to Pawlowicz et al. (2002), tidal analysis and prediction using the T_Tide toolbox are recommended to minimize data gaps. The length (duration) of water level data that analyze using THA absolutely affected the prediction accuracy. Research by Parker, 2007 demonstrated that longer water level time series allow for the analysis of more tidal constituents, leading to more accurate tidal predictions. It's important to note that in this study, the predictions only consider harmonic tidal components without adding non-tidal residual components or the sea level rise trend caused by climate change. Naturally, the predicted values over a long time period may slightly differ from the observations.

The histogram grouping of accuracy percentages in Figure 7 demonstrates variations in prediction accuracy over time. Generally, most months are dominated by predictions exceeding 90% accuracy. More than 60% of the 55 MAWS stations have accuracy exceeding 90% during the period from January 2022 to April 2023. Meanwhile, accuracy percentages between 70-90% are observed in less than 35% each month, and only about 10% of MAWS stations within the 50-70% accuracy range. Figure 7 also shows an increase in accuracy percentages exceeding 90% and a decrease in those within the 70-90% and 50-70%. This is due to the increasing number of MAWS station installations with improved water level sensor quality. Monthly variations in prediction accuracy are also related to variations in the quality of observational data over time. The variation in observational data quality is influenced by various factors such as communication systems, transmission, and the general electronic equipment conditions.

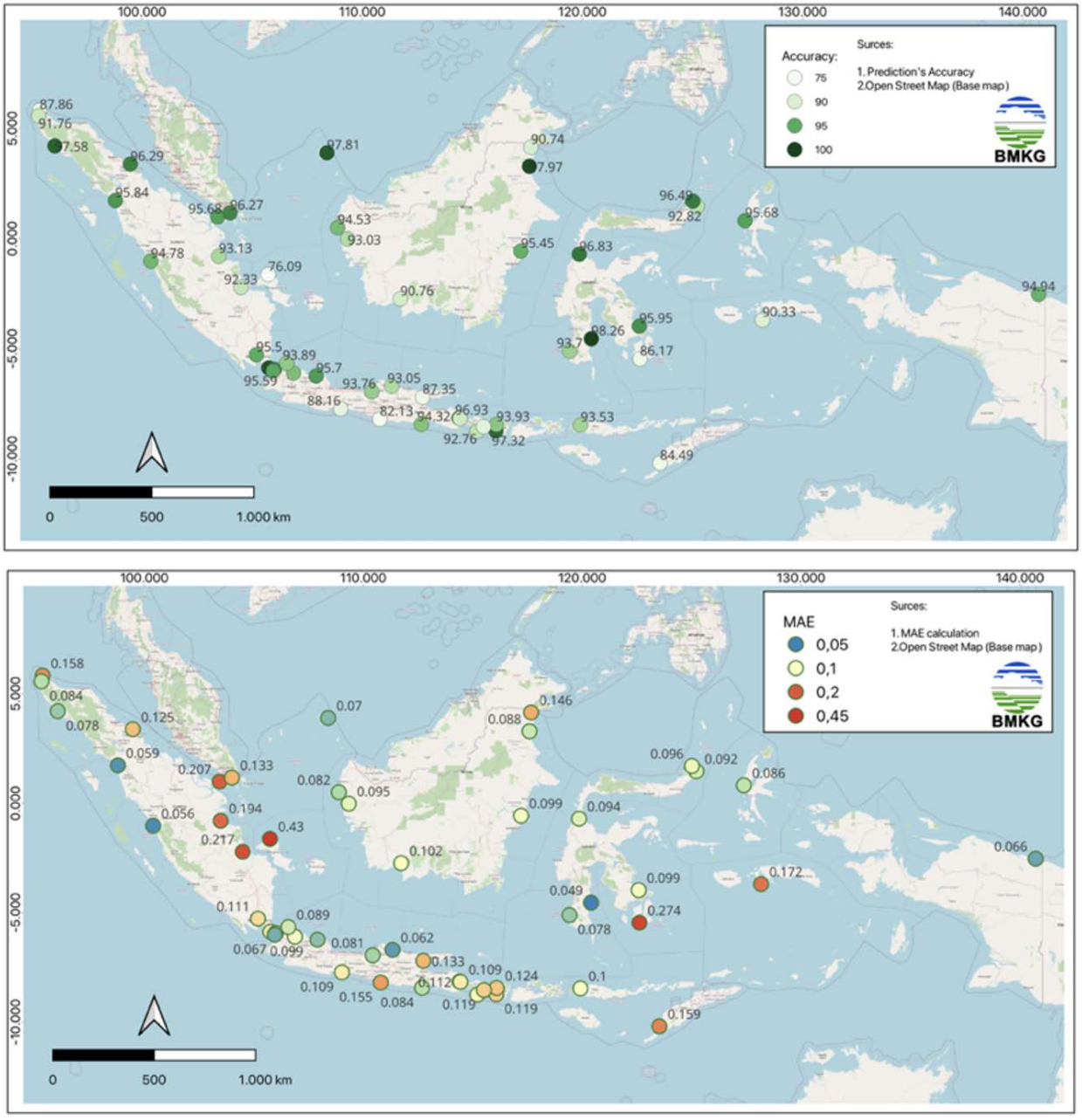

Figure 6. The average of accuracy percentage (MAPE, top) and Mean Absolute Bias (MAE, bottom) of tidal predictions for the period of January 2022 to April 2023.

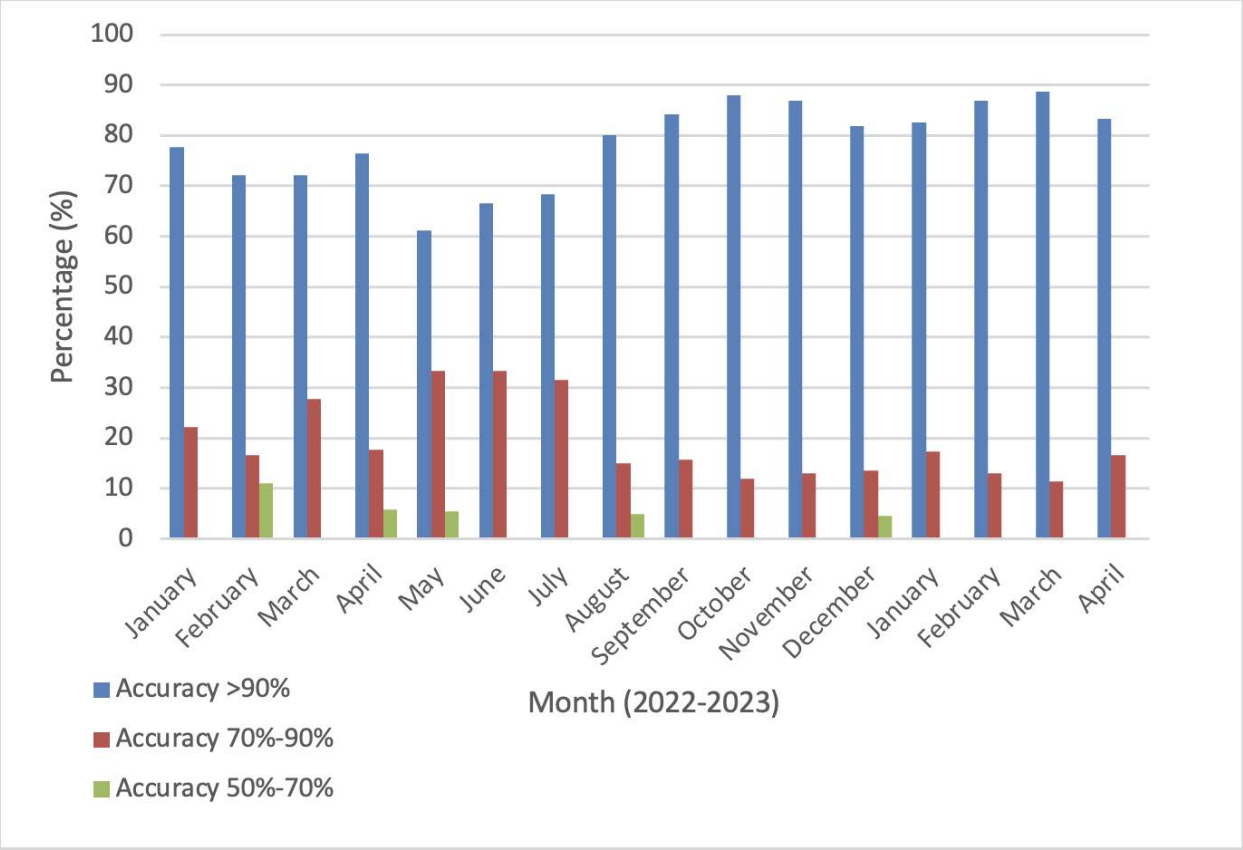

Figure 7. Histogram of accuracy percentage of tidal predictions for the period of January 2022 to April 2023.

Tidal prediction dashboard

Figure 8 displays the implemented tidal prediction dashboard. This tools consists of four sections, each section labelled A-D with different border color as shown in Figure 8. Part A (red border) serves as the control section, where users can select various controls, such as choosing the MAWS station to be displayed, the type of datum to be used, and the desired time range. In the datum section, two types of datum can be selected: Mean Sea Level (MSL) datum and Mean Lower Low Water (MLLW) datum, depending on the user's needs. MSL datum represents the average sea level observed over a specific period, while MLLW represents the average lowest tide within a day over a certain period. MLLW datum is also used by other institutions like National Oceanic and Atmospheric Administration (NOAA). In the time control section, users can select the desired time within a one-year range. Prediction values will be updated annually at the end of the year. Additionally, Part A contains a "User's Guide," link which serves as the manual for the conducted predictions, providing user instruction and scientific documentation for the dashboard. Finally, a map at the bottom displays the locations of the tidal prediction stations. This map dynamically updates to reflect the currently selected MAWS station.

Part B (blue circle) consists of a tidal elevation graph that adjusts its display based on the selected location and time. The bottom of the graph displays information about elevation units, datum, and the time zone used. The time zone utilized in this dashboard is Coordinated Universal Time (UTC) (WIB+7). Part C is a table of predicted elevation values that correspond to the chosen location and time in the control section in Part A. This table also offers an option to download the data by clicking the three dots in the upper right corner and selecting "export". Finally, Part D provides information about tidal elevation and time over a 12-hour period, which can serve as a reference for various maritime activities. Figure 9 illustrates an example of the dashboard display when customized to select the Bajoe station, MSL datum, and a prediction period in July 2023.

Websites built with Google Looker Studio can experience slower loading times due to large amounts of stored data. This can be further impacted by individual internet connection speeds. BMKG is commited certainly work on developing a more

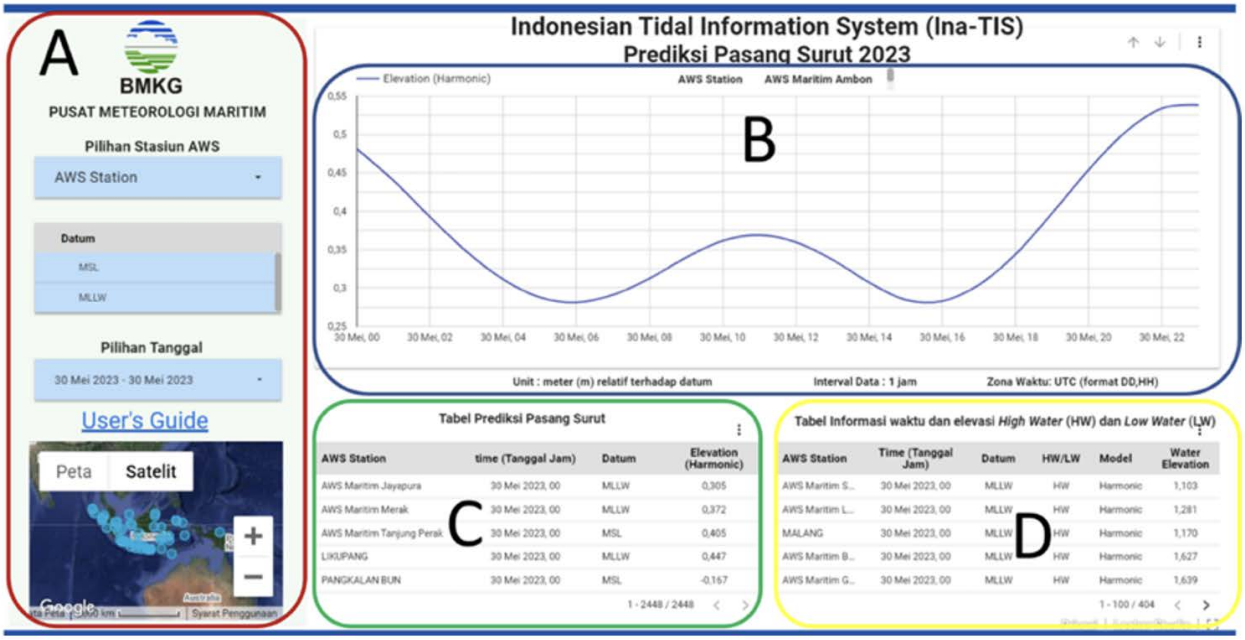

Figure 8. The initial display of the INATIS dashboard when first opened on the page https://maritim.bmkg.go.id/tide

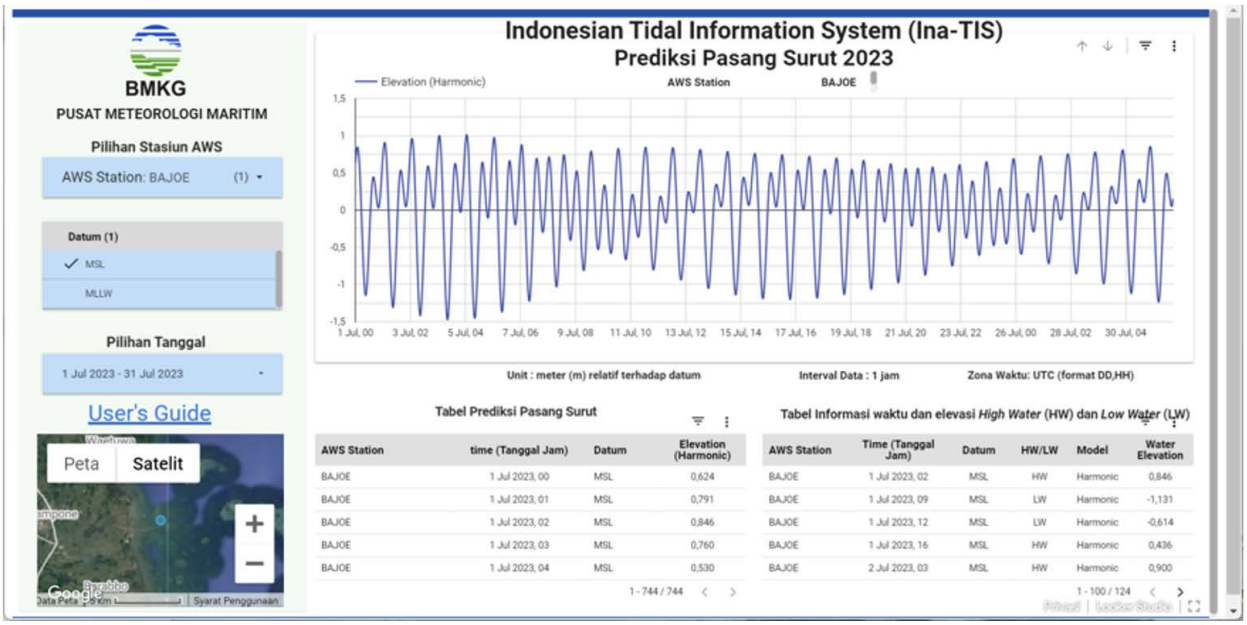

Figure 9. The display of the INATIS dashboard for Bajoe station with a MSL datum and prediction period in July 2023.

lightweight system to facilitate various users and improve loading efficiency.

CONCLUSIONS

Tidal predictions using classical harmonic analysis methods have demonstrated good accuracy, with an average accuracy reaching 93.21%. Monthly variations in prediction accuracy are influenced not only by the quality of data used for predictions but also by the quality of observational data used for verification. The tidal predictions have been successfully displayed on an open-source platform at https://maritim.bmkg.go.id/tide. This prediction information can serve as a reference for early warning systems for coastal flooding due to tidal influences. The prediction accuracy will continue to improve with the lengthening time series and availability of data to obtain more tidal components.

REFERENCES

Dasgupta, S., Laplante, B., Meisner, C., Wheeler, D., and Yan J. 2009. The impact of sea level rise on developing countries: A comparative analysis. *Climate Change*, 93(3–4):379–388. doi:10.1007/s10584-008-9499-5.

Egbert, G.D., and Ray, R.D. 2017. Tidal prediction. *Marine Research,* 75(3):189–237. doi:10.1357/002224017821836761.

Frederikse, T., Landerer. F., Caron, L., Adhikari, S., Parkes, D., Humphrey, V.W., Dangendorf, S., Hogarth, P., Zanna, L., and Cheng L. 2020. The causes of sea-level rise since 1900. *Nature*, 584(7821):393–397. doi:10.1038/s41586-020-2591-3.

Granata, F., and Di Nunno, F. 2021. Artificial Intelligence models for prediction of the tide level in Venice. *Stochastic Environmental Research and Risk Assessment*, 35(12):2537–2548. doi:10.1007/s00477-021-02018-9.

Haditiar, Y., Putri, M.R., Ismail, N., Muchlisin, Z.A., Ikhwan, M., and Rizal, S. 2020. Numerical study of tides in the Malacca Strait with a 3-D model. *Heliyon*, 6(9):e04828. doi:10.1016/j.heliyon.2020.e04828.

IOOS. 2016. Manual for Real-Time Quality Control of Hgh Frequency Radar Surface Current Data. May.

Lewis, C.D., 1982. *Industrial and Business Forecasting Methods: A Practical Guide to Exponential Smoothing and Curve Fitting*. Butterworth Heinemann.

Li, S., Liu, L., Cai, S., and Wang G. 2019. Tidal harmonic analysis and prediction with least-squares estimation and inaction method. *Estuarine, Coastal, and Shelf Science*, 220:196–208. doi:10.1016/j.ecss.2019.02.047.

Parker, B.B. 2007. *Tidal analysis and prediction.* Silver Spring, MD, NOAA NOS Center for Operational Oceanographic Products and Services, 378pp (NOAA Special Publication NOS CO-OPS 3). DOI: 10.25607/OBP-191.

Pawlowicz, R., Beardsley, B., and Lentz, S. 2002. Classical tidal harmonic analysis including error estimates in MATLAB using T TIDE. *Computer and Geoscience*, 28:929–937.

Riama, N.F., Sari, R.F., Rahmayanti, H., Sulistya, W., and Nurrahmat, M.H. 2021. The level of public acceptance to the development of a coastal flooding early warning system in Jakarta. *Sustainability,* 13(2):1–24. doi:10.3390/su13020566.

Riazi, A. 2020. Accurate tide level estimation: A deep learning approach. *Ocean Engineering*, 198:107013. doi:10.1016/j.oceaneng.2020.107013.

Small, C., and Nicholls, R.J. 2003. A global analysis of human settlement in coastal zones. *Coastal Research,* 19(3):584–599.

Snipes, G. 2018. Google Data Studio [Product Review]. *Journal of Librarianship and Scholarly Communication*, 6 (General Issue), eP2214. DOI: 10.7710/2162-3309.2214

Storto, A., Bonaduce, A., Feng, X., and Yang, C. 2019. Steric sea level changes from ocean reanalyses at global and regional scales. *Water,* 11(10). doi:10.3390/w11101987.

Su, Y., and Jiang, X. 2023. Prediction of tide level based on variable weight combination of LightGBM and CNN-BiGRU model. *Scientific Report,* 13(1):1–13. doi:10.1038/s41598-022-26213-y.

Thomson, R.E., and Emery, W. 2014. *Data Analysis Method in Physical Oceanography*. Third Volume. Elsevier B.V.

Ward, P.J., Marfai, M.A., Yulianto, F., Hizbaron, D.R., and Aerts, J.C.J.H. 2011. Coastal inundation and damage exposure estimation: A case study for Jakarta. *Natural Hazards*, 56(3):899–916. doi:10.1007/s11069-010-9599-1.

Widlansky, M.J., Long, X., and Schloesser, F. 2020. Increase in sea level variability with ocean warming associated with the nonlinear thermal expansion of seawater. *Communication Earth and Environmet*, 1(1):1–12. doi:10.1038/s43247-020-0008-8.

Zhang, Y.H., Fernandez-Montblanc, T., Pringle, W., Yu, H.C., Cui, L., and Moghimi, S. 2023. Global seamless tidal simulation using a 3D unstructured grid model (SCHISM v5.10.0). *Geoscience Model Development,* 16:2565-2581. doi: 10.5194/gmd-16-2565-2023.

Guide for Authors - Geoscience Publications
Bulletin of the Marine Geology

Writing should be submitted according to the following restrictions:

1. Manuscript should be written in English and be submitted online via journal website http://ejournal.mgi.esdm.go.id. Online Submission will be free. The author must login in order to make submission.
2. Manuscript should contains at least 2.000 words and at least 8 pages of manuscript that including embedded figures and tables, without any appendix, and the file should be in Microsoft Office (.doc/.docx) format. It should be prepared in A4 paper (21cm x 29.7cm) using 2.5 cm for left and right margins and 2 cm for top and bottom margins, additionally the paragraph should be used 1 line spacing, 11 TNR.
3. Title, Abstract, and Keywords should be written in English
   - Abstract should be written in English and Bahasa Indonesia version
   - Title should be less than 15 words, title case, small caps, centered, bold, font type Times New Roman (TNR), font size 16, and single spaced.
   - Abstract contains neither pictures nor tables, justified, in 11 TNR, single spaced, and should not exceed 250 words.
   - Keywords contain four to six words/phrases separated with coma and should be justified, 10 TNR and single spaced.
   - Please provide all email address of all authors for our database concern, however, in the published version, only the email address of the first author will be appeared.
4. Manuscript body consists of: Introduction, Method, Result, Discussion, and Conclusion completed by Acknowledgment and References in capital and bold.
5. Heading should be made in four levels. Level five cannot be accepted.
   - Heading 1: title caps, left aligned, bold, 14 TNR, single spaced
   - Heading 2: title case, left aligned, bold, 11 TNR, single spaced
   - Heading 3: title case, left aligned, italic, 11 TNR, single spaced
   - Heading 4 is not recommended, however, it could still be accepted with the format of: sentence case, left indent 5 mm, hanging indent 5 mm, italic, 11 TNR, single spaced
   - Heading 5 cannot be accepted in the manuscript.
6. Figure and table can be either in black and white or in color, they should be clearly readable and in a proportional measure to the overall page. Caption should be numbered, in 9 TNR and single spaced. For lay outing purpose, please provide the respective captioned figure/table with extension .tif/.jpg/.jpeg within a particular folder apart from the manuscript. Please note the figure source/citation/reference if it is taken and/or modified from previous publication.
7. Mathematical equation should be clearly written, numbered orderly, and accompanied with any information needed.
8. Header and footer including page number must not be used. All hypertext links and section bookmarks will be removed from papers. If you need to refer to an Internet email address or URL in your paper, you must type out the address or URL fully in Regular font.
9. Citation and Reference. Following are the detail organization of the references guidelines:
   a. References are written in alphabetical order according to the family name of the first author.
   b. If there is more than one references made by similar author, References are arranged in order of time, and then in alphabetical order.
   c. All the references should be cited in the text. In the text, reference is cited with author family name and the year of publication. If it is written by 2 authors, the family name of both authors are noted, followed by the year of publication, if it is written by more than 2 authors, the reference is cited with the first author family name, followed by *et al.,* and the year of publication. For example: (Kennett, 1981); (Usman and Panuju, 2013); (Susilohadi *et al.*, 2009). Several references are written in alphabetical order, for example: (Kennett, 1981; Susilohadi *et al.,* 2009; and Usman and Panuju, 2013).
   d. References are consist of paper, proceeding, or book that are published, or unpublished report including internal report, dissertation, or thesis.
   e. References can be taken from website, by writing the hyperlink, and the time when it is accessed. Wikipedia, personal blog, or non scientific website is not allowed to be taken into account.

f. References should be ten references in minimum, at least two of them were published in the last five years.

g. Only the family name of the authors are written, followed by the abbreviation of their first name and middle name (if available). If the reference is written by more than one author, all authors should be written, abbreviation (e.g. dkk, *et al,* or drr) is not allowed..

h. All the information of the references must be noted, including publisher, journal volume, number (if available), and page number.

- For book, the book title should be written in italic, for example:

  Kennett, J.P., 1981. *Marine Geology.* Prentice Hall, 813p.

- For periodicals, the name of the journal should be written in italic, for example:

  Susilohadi, S., Gaedicke, C., and Djajadihardja, Y.S., 2009. Structures and sedimentary deposition in the Sunda Strait, Indonesia, *Tectonophysics,* 467 (1): 55-71.

- (Tectonophysics is the name of the journal, 467 is the volume, 1 is issued number, 55 – 71 is page number)

  Usman, E., and Panuju, 2013. Study of Gas Potency Based on Gravity Anomaly Modeling And Seismic Profile Analysis at Banggai-Sula Basin. *Bulletin of the Marine Geology,* 28 (2): 51-60.

- For edited symposia, special issues, etc. published in periodical:

  Kenneth, S. J., 2009. Marine biogeochemistry in 2025. In: D. Glickson (Editor), *Oceanography in 2025: Proceedings of a workshop.* The National Academic Press, Washington D. C.: 130 – 134.

- For websites:

  <http://palaeo-electronica.org/2003_1/benthic/issue1_03.htm> [Accessed on 30 November 2011].

- Unpublished references:

  Darlan, Y., Kamiludin, U., Kurnio, H., Rahardian, R., Hutagaol, J. P., Sianipar, A. H., and Sinaga, A. C., 2005. *Eksplorasi prospektif gas biogenik kelautan di Perairan Muara Kakap dan sekitarnya - Kalimantan Barat.* Pusat Penelitian dan Pengembangan Geologi Kelautan, Bandung, Badan Penelitian dan Pengembangan Energi dan Sumberdaya Mineral, Departemen Energi dan Sumberdaya Mineral. Internal report, 104p. Unpublished.

SERTIFIKAT

Direktorat Jenderal Penguatan Riset dan Pengembangan,
Kementerian Riset, Teknologi, dan Pendidikan Tinggi

RISTEKDIKTI

Kutipan dari Keputusan Direktur Jenderal Penguatan Riset dan Pengembangan,
Kementerian Riset, Teknologi, dan Pendidikan Tinggi Republik Indonesia
Nomor: 21/E/KPT/2018, Tanggal 9 Juli 2018
Tentang Hasil Akreditasi Jurnal Ilmiah Periode I Tahun 2018

Nama Jurnal Imiah

Bulletin of the Marine Geology

E-ISSN: 2527-8843
Penerbit: Puslitbang Geologi Kelautan, Kementerian ESDM

Ditetapkan sebagai Jurnal Ilmiah

TERAKREDITASI PERINGKAT 2

TERAKREDITASI

Akreditasi berlaku selama 5 (lima) tahun, yaitu
Volume 31 Nomor 1 Tahun 2016 sampai Volume 35 Nomor 2 Tahun 2020

Jakarta, 9 Juli 2018
Direktur Jenderal Penguatan Riset dan Pengembangan

Dr. Muhammad Dimyati
NIP. 195912171984021001

MARINE GEOLOGICAL INSTITUTE

GEOLOGICAL AGENCY
MINISTRY OF ENERGY AND MINERAL RESOURCES
Jalan Dr, Junjunan No. 236, Bandung-40174, Indonesia
http://www.mgi.esdm.go.id, E-mail: ejournal.p3gl@gmail.com

ISSN 1410 - 6175
9 771410 617003